Characterization of Cadmium-Induced BiP Accumulation in *Xenopus laevis* A6 Kidney Epithelial Cells

by

Cody Shirriff

A thesis
presented to the University of Waterloo
in the fulfillment of the
thesis requirement for the degree of
Master of Science
in
Biology

Waterloo, Ontario, Canada, 2016

Author's Declaration

I hereby declare that I am the sole author of this thesis. This is a true copy of the thesis, including any required final versions, as accepted by my examiners. I understand that my thesis may be made electronically available to the public.

Abstract

In vertebrates, cadmium exposure is found to cause respiratory, neurological and kidney disorders. At the cellular level, cadmium can damage or modify proteins resulting in the production of toxic protein aggregates. The formation of protein aggregates can be inhibited by the accumulation of heat shock proteins (HSPs), a class of molecular chaperones. Immunoglobulin binding protein (BiP) is an endoplasmic reticulum (ER)-resident heat shock protein that binds to nascent proteins on entry into the ER and assists in their folding and assembly. Little information is available on the effect of cadmium on BiP accumulation or function in vertebrates. In this study, cadmium treatment of *Xenopus laevis* A6 kidney epithelial cells induced a dose- and time-dependent increase in BiP accumulation that was the result of de novo transcription and translation. In cells recovering from cadmium exposure, elevated levels of BiP were still detectable after 48 and 72 h. The exposure of cells to a low concentration of cadmium at 30 °C greatly enhanced BiP accumulation compared to cadmium treatment at 22 °C. Glutathione levels may modulate the UPR since treatment of cells with the glutathione synthesis inhibitor, buthionine sulfoximine, enhanced cadmium-induced BiP accumulation. Finally, immunocytochemistry revealed that cadmium-induced BiP accumulation occurred primarily in a punctate pattern in the perinuclear region. In some cells treated with 200 μM cadmium or 30 μM MG132, relatively large BiP antibody staining structures were observed that co-localized with a Proteostat dye that has been used to detect aggregated protein or aggresome-like structures. Analysis of individual z-planes revealed that BiP was detected in the center of the Proteostat-stained structures. These structures were also observed in cells treated with 100 μM cadmium chloride at 30 °C or 100 μM cadmium chloride after pretreatment with the glutathione inhibitor, buthionine sulfoximine. This study has shown for the first time in amphibians that cadmium

chloride induced an increase in BiP levels, which is likely to counteract the toxic accumulation of aggregated protein in the ER. The sequestration of protein aggregates by a molecular chaperone may be significant to the understanding of the pathology of certain diseases that result in intracellular inclusion bodies such as Alzheimer's disease, Parkinson's disease and amyloidosis.

Acknowledgements

I would like to extend a deep level of gratitude and appreciation towards Dr. John J. Heikkila. His infallible patience, wisdom and positive attitude guided me through the rocky terrain of research. I will forever carry the lessons that he shared over the last two years (and his numerous puns). I consider myself lucky that he was my supervisor.

I would also like to extend my appreciation towards my committee members, Dr. Mungo Marsden and Dr. Paul Craig, for taking the time to critically analyze this thesis.

Imran Khamis and James Campbell, my two office brothers, added a great amount of comfort to my graduate student experience. Imran introduced me to the Heikkila Lab, for which I am grateful. I learned from James that humor and lab work are not mutually exclusive.

Two friends that need to be mentioned are Matt Mcleod and Mohini Nema. We shared a lot of laughs, mulled wine, odd dinner experiences, Fridays at the grad house, etc. It was always a pleasure hanging out with those two after long hours spent in the lab.

I appreciated visits from my friend on the second floor, Justin Knapp. It was nice watching his squash game improve over the last few months. It was not nice watching him improve to the point of beating me. I hope to repay the favor in golf some day.

Finally, I am grateful for the encouragement provided by my family: Steve, Lisa and Wylie. This work was a direct result of their love and support. Thank you.

Table of Contents

List of Figures

List of Tables

List of Abbreviations

ANOVA	analysis of variance
APS	ammonium persulfate
ATF6	activating transcription factor 6
ATP	adenosine triphosphate
BAG3	B-cell lymphoma 2-associated athonogene-3
BCA	bicinchoninic acid
BCIP	5-bromo-4-chloro-3-indolyl phosphate
BiP	Immunoglobulin binding protein
BSA	bovine serum albumin
BSO	buthionine sulfoximine
C	control
CAT	chloramphenicol acetyltransferase
c-MYC	v-myc myeolocytomatosis viral oncogene homolog
CHIP	carboxyl terminal of HSP70/HSP90 interacting protein
Cul3-RBX1	Cullin 3-ring box 1
DAPI	4,6-diamindino-2-phenylindole
DMSO	dimethylsulfoxide
DMT1	divalent metal ion transporter 1
EDTA	ethylenediaminetetraacetic acid
ER	endoplasmic reticulum
ERAC	endoplasmic reticulum-associated compartment
ERAD	endoplasmic reticulum-associated degradation
ERSE	endoplasmic reticulum stress element
eIF2α	eukaryotic translation factor 2-alpha
FBS	fetal bovine serum
FOXA-1	forkhead box a-1
GRP	glucose-regulated protein
GSH	glutathione
GSSH	glutathione disulfide
HeLa	Henrietta Lacks
HBSS	Hank's balanced salt solution
HDAC6	histone deacetylase 6
HEPES	4-(2-hydroxyethyl)-1-piperazineethanesulfonic acid
HO-1	heme oxygenase-1
HSC70	heat shock cognate 70
HSE	heat shock element
HSF	heat shock factor
HSP	heat shock protein
IRE1	inositol-requiring enzyme 1
Keap-1	Kelch-like ECH associated protein
L-15	Leibovitz-15
LLC-PK1	Lilly-laboratory cell – porcine kidney 1
LSCM	laser scanning confocal microscopy
MAF	musculoaponeurotic fibrosarcoma

MARE	Maf recognition elements
MAPK	mitogen-activated protein kinase
MG132	carbobenzoxy-L-leucyl-L-leucyl-L-leucinal
MRE	metal response element
NBT	4-nitro blue tetrazoleum
NRF-2	nuclear factor (erythroid-derived 2)-like 2
PAK-2	p21 protein (cdc42Rac)-activated kinase-2
PERK	protein kinase RNA-like ER kinase
PEX11β	peroxisomal biogenesis factor 11 β
PBS	phosphate-buffered saline
ROS	reactive oxygen species
SP1	specificity protein 1
SDS-PAGE	sodium dodecyl sulfate-polyacrylamide gel electrophoresis
sHSP	small heat shock protein
TEMED	tetramethylenediamine
TBS-T	Tris-buffered saline solution-tween 20
Tris	Tris(hydroxymethyl)aminomethane
TRITC	tetramethylrhodamine-5-isothiocyanate phalloidin
UCH-1	ubiquitin carboxy-terminal hydrolase-1
UPR	unfolded protein response
UPS	ubiquitin-proteasome system
XBP1	x-box binding protein 1
ZIP	zinc-regulated transporter, iron-regulated transporter related protein

1.0 Introduction

1.1 Proteotoxic stress

Proteotoxic stress refers to a challenge imposed on the homeostasis of the cellular pathways that maintain the synthesis, folding, translocation and degradation of proteins (Balch et al., 2008). A proteotoxic stress can be the consequence of environmental stress (e.g. heat shock, heavy metals, proteasomal inhibitors) or certain disease states (e.g. Alzheimer's, Parkinson's, cystic fibrosis). For example, the exposure of cells to heat shock can disrupt the conformational stability of native proteins by affecting hydrogen bonds, van der Waal forces, salt bridges and hydrophobic interactions (Daniel et al., 1996). Hydrophobic and backbone moieties that are buried in the interior of native protein are exposed when proteins become unfolded/misfolded, which increases the probability of aggregation since hydrophobic forces drive the interaction between non-native proteins (Chiti & Dobson, 2009; Tyedmers et al., 2010; Vabulas et al., 2010). Additionally, protein aggregation results in the loss of their function within the cell, which can disrupt biochemical pathways (Powers et al., 2009). The process of protein aggregation was shown to be concentration dependent and enhanced by the cell's crowded environment (Zimmerman & Trach, 1991; Ellis & Minton, 2006; Chiti & Dobson, 2009). Two modulators of protein homeostasis that can inhibit or reduce the level of stress-induced protein aggregation are the heat shock and unfolded protein response (Morimoto, 2008; Powers et al., 2009).

1.2 Heat shock proteins

Heat shock proteins (HSPs) are highly conserved in evolution as they have been reported in essentially all organisms from bacteria to humans (Lindquist & Craig, 1988; Kregel, 2002). In

eukaryotic cells, there are at least 6 HSP families that have been classified by means of size and amino acid sequence and include HSP90, HSP70, HSP60, HSP40 and small HSPs (sHSPs). Some HSPs are constitutively expressed while others are stress-inducible (Katchinski, 2004). Stress-inducible HSPs can protect the cell by inhibiting aggregation of unfolded/misfolded protein. Once normal conditions return, some stress-inducible HSPs can refold their client proteins to restore their function. Stress-inducible HSPs appear to be involved in the protection of cells from exposure to heavy metals, hydrogen peroxide, extreme temperatures or ethanol toxicity (Richter et al., 2010). Other HSPs, such as HSP40, work as co-chaperones that regulate the activity and substrate specificity of other HSPs (Fan et al., 2003). In addition to their roles during stress conditions, HSPs can play a role in normal cellular function by assisting in protein translation, translocation and protein refolding (Kang et al., 1990; Frydman et al., 2001).

1.2.1 HSP70 Family

The HSP70 family has been highly conserved during evolution (Katchinski, 2004; Daugaard et al., 2007). Eukaryotic organisms contain multiple copies of HSP70 family members specific for different cellular compartments (Katchinski, 2004). This includes stress-inducible HSP70 and constitutively-expressed heat shock cognate 70 (HSC70) found primarily in the cytosol, mitochondrial HSP70, and the endoplasmic reticulum (ER) protein, immunoglobulin binding protein (BiP; discussed in section 1.4), which is also known as glucose-regulated protein 78 (GRP78; Daugaard et al., 2007). All HSP70 proteins share a conserved ATPase domain, a protease-sensitive site, a peptide binding domain and a G/P-rich C-terminal domain (Daugaard et al., 2007). The N-terminal ATP-binding domain is well conserved between HSP70 family members compared to the C-terminal substrate-binding domain (Brocchieri et al.,

2008). Eukaryotic HSP70 family members share a high amount of amino acid identity as well as with homologs in evolutionarily distant species. For example, *Drosophila* HSP70 shares 73% amino acid identity with human HSP70 (Hunt & Morimoto, 1985). The human genome contains 47 hsp70 sequences consisting of 17 genes and 30 pseudogenes, which can be divided into 7 evolutionarily distinct groups that share a high degree of sequence similarity among them (Brocchieri et al., 2008).

1.2.2 Cytosolic stress-inducible HSP70

In human cell lines, cytosolic HSP70 was induced by stressful conditions including heat shock, oxidative stress and the presence of heavy metals as well as other stressors (Vilaboa et al., 1997). HSP70 was determined to act as an ATP-dependent molecular chaperone since it bound to the hydrophobic residues of denatured client proteins to inhibit their aggregation followed by refolding of the protein once normal conditions were re-established (Katschinski, 2004; Daugaard et al., 2007). HSP70 was reported to prevent aggregation by interacting with growing polypeptide chains under stressful conditions (Beckman et al., 1990; Shalgi et al., 2013) Stress-inducible HSP70 can also protect from programmed cell death by acting on upstream or downstream factors of caspase activation (Mosser et al., 2000).

There are two human stress-inducible *hsp70* genes, *hsp70-1a* and *hsp70-1b* (Brocchieri et al., 2008; Murphy, 2013). *Hsp70-1a* and *hsp70-1b* are intronless and produce nearly identical proteins differing by two amino acids (Murphy, 2013). The promoter for both *hsp70-1a* and *hsp70-1b* contain a TATA box, two CCAAT boxes, at least two HSEs, a serum response element, a metal response element (MRE) and binding sites for transcription factors such as specificity protein 1 (SP1), v-myc myeolocytomatosis viral oncogene homolog (c-MYC) and

forkhead box a-1 (FOXA-1;Wu et al., 1986; Morgan et al., 1987, Morgan, 1989; Murphy, 2013). The activation of *hsp70-1* can occur under certain stress conditions, which includes heat shock, hypoxia, low pH and redox imbalance (Silver & Noble, 2012). The transcriptional regulation of *hsp70-1* under heat stress has been extensively studied (Refer to Section 3 for the heat shock response).

In *Xenopus laevis*, there has been one cDNA and four intronless *hsp70A, B, C and D* genes isolated, however the full coding sequence is only available for *hsp70A* and *hsp70B* (Bienz, 1984; Horrell et al., 1987; Heikkila, 2010). The 5' regulatory region for *hsp70A* and *hsp70B* contains 3 heat shock elements (HSEs) in addition to a TATA and CCAAT box. The amino acid sequence for HSP70A shares a 74% identity with *Drosophila* HSP70 (Heikkila, 2010). Increased accumulation of *Xenopus* HSP70 has been reported in A6 cells that were exposed to stressors such as heat shock, cadmium chloride, sodium arsenite, proteasomal inhibitors, curcumin, celastrol, withaferin A and hydrogen peroxide (Muller et al., 2004; Woolfson & Heikkila, 2009; Walcott & Heikkila, 2010; Young & Heikkila, 2010; Khan & Heikkila, 2011; Brunt et al., 2012; Khan et al., 2012; Khamis & Heikkila, 2013). In A6 cells recovering from heat shock, HSP70 accumulation declined to control levels after 24 h but remained elevated when cells were also treated with a proteasome inhibitor, suggesting HSP70 was being degraded by the proteasome (Khan & Heikkila, 2014).

1.3 The heat shock response

In 1964, Ferruccio Ritossa reported that *Drosophila* larvae exposed to an elevated temperature of 37 °C resulted in the formation of specific puffs in salivary gland chromosomes (Ritossa, 1964). These puffs were later characterized as transcriptionally active sites (Berendes,

1968). Since then it has been proposed that elevated temperature can induce the synthesis of HSPs through the heat shock response (HSR), which is the activation of transcription of *hsp* genes leading to the transient production of HSPs. The HSR has been studied in numerous systems and under a variety of conditions (Pardue et al., 1992; Feder & Hofman, 1999; Morimoto, 2008). Upon the activation of the HSR, stress-inducible HSPs were determined to bind to unfolded protein, inhibit their aggregation, and assist in their refolding once environmental conditions returned to normal.

Heat shock factors (HSFs) are the key transcriptional regulators of *hsp* gene transcription (Akerfelt et al., 2010). In 1984, there were two reports published on the presence of a HSF bound to the upstream regulatory region of *hsp* genes in *Drosophila* (Parker & Topol, 1984; Wu, 1984). Later studies with vertebrates revealed the presence of HSF1, HSF2, HSF3 and HSF4. HSF1 is the key regulator of the HSR in mammals and is the functional homologue to HSF found in *Drosophila* and yeast (Pirkkala et al., 2001). HSF2 is tissue-specific (testes, heart and brain for example) and is found in certain stages in development (Goodson et al., 1995; Pirkkala et al., 2001). HSF3 was reported in birds and is stress-responsive (Nakai & Morimoto, 1993; Pirkkala et al., 2001; Fujimoto et al., 2010). Finally, HSF4 has two isoforms that have different regulatory effects, HSF4a and HSF4b, which are expressed in a tissue-specific manner (Tanabe et al., 1999; Pirkkala et al., 2001).

In a DNA mobility shift assay, HSF binding to a synthetic oligonucleotide corresponding to the HSE of the *hsp70B* gene was reported to be heat-inducible at all developmental stages in *Xenopus laevis* including the pre-midblastula stages, which are unable to express HSP genes (Ovsenek & Heikkila, 1990). Also, cDNA sequences have been isolated and sequenced for *Xenopus laevis* HSF1 and HSF2, respectively (Stump et al., 1995; Hilgarth et al., 2004). Both

sequences for *Xenopus laevis* HSF1 and HSF2 share high similarity to other vertebrate HSFs (Stump et al., 1995; Hilgarth et al., 2004).

The general model for the HSR begins with a pre-existing monomeric form of HSF1 in the cell bound to heat shock protein 90 (HSP90) and histone deacetylase 6 (HDAC6) under normal conditions (Figure 1; Voellmy, 2004; Boyault et al., 2007; Pernet et al., 2014). In response to stressful conditions, monomeric HSF1 undergoes a conformational change, which allows HSF1 to trimerize and enter the nucleus (Hentze et al., 2016). It then binds a *cis*-acting element in the upstream region of stress-inducible *hsp* genes, the heat shock element (HSE), and recruits RNA polymerase II to activate transcription (Voellmy & Boellman, 2007; Hentze et al., 2016). The transition from monomeric HSF1 to a trimer was reported to be concentration-dependent (Hentze et al., 2016).

1.4 Immunoglobulin binding protein (BiP)

1.4.1 BiP discovery

In the 1970s, researchers reported that the infection of chick embryo fibroblast cells with an avian RNA tumor virus induced rapid cell divisions, which resulted in glucose deprivation and the concomitant accumulation of 78 and 94 kDa polypeptides (Stone, 1974; Pouysségur et al., 1977). These proteins were referred to as glucose-regulated protein 78 (GRP78) and glucose-regulated protein 94 (GRP94; Pouysségur et al., 1977; Shiu et al., 1977). Tunicamycin, an N-linked glycosylation inhibitor, also enhanced the relative level of GRPs (Olden et al., 1979). GRP78 and GRP94 accumulated in high amounts in ER fractions from glucose-starved avian cells, suggesting these proteins were ER residents (Zala et al., 1980). Other studies revealed that GRP78 was identical to immunoglobulin binding protein (BiP) that was found covalently attached to the heavy chain of immunoglobulin proteins produced in lymphocytes and

Figure 1. The heat shock response**.** Stress-induced unfolded protein accumulation in the cytoplasm results in the dissociation of HSP90 and HDAC6 from the HSF1 monomer, which then trimerizes, enters the nucleus and binds to HSEs to activate transcription of *hsp* genes.

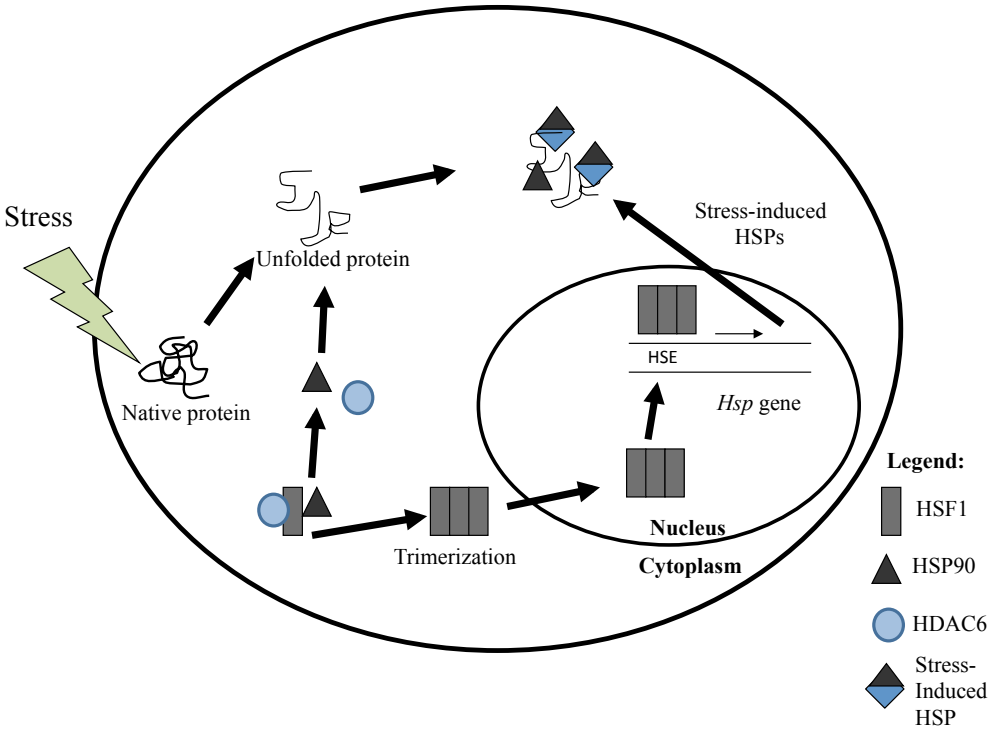
Stress
Native protein
Unfolded protein
Stress-induced
HSPs
HSE
Hsp gene
Trimerization
Nucleus
Cytoplasm
Legend:
HSF1
HSP90
HDAC6
Stress-
Induced
HSP

hybridomas (Haas & Wabl, 1983). BiP/GRP78 was later determined to be a member of the *hsp70* gene family (Munro & Pelham, 1986).

1.4.2 BiP structure

BiP is highly conserved and shares more sequence identity with homologues from different species than with other HSP70 family proteins found within the same organism (Haas, 1994). For example, rat BiP shares 98% sequence identity with hamster BiP compared to 62% with rat HSP70 (Haas, 1994). BiP is composed of an ATPase and C-terminal peptide-binding domain connected via a linker, as well a KDEL ER retention signal sequence (Lys-Asp-Glu-Leu; Munro & Pelham, 1986; MacIas et al., 2011). Normally, the KDEL ER retention sequence prevents BiP secretion from the ER. However, BiP and other ER chaperones containing the KDEL (e.g. GRP94 and protein disulphide isomerases) have been documented to leave the ER under cell stress or through anterograde transportation under normal conditions (Capitani & Sallese, 2009). Crystal structures were determined for human BiP in an ATP-bound state as well as the BiP substrate-binding domain with a bound peptide and the ATPase domain in complex with ADP (Wisniewska et al., 2010; Yang et al., 2015)

1.4.3 BiP function within the endoplasmic reticulum

The ER mediates early steps involved in the biosynthetic pathway of secretory and surface proteins. Normally, all proteins destined for secretion or the cell surface contain a hydrophobic ER signal sequence usually at the N-terminus (Lodish et al., 2000). The translation of secretory and surface proteins occurs either through co-translational translocation or post-translational translocation. Co-translational translation occurs when proteins containing an ER signal sequence guide ribosomes to the ER membrane at a translocon gate, permitting

translocation while translation occurs (Ma & Hendershot, 2004; Nyathi et al., 2013). Studies performed in yeast suggested that BiP plays an essential role in the functioning of the translocon gate (Alder et al., 2005; Nyathi et al., 2013). BiP was also determined to bind nascent unfolded polypeptides in the ER lumen and to prevent their degradation and/or aggregation before they reached a folded-competent state (Sanders & Shekman, 1992). Post-translational modifications of the nascent polypeptide can then occur, which include N-linked glycosylations and disulphide bonds (Ma & Hendershot, 2004). Many modified proteins are then transited to other organelles, such as the Golgi apparatus, mitochondria or lysosomes, or are secreted from the cell (Lodish et al., 2000). ER molecular chaperones monitor the maturation of newly translated secretory proteins in the complex ER environment that is oxidizing, calcium-rich and highly crowded (Ma & Hendershot, 2004). BiP plays a significant role in this process by binding misfolded protein, preventing aggregation and re-folding proteins in an ATP-dependent manner (Zhu & Lee, 2015). When ATP occupies the ATPase domain of BiP, the substrate-binding domain is in an open conformation, allowing substrates to bind and release with low affinity (Otero et al., 2010). The hydrolysis of ATP closes the substrate binding which stabilizes the interaction of BiP with the substrate (Mayer & Bukau, 2005; Otero et al., 2010). ADP is exchanged for ATP and the substrate protein is released, allowing an opportunity to re-fold (Mayer & Bukau, 2005; Otero et al., 2010). BiP has high binding affinity with substrates containing hydrophobic residues exposed on misfolded proteins (Flynn et al., 1991; Haas, 1994).

BiP was found to directly bind calcium, regulate the unfolded protein response (UPR; discussed in the section 4.5) and aid in endoplasmic reticulum associated degradation (ERAD; Lee, 2001; Ni et al., 2011). The model for ERAD proposes that a misfolded protein in the ER is targeted, carried to a retrotranslocon in the ER membrane and exported to the cytosol for

degradation by the 26S proteasome (Okuda-Shmizu & Hendershot, 2007). Studies in yeast suggested that BiP was required for the retrotranslocation of several non-glycosylated ERAD substrates (Plemper et al., 1997; Brodsky et al., 1999). Also, mammalian studies reported that soluble non-glycosylated BiP substrates were retrotranslocated and degraded by the 26S proteasome (Skowronek et al., 1998; Okuda-Shmizu & Hendershot, 2007).

In addition to the ER, BiP has been identified at low levels in the nucleus, cytosol, mitochondria and extracellular membrane (Ni et al., 2011). Cells exposed to thapsigargin (an ER calcium-ATPase inhibitor) or cells ectopically expressing BiP as well as certain tumor cells, such as gastric cancer cells and pancreatic cancer cells, have been shown to have BiP on their cell surface (Quinones et al., 2008; Ni et al., 2011). In cancer cells, cell surface BiP is thought to play a role in mediating tumor cell signalling (Misra et al., 2004; Ni et al., 2011). For example, cell surface BiP binds alpha$_2$-macroglobulin, activates p21 protein (cdc42rac)-activated kinase-2 (PAK-2) and leads to an increase cell motility for metastasis (Misra et al., 2004).

1.4.4 *Xenopus laevis* BiP

Two *Xenopus laevis* BiP cDNAs have been isolated and sequenced (Beggah et al., 1996; Miskovic et al., 1997). Miskovic et al. (1997) reported they share 97% identity with each other and share approximately 90% identity with chicken, rat and human BiP sequences than *Xenopus* HSP70 (57%) or HSC70 (55%) amino acid sequences. *Bip* mRNA was detected in all stages of development, from unfertilized eggs to 4-day tadpoles (Winning et al., 1991). Furthermore, A23187 and tunicamycin first enhanced *bip* mRNA accumulation at the neurula stage (Miskovic et al., 1999). In *Xenopus laevis* A6 kidney epithelial cells, *bip* mRNA and BiP protein levels were enhanced by treatment with heat shock, tunicamycin or A23187 (Winning et al., 1989;

Winning et al., 1991; Miskovic et al., 1997). Recently, our laboratory found that BiP was also induced by the proteasomal inhibitors, MG132 and withaferin A, as determined by immunoblot and immunocytochemical analysis (Khan et al., 2012).

1.4.5 The unfolded protein response (UPR)

The accumulation of unfolded proteins within the ER lumen was found to upregulate stress-inducible BiP through the unfolded protein response (UPR; see Figure 2; Lièvremont et al., 1997; Lee, 2005; Ron & Walter, 2007; Walter & Ron, 2011). Under normal conditions, BiP inhibits the activity of three ER transmembrane proteins: activating transcription factor 6 (ATF6), inositol-requiring enzyme 1 (IRE1) and protein kinase RNA-like ER kinase (PERK; Ron & Walter, 2007). As proteins unfold and accumulate in the ER lumen, BiP dissociates from ATF6, IRE1 and PERK to bind the unfolded proteins (Bertolloti et al., 2000; Shen et al., 2002). Upon release of BiP, ATF6 translocates to the Golgi apparatus where it is cleaved to become the transcription factor, ATF6f, which is capable of inducing BiP gene expression (Kokame et al., 2001; Shen et al., 2002). IRE1 dissociates from BiP to gain endoribonuclease activity (Schröder & Kaufman, 2005). IRE1 can then splice x-box binding protein 1 (XBP1) mRNA to allow translation of the XBP1s protein, a transcription factor that is involved in inducing the expression of BiP, endoplasmic reticulum associated degradation (ERAD) genes and other genes associated with the unfolded protein response (Yoshida et al., 1998; Smith et al., 2011; Walter & Ron, 2011). PERK then dissociates from BiP and phosphorylates eukaryotic translation factor 2-alpha (eIF2α), which inhibits protein translation thus preventing further protein accumulation in the ER (Schröder & Kaufman, 2005). In mammalian studies, XBP1s and ATF6f have been reported to bind upstream cis-regulatory elements called endoplasmic reticulum stress elements (ERSE) to

Figure 2. The unfolded protein response. Under normal conditions, BiP inhibits the activation of the unfolded protein response by binding ATF6, IRE1 and PERK. An increase in unfolded proteins within the ER lumen results in the dissociation of BiP from ATF6, IRE1 and PERK allowing it to bind the unfolded protein. ATF6 translocates to the Golgi apparatus to undergo processing to become ATF6f, a transcription factor able to induce BiP expression. Activated IRE1 gains endoribonuclease activity, which splices XBP1 mRNA into XBP1s mRNA. Subsequent translation into XBP1s protein enables induction of ERAD and BiP gene expression. Activated PERK phosphorylates eIF2α, which can inhibit translation. Image adapted from Todd et al., 2008.

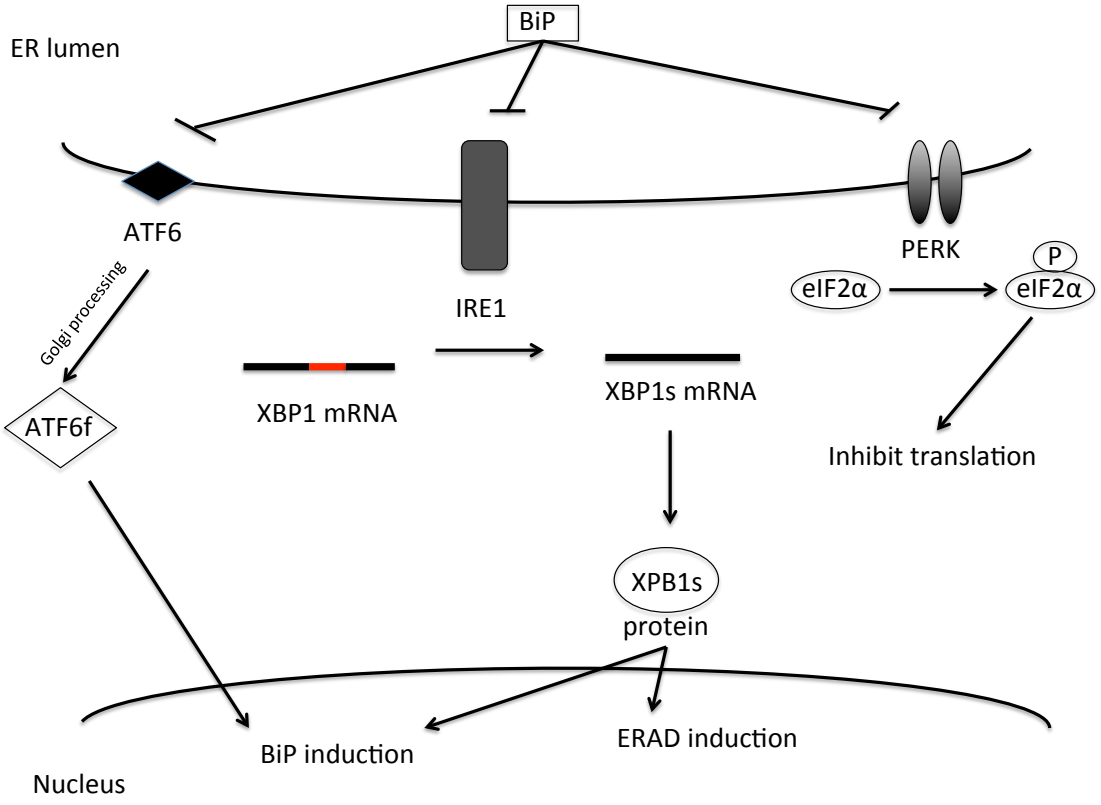
ER lumen
BiP
ATF6
IRE1
PERK
P
eIF2α
eIF2α
Golgi processing
ATF6f
XBP1 mRNA
XBP1s mRNA
Inhibit translation
XPB1s
protein
BiP induction
ERAD induction
Nucleus

enhance BiP expression (Yoshida et al., 1998; Yamamoto et al., 2004). Duplicate copies of mammalian ERSE (CCAAT-N9-CCACG) fused to a chloramphenicol transferase (CAT) coding sequence were required for stress-induced expression in HeLa cells treated with tunicamycin, an N-linked glycosylation inhibitor (Yoshida et al., 1998; Roy & Lee, 1999).

1.5 Small heat shock proteins

Small HSPs (sHSPs) have been reported in a range of organisms that include bacteria, plants, insects, tardigrades, nematodes, crustaceans, amphibians, and mammals (Allen et al., 1992; Linder et al., 1996; Wotton et al., 1996; Ohan et al., 1998; Sun et al., 2002; Sun & MacRae, 2005; Morrow et al., 2006; Schokraie et al., 2011). Amino acid sequences of sHSP families, such as Hsp27, are well conserved within a species but are more divergent across species (de Jong et al., 1998; Stromer et al., 2003). In response to proteotoxic stress, sHSPs interact efficiently with a wide range of partially unfolded protein substrates including enzymes and cytoskeletal proteins (Lentze & Narberhaus, 2004; Sudnitsyna et al., 2012).

In addition to inhibiting the cell from the accumulation of aggregated protein, sHSPs were reported to have roles in cellular differentiation, apoptosis, proliferation and the modulation of the redox state (Mounier & Arrigo, 2002; Arrigo, 2007; Heikkila, 2010; Sudnitsyna et al., 2012). Moreover, expression of sHSPs in unstressed cells decreased the basal level of intracellular reactive oxygen species (ROS) in addition to reducing the ROS generative by oxidative stress (Arrigo, 2007). Glutathione seems to play a major role in the ability of sHSPs to modulate a cell's redox state (Mehlen et al., 1996). Furthermore, a *X. laevis* sHSP, HSP30, was associated with aggresome-like inclusion bodies in A6 cells treated with cadmium chloride, sodium arsenite or proteosomal inhibitor (Khan et al., 2015). As will be described in Section 8.0,

an aggresome is a membrane-free pericentriolar inclusion body containing misfolded and ubiquitinated protein surrounded by a vimentin cage (Johnston et al., 1998).

1.6 Heme oxygenase-1

Heme-oxygenase 1 (HO-1), also known as heat shock protein 32 (HSP32), is a stress-inducible enzyme that catalyzes the degradation of heme into biliverdin, free iron and carbon monoxide (Paine et al., 2010). Biliverdin reductase subsequently catalyzes the conversion of biliverdin to bilirubin, a potent antioxidant (Paine et al., 2010). Stress-induced HO-1 accumulation was reported to increase cell survival by inhibiting apoptosis and reducing oxidative stress (Kapitinulk & Maine, 2010). HO-1 is controlled mainly at the transcriptional level (Ryter et al, 2006). Nuclear factor erythroid-2-related factor-2 (NRF2) is the principal regulator of HO-1 gene expression (Alam & Cook, 2007; Macleod et al, 2009). Under normal conditions, NRF2 is ubiquitinated by Cullin 3-ring box 1 (Cul3-RBX1) and is readily degraded by the proteasome (Kobayashi et al, 2004). A substrate adaptor for NRF2 ubiquitination known as kelch-like erythroid-derived cap-n-collar-homology associated protein 1 (KEAP-1) is modified by redox-dependent stimuli at two cysteine residues, which permits NRF2 to avoid degradation and accumulate in the nucleus (Zhang & Hannink, 2003; Kobayashi et al., 2004; Macleod et al., 2009). NRF2 forms a heterodimer with musculaponeurotic fibrosarcoma (MAF) proteins, which activates HO-1 gene expression by binding to Maf recognition elements (MARE; Nioi et al., 2003; Li et al., 2008). Heavy metals and proteasome inhibitors were found to induce the expression of HO-1 genes in mammals by NRF2 translocation induced by p38 mitogen-activated protein kinase (p38 MAPK; Alam et al., 2000; Wen-Tung et al., 2004; Yamamoto, 2010). HO-1 induction by cadmium or MG132 has also been reported to involve NRF2 binding

to MARE in mammalian studies (Alam et al., 2000; Cai, 2013). In addition, mammalian cells treated with an inhibitor of glutathione synthesis, buthionine sulfoximine (BSO), showed an increase in HO-1 mRNA and protein accumulation (Saunder et al., 1991; Ewing & Maines, 1993; Li et al., 2013).

In *Xenopus laevis*, HO-1 was suggested as having important roles in development, since it was detected in neural crest lineages, pronephron cells and pronephric tubule cells (Shi et al., 2008). As will be mentioned later, our laboratory has characterized HO-1 accumulation under heavy metal stress and proteasome inhibition in *Xenopus laevis* A6 kidney epithelial cells (Music et al., 2014).

1.7 Ubiquitin-Proteasome System

Cells are able to degrade proteins and maintain protein homeostasis through the ubiquitin-proteosome system (UPS). The UPS is a non-lysosomal proteolytic pathway that occurs in two general steps. First, a damaged or misfolded protein is targeted for degradation by the attachment of multiple ubiquitin molecules (Ciechanover, 1994). Secondly, the ubiquitinated protein is brought to the 26S protease complex for degradation (Ciechanover, 1994). The 26S protease complex consists of a 19S regulator and a 20S proteolytic core. The 19S regulator identifies ubiquitinated proteins and transfers them to the 20S proteolytic core for degradation (Figure 3; Lee & Goldberg, 1998; Demartino & Gillette, 2007).

Proteins are targeted for degradation by the attachment of ubiquitin proteins to lysine residues on the targeted protein. Three sets of enzymes coordinate the attachment of ubiquitin, ubiquitin-activating enzymes (E1), ubiquitin-conjugating enzymes (E2) and ubiquitin ligases (E3; Ravid & Hochstrasser, 2008). E1 hydrolyzes ATP and adenylylates ubiquitin, which is then

transferred to E1's active-site in concert with the adenylylation of a second ubiquitin (Ravid &

Figure 3. Ubiquitin-proteasome system. A) Multiple ubiquitin molecules are added to unfolded/misfolded protein by ubiquitin-conjugating enzymes. The targetted protein is then cleaved into smaller peptides by the 26S Proteasome complex. B) Structure of the 26S Proteasome complex containing the 19S regulator subunits and the 20S proteolytic core composed of 2 alpha and 2 beta rings (Image adapted from Lee & Goldberg, 1998).

A

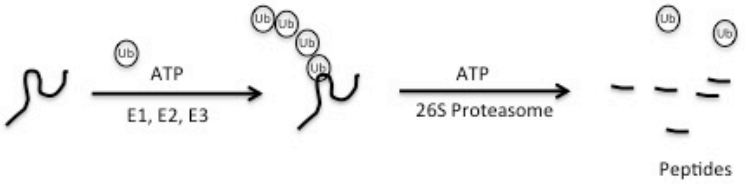
Ub
ATP
E1, E2, E3
Ub
Ub
Ub
Ub
ATP
26S Proteasome
Ub
Ub
Peptides

B

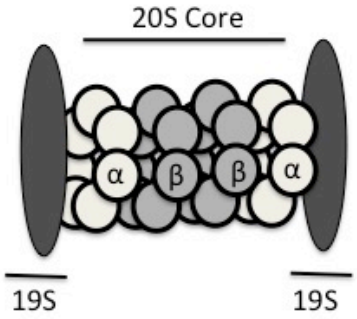
20S Core
α
β
β
α
19S
19S

Hochstrasser, 2008). Adenylated ubiquitin is then transferred to E2. E3 recognizes the protein for ubiquitination and catalyzes the transfer of ubiquitin from E2 to the lysine residue of the targeted protein (Ardley & Robinson, 2005; Ravid & Hochstrasser, 2008). E3 enzymes are capable of polyubiquination, where several ubiquitin proteins are attached to targeted proteins (Thrower et al., 2000). Polyubiquitination is a proteolytic signal for the 26S proteasome (Thrower et al. 2000, Ardley & Robinson, 2005).

The UPS plays a role for cellular processes such as cellular differentiation, cell cycle progression, proliferation and apoptosis (Landis-Piwowar et al., 2006). The inhibition of the proteasome can result in the increased accumulation of ubiquitinated protein, which has been documented in *Xenopus* A6 cells treated with MG132, withaferin A, celastrol, cadmium chloride or sodium arsenite (Walcott & Heikkila, 2010; Brunt et al., 2012; Khan et al., 2012).

1.8 Aggresomes and ERACs

When the UPS is inhibited or overwhelmed, eukaryotic cells form organized structures called aggresomes. Aggresomes are membrane-free pericentriolar inclusion bodies that contain ubiquitinated and misfolded proteins that are surrounded by a vimentin cage (a type III intermediate filament; Johnston et al., 1998). Aggregated protein is brought to the aggresome by dynein-dependent retrograde transportation on microtubules (Figure 4; Kopito, 2000; Corchero, 2016). The transportation of aggregated protein is facilitated by the protein deacetylase, HDAC6 (Kawaguchi et al., 2003). It was found that inhibition of microtubule polymerization prevented aggresome formation by preventing the retrograde transportation of unfolded protein, which led to an increase in cytotoxic misfolded protein throughout the cytoplasm (Kopito, 2000;

Figure 4. Schematic of aggresome formation. Misfolded protein is brought to the pericentriolar region by dynein-dependent transportation on microtubules. The misfolded protein accumulating next to the nucleus (red) is wrapped in a vimentin cage (green). Image adapted from Corchero, 2016.

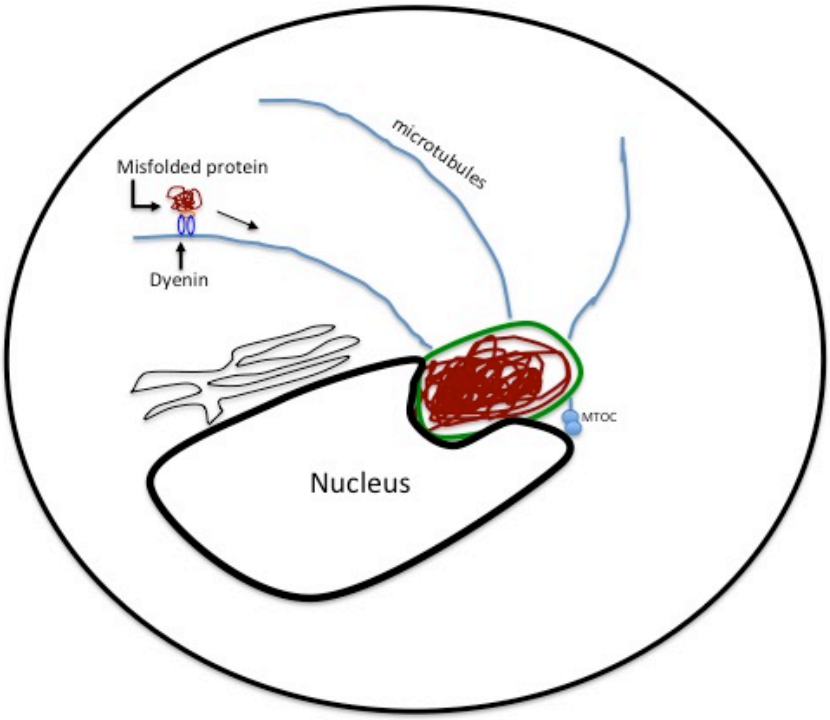
microtubules
Misfolded protein
Dyenin
MTOC
Nucleus

Kawaguchi et al., 2003). Inhibiting the proteasome with MG132 was found to induce aggresome formation in human embryonic kidney, HeLa, neuroblastoma and breast epithelial cells (Zaarur et al., 2008; Ouyang et al., 2012; Taylor et al., 2012; Salemi et al., 2014). In addition, sodium arsenite and cadmium chloride induced aggresome formation in yeast and human embryonic kidney cells (Heir et al., 2006; Song et al., 2008; Jacobsen et al., 2012).

HSP70 has been reported to promote aggresome formation through interaction with ubiquitin ligase carboxyl terminal of HSP70/HSP90 interacting protein (CHIP) and B cell lymphoma-2 associated anthonogene 3 (BAG3; Gamerdinger et al., 2011; Zhang & Qian, 2011). Abrogating the interaction between HSP70 and CHIP or B-cell lymphoma 2-associated athonogene-3 (BAG3) prevented aggresome formation (Gamerdinger et al., 2011; Zhang & Qian, 2011). Previous studies with mammalian cells treated with the proteosomal inhibitor, MG132, reported the co-localization of HSP27, alphaB-crystallin, and BiP with aggresomes (Bauer & Richter-Landsberg, 2006; Goldbaum et al., 2009; Bolhuis & Richter-Landsberg, 2010; Ito et al., 2012; Sabatelli et al., 2014; Malek et al., 2015). Furthermore, Ardley et al. (2004) observed co-localization of BiP with mutant ubiquitin carboxy-terminal hydrolase-1 (UCH-1), a mutant protein that is involved in aggresome formation, within inclusions formed in monkey kidney cells overexpressing UCH-1. Recently, the treatment of *Xenopus* A6 cells with MG132, cadmium chloride or sodium arsenite induced the presence of HSP30 associated aggresome-like inclusion bodies as determined by means of a Proteostat aggresome dye and co-localization of immunocytochemical markers, gamma-tubulin and vimentin (Khan et al., 2015).

Other organized inclusion body structures have been reported. A study examining mutant proteins that accumulate and misfold in the ER of yeast reported inclusion bodies associated with the ER, named ER-associated compartments (ERACs; Huyer et al., 2004). Electron microscopy

suggested ERACS were comprised of tubular-vesicles directly connected to the ER (Huyer et al., 2004). ERACs localized next to the nucleus and associated with ER lumenal and membrane proteins in addition to BiP, as determined by co-localization studies (Huyer et al., 2004; Bagola & Sommer, 2008). ERACs and aggresomes share similar features such as localization next to the nucleus, presence of ubiquitinated proteins and association with molecular chaperones. It remains to be determined whether these inclusion bodies are related or serve distinct functions (Bagola & Sommer, 2008).

1.9 Cadmium

Cadmium is an environmental pollutant produced mainly by non-ferrous metal production and combustion of fossil fuels (Cullen & Maldonado, 2013). Chronic exposure to cadmium has been associated with numerous human health problems such as lung cancer, Alzheimer's disease, and kidney dysfunction (WHO, 2008; Nordberg, 2009). The kidney is the principal organ that is negatively affected by long-term cadmium exposure (Groten et al., 1991; Nordberg, 2009). Circulating cadmium in the glomerulus followed by proximal tubular uptake and transport to distal nephron segments is a general mechanism to explain cadmium-induced nephrotoxicity that has been reported in both proximal and distal tubular epithelial cells (Friedman & Gesek, 1994; Faurskov & Bjerregaard, 2002).

Cadmium enters the cell mainly through metal transporters such as zinc-regulated transporter, iron-regulated transporter related protein 8 (ZIP8), ZIP14 and divalent metal ion transporter 1 (DMT1; Fujisharo et al., 2012). Once inside the cell, cadmium was determined to have effects on cell cycle progression, differentiation, apoptosis, DNA replication/repair and gene expression (Bertin & Averbeck, 2006). Cadmium interferes with proteins containing thiol

groups or zinc finger domains, which cause an increase in the intracellular level of denatured/abnormal protein (Waisberg et al., 2003). These conditions can activate the heat shock response resulting in the accumulation of HSPs.

Cadmium is highly soluble in water and is present in many aquatic environments (Kumar & Singh, 2010). In amphibians and fish, cadmium can enter through passive diffusion or carrier transport through the gills (Kumar & Singh, 2010). Acute or chronic cadmium exposure to adult amphibians, such as *Rana temporaria* or *Xenopus laevis*, resulted in the accumulation of cadmium in organs such as the liver, kidney, gonads and skin (Vasil'eva et al., 1987; Vogiatzis and Loumbourdis, 1997; Fort et al., 2001; Loumbourdis & Vogiatzis, 2002; Othman et al., 2009; Simoncelli et al., 2015). Several studies have examined the effect of cadmium cellular toxicity in *Xenopus laevis* A6 kidney epithelial cells (Faurskov & Bjerregaard, 2002; Bjerregaard, 2007; Woolfson & Heikkila, 2009; Brunt et al., 2012; Music et al., 2014). The *Xenopus* A6 cell line was reported to produce a transient spike in cytosolic calcium in a dose-dependent relationship with cadmium treatments (Faurskov & Bjerregaard, 2002). Our laboratory has previously characterized cadmium chloride-induced accumulation of HSP30 and HSP70 proteins in *Xenopus laevis* A6 kidney epithelial cells (Woolfson & Heikkila, 2009; Brunt et al., 2012; Khamis & Heikkila, 2013; Music et al., 2014).

Another mechanism associated with cadmium cytotoxicity is its ability to induce an imbalance in the cellular redox state. Cadmium was shown to decrease the availability of antioxidants such as glutathione (GSH) while concurrently increasing reactive oxygen species produced by the mitochondria (Waisberg et al., 2003; Bertin & Averbeck, 2006). GSH is a low molecular weight thiol that exists in high concentrations (0.1 to 10 mM) within animal cells (Schafer & Buetner, 2001; Mah & Jalilehvand, 2010). GSH can directly scavenge ROS (eg.

hydrogen peroxide, hydroxyl radical, lipid peroxyl radical, etc.) by serving as an electron donor (Schafer & Buetner, 2001; Pompella et al., 2003). These redox reactions convert GSH to its oxidized form, glutathione disulfide (GSSG; Schafer & Buetner, 2001). The ratio between reduced and oxidized GSH is often a measure of the redox state of a cell and can be indicative of certain age-related diseases, such as Alzheimer's and Parkinson's (Schafer & Buetner, 2001; Pocernich & Butterfield, 2010; Carroll et al., 2016; Bratt et al., 2016). In addition to scavenging ROS, GSH can form a complex with cadmium, which is thought to be an initial step in cellular detoxification of cadmium exposure (Fauchon et al., 2002; Mah & Jalilehvand, 2010). Treatment of cells with buthionine sulfoxomine (BSO), an inhibitor of γ-glutamylcysteine synthetase, which is involved in glutathione synthesis, has been shown to lower intracellular levels of GSH (Griffith, 1982; Galan et al., 2001; Schafer & Buetner, 2001). Glutathione depletion by BSO pretreatment was found to enhance alpha-crystallin, HSP27 and HSP70 accumulation in rat glioma cells treated with sodium arsenite (Ito et al., 1998). Furthermore, human promonocytic cells and amniotic cells pretreated with BSO and a low concentration of cadmium resulted in enhanced HSP70 expression, suggesting glutathione depletion resulted in an increase in cadmium-sensitivity (Abe et al., 1994; Galan et al., 2001).

Cadmium-induced oxidative stress has also been reported to impede the ubiquitination of NRF2, enabling transcription of the heme oxygenase-1 (*ho-1*) gene (Alam et al., 2000). Cadmium-induced HO-1 accumulation has been characterized in a variety of cell types, including mammalian and *Xenopus laevis* A6 cells (Masuya et al., 1998; Alam et al., 2000; Miyamoto et al., 2009; Music et al., 2014). Cadmium was also reported to impair the UPS in both mammalian and *Xenopus* model systems, which resulted in the formation of aggresomes (Li et al., 2008; Song et al., 2008; Yu et al., 2011; Brunt et al., 2012; Khan et al., 2015).

1.10. *Xenopus laevis* A6 kidney epithelial cells as a model system

Xenopus laevis is an aquatic African clawed frog that has been extensively used in the study of vertebrate embryology and development, cell biology, neurobiology and toxicology. Our basic knowledge about transcriptional and translational processes in eukaryotes has been greatly aided by work with *Xenopus* (Wheeler & Brandi, 2009; Heikkila, 2010). Furthermore, the findings obtained are generally applicable to human. In 1968, Rafferty isolated several cell lines from *Xenopus laevis,* one of which was the A6 cell line from the renal proximal tubules of adult male *Xenopus laevis* (Rafferty, 1968). A6 cells are well-characterized, hardy, fast growing and ideal for immunocytochemistry (Rafferty, 1975; Heikkila, 2010). A variety of research studies in molecular biology and cell physiology have used A6 cells, which includes the examination of the toxicity of copper oxide nanoparticles, optimization of gene delivery methods, characterizing the type I interferon response, analyzing the function of peroxisomes and studying the regulation of sodium channels (Ramirez-Gordillo et al., 2011; Grayfer et al., 2014; Fox et al., 2014; Thilt et al., 2015; Wang et al., 2015). For instance, the knockdown of peroxisomal biogenesis factor 11 β (PEX11β) by morpholino was reported to reduce the number of peroxisomes and the accumulation of proteins associated with peroxisome formation (Fox et al., 2014). They have also been extensively used to characterize stress-inducible and constitutive expression of *hsp* gene expression (Heikkila, 2010).

1.11. Research objectives

The toxicity of cadmium is a concern for human and animal health near cadmium-emitting industry (Mason et al., 2000; Audry et al., 2004; Arnason et al., 2003; Brumbaugh et al., 2005;

WHO, 2008; Nordberg, 2009). Since cadmium contamination can be found in freshwater habitats, amphibians may be susceptible to its deleterious effects (Waisberg, 2003). The effect of cadmium on the expression and function of amphibian stress protein genes may contribute to an improved understanding of the cellular effects of this toxicant. The present study will examine the effect of cadmium on BiP gene expression in *Xenopus laevis* A6 kidney epithelial cells.

The following is the list of the primary objectives for my Master's thesis research using the *Xenopus laevis* A6 kidney epithelial cell line:

1) To examine the effect of cadmium chloride on the relative levels of BiP by immunoblot and immunocytochemistry.

2) To examine the possible association of aggregated protein with large perinuclear BiP structures in cadmium chloride-treated cells using immunocytochemistry.

3) To examine the effect of buthionine sulfoximine, a glutathione synthesis inhibitor, on the relative levels of cadmium chloride-induced BiP accumulation and induction of putative BiP/aggregated protein complexes.

4) To examine the effect of an elevated temperature of 30 ^{o}C on cadmium chloride-induced BiP accumulation and the formation of putative BiP/aggregated protein complexes.

2.0 Materials and Methods

2.1 Amino acid sequence alignment and phylogenetic analysis

The *X. laevis* BiP amino acid sequence (Genbank accession no. AAB41582.1) was derived from *bip* cDNA that was originally isolated by Miskovic et al. (1997). A pairwise sequence alignment was performed between *X. laevis* BiP and *H. sapiens* BiP using the EMBOSS needle program with a BLOSUM90 matrix using the default parameters. Furthermore, the *X. laevis* BiP amino acid sequence was aligned with BiP from *H. sapiens*, *R. norvegicus, P. bivattatus, A. carolinensis, G. gallus, H. leucocephalus, F. heteroclitus, P. mexicana* using the sequence alignment program of Clustal Omega (Version O.2.1; Sievers et al., 2011). For phylogenetic analysis, representative BiP and BiP amino acid sequences obtained from amphibians, reptiles, mammals and fish were aligned using ClustalW. A neighbour-joining tree was generated in MEGA 7.0.14 based on the neighbor-joining method created by Saitou & Nei (1987). A maximum-likelihood tree was constructed using a Jones-Taylor-Thornton model with MEGA 7.0.14 (Jones et al., 1992; Kumar et al., 2016). The tree was rooted with *C. elegans* HSC70. The reliability of the tree was estimated by bootstrapping with 1000 replicates.

The upstream regulatory region of *X. laevis* (J-strain, V9.1) and *X. tropicalis bip* genes were obtained from Xenbase (http://www.xenbase.org/, RRID:SCR_003280; Karpink at al., 2015). The upstream regulatory region for *H. sapiens* was obtained from NCBI (Genbank accession no. X59969). A multiple sequence alignment was performed using the Clustal Omega program version 1.2.2 provided by the European Molecular Biology Laboratory - European Bioinformatics Institute (EMBL-EBI; McWilliam et al., 2013).

Maintenance and treatment of *Xenopus laevis* A6 kidney epithelial cells

Xenopus laevis A6 kidney epithelial cells (CCL-102) were purchased from American Type Culture Collection (Rockville, MD, USA) and grown at 22 °C in T-75 cm^2 BD Falcon tissue culture flasks (VWR, Mississauga, ON) as described previously (Khamis et al., 2013; Khan and Heikkila, 2014). Briefly, cells were maintained with 70% Leibovitz (L)-15 media supplemented with 10% (v/v) fetal bovine serum (FBS) and 100 U/mL penicillin and 100 μg/mL streptomycin (all from Sigma-Aldrich, Oakville, ON, Canada). When cells reached confluency, they were washed with 1 mL versene [0.02% (w/v) KCl, 0.8% (w/v) NaCl, 0.02% KH_2PO_4, 0.115% (w/v) $NaHPO_4$, 0.02% (w/v) Na_2EDTA], followed by 2 mL of versene. The cells were then treated with 1 mL of 1x trypsin (Sigma-Aldrich) in Hank's balance salt Solution (HBSS) for 1 min before resuspending cells in new flasks with fresh media. When cells reached 90% confluency, treatments were administered. A6 cells were treated with 25, 50, 100, 200 or 400 μM cadmium chloride (Sigma-Aldrich) prepared from a 100 mM stock solution made with sterile water. In cadmium chloride time course experiments, cells were exposed to 200 μM cadmium chloride for 4, 8, 12, 16 or 24 h. In recovery experiments, cells were treated with 200 μM cadmium chloride for 8 h followed by 3 rinses with Hank's balanced salt solution before adding fresh media. MG132 (carbobenzoxy-L-leucyl-L-leucinal; Sigma-Aldrich) was dissolved in dimethylsulphoxide (DMSO; Sigma-Aldrich) and kept in 5 mg/mL stock solutions before treatment of cells with 30 μM MG132. In some experiments, flasks were incubated at 30 °C in a water bath for 5 h in the absence or presence of 100 μM cadmium chloride. In actinomycin D (Sigma-Aldrich) experiments, cells were pretreated for 30 min before washing three times with HBSS and adding media with or without cadmium chloride. In cycloheximide (Sigma-Aldrich) experiments, cells were pretreated with 100 μM cycloheximide for 6 h before washing three times with HBSS and adding media with or without cadmium chloride. Tunicamycin (Sigma-

Aldrich) in DMSO at 50 mM was given to cells at 2 μg/mL. A23187 (Sigma-Aldrich) in DMSO at 2 mM was given to cells at 7 μM. In experiments employing the glutathione depleting agent, DL-buthionine sulfoximine (BSO; Sigma-Aldrich), a 215 mM stock solution of was freshly prepared before each treatment by dissolving it in sterile water. Cells were treated with 10 mM BSO for 4 h before cadmium chloride treatment. The concentration of BSO employed was previously used to reduce glutathione level in *X. laevis* oocytes (Kannan et al., 1996, Kannan et al., 1998). At the end of the various treatments, A6 cells were harvested and stored at -80 °C.

Protein isolation and quantification

Total protein isolation from A6 cells was performed as described by Young et al. (2009). Briefly, cells were lysed with 300 μL of lysis buffer containing homogenization buffer (200 mM sucrose, 2 mM EGTA, 1 mM EDTA, 40 mM NaCl, 30 mM HEPES, pH 7.4), 1% (v/v) protease inhibitor cocktail (Promega, Madison, WI) and 1% (v/v) SDS. The cells were then sonicated on ice using a Fisher Scientific Model 100 (Waltham, MA, USA) with an output of 10 mW. Cell debris was removed from soluble protein by centrifugation at 14,000 rpm for 1 h at 4°C. The bicinchonic acid (BCA) protein assay was used to determine protein concentration as per the manufacturer's instructions (Pierce, Rockford, IL). Bovine serum albumin (BSA) was used as a protein standard by diluting it in ultrapure Milli-Q water to concentrations ranging from 0 to 2 mg/mL. Protein samples were diluted 1:2 in ultrapure Milli-Q water. BSA standards and protein samples in 10 μL volumes were loaded into a 96-well polystyrene plate in triplicate. Eighty μL of BCA reagent A and B (Pierce) was added to each standard and protein samples and the plate was incubated at 37 °C for 30 min. The plate was read at 562 nm using a Versameax Tunable microplate reader (Molecular Devices, Sunnyvale, CA, USA) and Softmax Pro software. The

BSA protein standards were used to generate a standard curve, which was used to determine the concentration of the protein samples.

Immunoblot analysis

Twenty μg of protein was loaded onto 12% sodium dodecyl sulphate polyacrylamide gel electrophoresis (SDS-PAGE) gels. Separating gels [12% (w/v) acrylamide, 0.32% (v/v) n'n'-bismethylene acrylamide, 0.375 M Tris pH 8.8, 1% (w/v) SDS, 0.2% (w/v) ammonium persulfate (APS), 0.14% (v/v) tetramethylenediamine (TEMED)] were prepared and allowed to polymerize for 25 min after 100% ethanol was layered on top of the gel. After the separating gel solidified, the ethanol was removed and the stacking gel [4% (v/v) acrylamide, 0.11% (v/v) n'n'-bismethylene acrylamide, 0.125 M Tris pH 6.8, 1% (w/v) SDS, 0.4% (w/v) APS, 0.21% TEMED] was added, followed by the insertion of combs to create lanes in each stacking gel and then allowed to polymerize. Protein samples (20 μg) were added to loading buffer [0.0625 M Tris pH 6.8, 10% (v/v) glycerol, 2% (w/v) SDS, 5% (v/v) β- mercaptoethanol, 0.00125% (w/v) bromophenol blue]. Samples were then boiled for 10 min, briefly cooled and loaded onto the SDS-PAGE gel. SDS-PAGE gels were electrophoresed using a BioRad Mini Protean III gel system (BioRad, Mississauga, ON) in 1x running buffer [25 mM Tris, 0.2 M glycine, 1 mM SDS] at 90 V until samples reached the separating gel at which point the voltage was increased to 160 V. Once electrophoresis was completed, the stacking gel was removed and the separating gel was soaked in transfer buffer [25 mM Tris, 192 mM glycine, 10% (v/v) methanol] for 15 min. Protein was transferred onto a nitrocellulose membrane, which had been soaked in transfer buffer for 30 min, using a BioRad Semi-Dry Transfer cell at 20 volts for 25 min. The nitrocellulose membrane was then incubated in Ponceau S stain [0.19% (w/v) Ponceau-S, 5% (v/v) acetic acid] for 10 min to determine protein transfer efficiency. The blots were rinsed with

distilled water and then blocked for 1 h in blocking solution containing 5% skim milk (Carnation, Markham, ON), Tris-buffered saline solution [20 mM Tris, 300 mM NaCl, pH 7.5], and 0.1% Tween-20 (Sigma-Aldrich). Immunodetection involved the incubation of the membranes with either polyclonal rabbit anti-human BiP antibody (1:500; Sigma-Aldrich; catalog no. G9043), polyclonal rabbit anti-human HO-1 antibody (1:500; Enzo Life Sciences, Farminghale, NY), polyclonal rabbit anti-*Xenopus* HSP70 (1:350; Gauley et al., 2008; Abgent, San Diego, CA, USA) or polyclonal rabbit anti-actin (1:200; Sigma-Aldrich). The immunogen to produce the anti-BiP antibody was from a synthetic human BiP protein (amino acids 71-91), which sequence is identical to the comparable site in *X. laevis* BiP. The membranes were washed three times with Tris-buffered saline solution with 0.1% Tween-20 (TBS-T) and then incubated with alkaline phosphatase conjugated goat anti-rabbit antibody (1:2000; BioRad) in blocking solution for 1 h. The membranes were then washed three times with TBS-T before incubating in detection solution [100 mM Tris pH 9.5, 100 mM NaCl, 50 mM $MgCl_2$, 0.3% nitro blue tetrazoleum; Roche, Ayr, ON] and 0.17% 5-bromo-4-chloro-3-idolyl phosphate toluidine salt (Roche) until bands were visible.

Densitometry

Densitometric analyses of the immunoblots in the range of linearity were performed using Image J software (Version 1.49; National Institute of Health), as previously performed by our laboratory (Khamis & Heikkila, 2013; Music et al., 2014; Khan et al., 2015). Band intensities for BiP, HSP70 and HO-1 were expressed as a percent of the maximum value for each sample. Standard error of the mean was included as error bars. Significance ($p<0.05\%$) between control and treatment intensity was determined using one-way ANOVA and Tukey's post-hoc test.

Immunocytochemical analysis and laser scanning confocal microscopy (LSCM)

Immunofluroescence analysis was carried out as previously described by our laboratory (Manwell & Heikkila, 2007; Khan et al., 2015). Cells were grown on base-washed glass coverslips that were flame-sterilized. Treatments were administered as previously mentioned. At the end of the treatment, coverslips were washed with phosphate buffered saline with magnesium and calcium (PBS; 1.37 M NaCl, 67 mM Na_2HPO_4, 26 mM KCl, 14.7 mM H_2PO_4, 1mM $CaCl_2$, 0.5 mM $MgCl_2$, pH 7.4) twice for 2 min. Cells were fixed by adding 3.7% paraformaldehyde in PBS to the coverslips for 15 min. Coverslips were washed three times for 5 min with PBS before permeabilizing with 0.3% Triton X-100 (TX-100; Sigma-Aldrich) in PBS for 10 min. Coverslips were then washed with PBS three times for 2 min before 3.7% bovine serum albumin (BSA) in PBS was added for 1 h or overnight incubation at 4°C. They were then incubated with rabbit anti-BiP antibody (1:500; Sigma-Aldrich; catalog number: G9043) in 3% BSA for 1 h. This was followed by 3 washes of PBS. Addition of secondary antibodies included using anti-rabbit Alexa Fluor 488 (1:2000; Invitrogen Molecular Probes, Carlsbad, CA). To visualize the actin cytoskeleton, the cells were incubated with rhodamine tetramethylrhodamine-5-isothiocyanate phalloidin (TRITC; Invitrogen Molecular Probes) for 15 min at 1:100 in 3.7% BSA in the dark. The Proteostat aggresome detection kit (Enzo Life Sciences, Plymouth Meeting, PA) was used as per the manufacturer's instructions. The coverslips were dried and mounted on glass slides with Vectashield mounting medium containing 4,6-diamindino-2-phenylindole (DAPI; Vector Laboratories Inc., Burlingame, CA) to stain nuclei. Nail polish was used to permanently attach coverslips to slides. The slides were then examined with a Zeiss 510 laser scanning confocal microscope mounted on axiovert 200 and ZEN 2009 software (Carl Zeiss Canada Ltd., Mississauga, ON).

3.0 Results

3.1 Sequence analysis of *X. laevis* BiP

Previously, our laboratory isolated an *X. laevis bip* cDNA (Genbank accession no. U55069.1) and analyzed the nucleotide and amino acid sequence (Miskovic et al., 1997). However, at that time there was a limited amount of *bip* gene sequence information available in Genbank. Thus, I have reassessed the *X. laevis* BiP amino acid sequence in light of available *bip* gene sequences from numerous other organisms and *X. laevis bip* gene regulatory sequences accessible as a result of the *X. laevis* genome sequencing project. A pairwise sequence alignment generated with a BLOSUM90 matrix suggested that *X. laevis* BiP (Genbank accession no. AAB41582.1) shared high amino acid sequence identity with *Homo sapiens* BiP (Genbank accession no. NP_005338.1) at key regions, such as the nucleotide-binding domain, a substrate-binding interface and a KDEL retention sequence (Fig. 5). However, the N-terminal ER signaling sequences did not share a high degree of identity.

In the present study, amino acid sequence comparison analysis using the Genbank blastp software revealed that *X. laevis* BiP shared 98% sequence identity with *X. tropicalis* BiP (Table 1). In addition, *X. laevis* BiP shared high amino acid sequence identity with BiP orthologs in reptiles (e.g. *Python bivattatus* [91%], *Anolis carolinensis* [90%]), mammals (e.g. *Homo sapiens* [93%], *Rattus norvegicus* [93%]), birds [*Gallus gallus* [93%], *Haliaeetus leucocephalus* [93%]), and fish (e.g. *Fundulus heteroclitus* [93%], *Poeciliopsis mexicana* [91%]). Finally, *X. laevis* BiP shared less amino acid sequence identity with *X. laevis* HSP70 family members including HSP70 (63%) and HSC70 (62%) than with BiP orthologs from other classes of vertebrates. A phylogenetic tree generated in MEGA 7.0

Figure 5. Pairwise sequence alignment of *X. laevis* and *H. sapiens* BiP. The amino acid sequences of *X. laevis* (Genbank accession no. AAB41582.1) and *H. sapiens* BiP (Genbank accession no. NP_005338.1) were aligned using the EMBOSS needle program with a BLOSUM90 matrix using the following parameters: gap open penalty = 10, gap open extend penalty = 0.5, end gap penalty = false, open gap penalty = 10 and the end gap penalty extend = 10. Colons represent conservative amino acid substitutions and periods represent semi-conservative substitutions. Deletions are indicated by dashes in the amino acid sequence. The various protein domains and key sequences were based on annotations available for *H. sapiens* BiP (accession No. NP_005338.1). The ER-directing signal sequence and the KDEL retention sequence are indicated. Black lines shown above and below the two BiP sequences indicate the predicted substrate-binding interface. The nucleotide-binding domain is highlighted in gray.

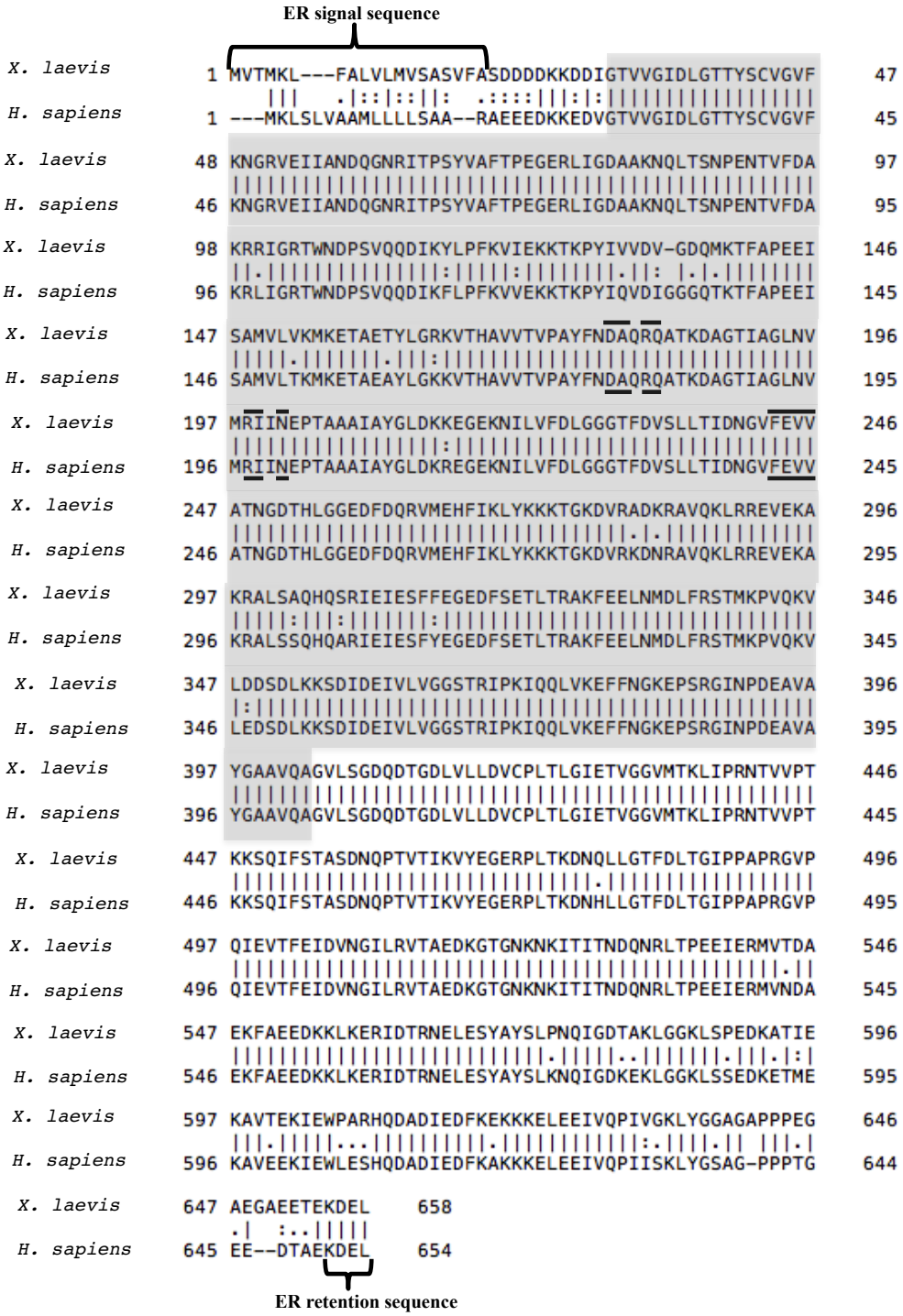
ER signal sequence
X. laevis 1 MVTMKL---FALVLMVSASVFASDDDDKKDDIGTVVGIDLGTTYSCVGVF 47
H. sapiens 1 ---MKLSLVAAMLLLLSAA--RAEEEDKKEDVGTVVGIDLGTTYSCVGVF 45
X. laevis 48 KNGRVEIIANDQGNRITPSYVAFTPEGERLIGDAAKNQLTSNPENTVFDA 97
H. sapiens 46 KNGRVEIIANDQGNRITPSYVAFTPEGERLIGDAAKNQLTSNPENTVFDA 95
X. laevis 98 KRRIGRTWNDPSVQQDIKYLPFKVIEKKTKPYIVVDV-GDQMKTFAPEEI 146
H. sapiens 96 KRLIGRTWNDPSVQQDIKFLPFKVVEKKTKPYIQVDIGGGQTKTFAPEEI 145
X. laevis 147 SAMVLVKMKETAETYLGRKVTHAVVTVPAYFNDAQRQATKDAGTIAGLNV 196
H. sapiens 146 SAMVLTKMKETAEAYLGKKVTHAVVTVPAYFNDAQRQATKDAGTIAGLNV 195
X. laevis 197 MRIINEPTAAAIAYGLDKKEGEKNILVFDLGGGTFDVSLLTIDNGVFEVV 246
H. sapiens 196 MRIINEPTAAAIAYGLDKREGEKNILVFDLGGGTFDVSLLTIDNGVFEVV 245
X. laevis 247 ATNGDTHLGGEDFDQRVMEHFIKLYKKKTGKDVRADKRAVQKLRREVEKA 296
H. sapiens 246 ATNGDTHLGGEDFDQRVMEHFIKLYKKKTGKDVRKDNRAVQKLRREVEKA 295
X. laevis 297 KRALSAQHQSRIEIESFFEGEDFSETLTRAKFEELNMDLFRSTMKPVQKV 346
H. sapiens 296 KRALSSQHQARIEIESFYEGEDFSETLTRAKFEELNMDLFRSTMKPVQKV 345
X. laevis 347 LDDSDLKKSDIDEIVLVGGSTRIPKIQQLVKEFFNGKEPSRGINPDEAVA 396
H. sapiens 346 LEDSDLKKSDIDEIVLVGGSTRIPKIQQLVKEFFNGKEPSRGINPDEAVA 395
X. laevis 397 YGAAVQAGVLSGDQDTGDLVLLDVCPLTLGIETVGGVMTKLIPRNTVVPT 446
H. sapiens 396 YGAAVQAGVLSGDQDTGDLVLLDVCPLTLGIETVGGVMTKLIPRNTVVPT 445
X. laevis 447 KKSQIFSTASDNQPTVTIKVYEGERPLTKDNQLLGTFDLTGIPPAPRGVP 496
H. sapiens 446 KKSQIFSTASDNQPTVTIKVYEGERPLTKDNHLLGTFDLTGIPPAPRGVP 495
X. laevis 497 QIEVTFEIDVNGILRVTAEDKGTGNKNKITITNDQNRLTPEEIERMVTDA 546
H. sapiens 496 QIEVTFEIDVNGILRVTAEDKGTGNKNKITITNDQNRLTPEEIERMVNDA 545
X. laevis 547 EKFAEEDKKLKERIDTRNELESYAYSLPNQIGDTAKLGGKLSPEDKATIE 596
H. sapiens 546 EKFAEEDKKLKERIDTRNELESYAYSLKNQIGDKEKLGGKLSSEDKETME 595
X. laevis 597 KAVTEKIEWPARHQDADIEDFKEKKKELEEIVQPIVGKLYGGAGAPPPEG 646
H. sapiens 596 KAVEEKIEWLESHQDADIEDFKAKKKELEEIVQPIISKLYGSAG-PPPTG 644
X. laevis 647 AEGAEETEKDEL 658
H. sapiens 645 EE--DTAEKDEL 654
ER retention sequence

Table I.

A comparison of BiP with other BiP and HSP70 amino acid sequences

Percent identity with *Xenopus laevis* BiP (AAB41582.1)	(%)
X. laevis BiP isoform (NP_001081462.1)	97
X. tropicalis BiP (XP_002941690.1)	98
P. bivittatus BiP (XP_007420669.1)	91
A. carolensis BiP (XP_003230508.1)	90
H. sapiens BiP (NP_005338.1)	93
R. norvegicus BiP (NP_037215.1)	93
P. mexicana BiP (XP_014856432.1)	91
F. heteroclitus BiP (XP_012729972.1)	90
G. gallus BiP (NP_990822.1)	93
H. leucocephalus BiP (NP_001094428.1)	93
X. laevis HSP70 (NP_001121147.1)	63
X. laevis HSC70.I (AAB97092)	62

An amino acid sequence comparison of *X. laevis* BiP with BiP from amphibian, reptile, fish, bird, mammalian and other members of the HSP70 family from *X. laevis*. Genbank accession numbers are indicated within the brackets.

(Kumar et al., 2016) that was constructed using the neighbor-joining method created by Saitou and Nei (1987) revealed that *X. laevis* and *X. tropicalis* BiP grouped more closely with reptilian, avian and mammalian BiP than with fish BiP (Fig. 6). A more robust clustering method called maximum-likelihood, based on the Jones-Taylor-Thornton matrix-based model (Jones et al., 1992), gave comparable results (Fig. 7).

The availability of the *X. laevis* genomic sequence (Xenbase version 9.1) allowed an examination of the upstream promoter region of the *bip* gene (Karpinka et al., 2015). Previous studies that examined the upstream regulatory region of the *H. sapiens bip* gene identified CAAT sites, a TATA box and endoplasmic reticulum stress elements (ERSEs; Yoshida et al., 1998; Kokame et al., 2001; Misiewicz et al., 2013). The consensus sequences for three CAAT sites, a TATA box and two ERSEs were located in the upstream region of the *X. laevis bip* gene (Fig. 8). Multiple sequence alignment of a section of the promoter region of *bip* genes from *X. laevis, X. tropicalis* and *H. sapiens* demonstrated the presence of conserved regulatory elements, namely two CAAT sites and two ERSEs (Fig. 9). The third putative CAAT site from the upstream regulatory region of the *X. laevis bip* gene did not align with a CAAT site from *H. sapiens* or the *X. tropicalis bip* gene (data not shown).

3.2 Accumulation of BiP in A6 cells treated with cadmium chloride, tunicamycin, A23187, or the proteasomal inhibitor, MG132

Previous studies in our laboratory characterized the expression of the *bip* gene in *Xenopus* A6 cells and demonstrated that this gene was upregulated in response to the N-linked glycosylation inhibitor, tunicamycin, the calcium ionophore, A23187, or the

Figure 6. Evolutionary relationships of vertebrate BiP amino acid sequences using the neighbour-joining method. Sequences were aligned using the ClustalW program and the phylogenetic tree was generated with the computer program MEGA7 using the neighbour-joining method of Saitou and Nei (1987). The percentage of replicate trees in which the associated taxa are clustered together in the bootstrap test (1000 replicates) are shown next to the branches (Felsenstein, 1985). The tree was drawn to scale with branch lengths in the same unit as those of the evolutionary distances used to infer the phylogenetic tree. The evolutionary distances in the units of the number of amino acid substitutions per site were computed using the Poisson correction method. The phylogenetic tree was rooted with *C. elegans* HSP70. The Genbank accession numbers of the different proteins are listed in Materials and methods.

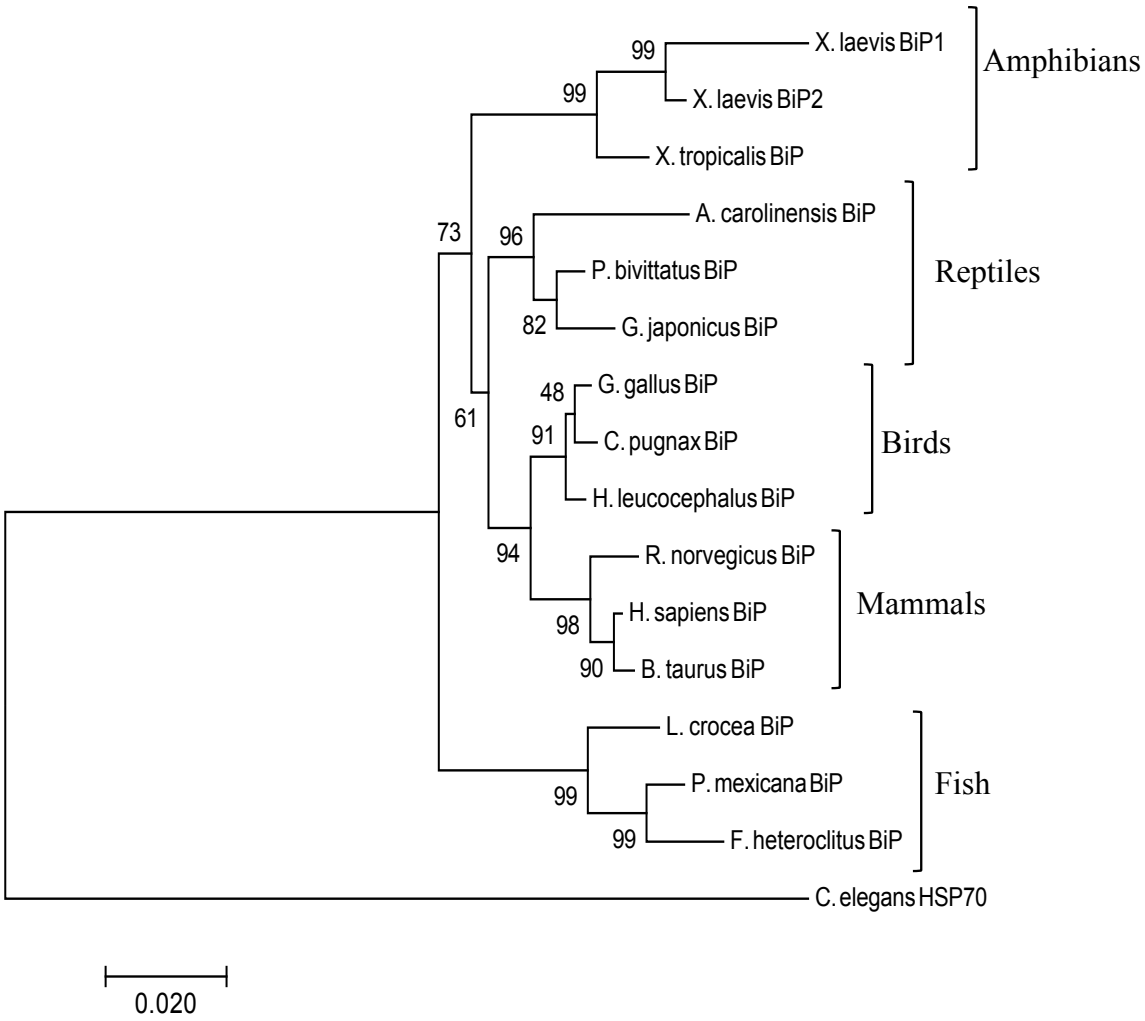
X. laevis BiP1
X. laevis BiP2
X. tropicalis BiP
Amphibians
A. carolinensis BiP
P. bivittatus BiP
G. japonicus BiP
Reptiles
G. gallus BiP
C. pugnax BiP
H. leucocephalus BiP
Birds
R. norvegicus BiP
H. sapiens BiP
B. taurus BiP
Mammals
L. crocea BiP
P. mexicana BiP
F. heteroclitus BiP
Fish
C. elegans HSP70
99
99
73
96
82
48
61
91
94
98
90
99
99
0.020

Figure 7. Phylogenetic analysis of vertebrate BiP amino acid sequences using maximum-likelihood analysis. The phylogenetic tree was constructed using the maximum-likelihood method based on the Jones-Taylor-Thornton matrix-based model of translated amino acid sequences (Jones et al., 1992). The percentage of trees in which the associated taxa clustered together is shown next to the branches. The number of bootstrap replications was 1000. The tree is drawn to scale with branch lengths measured in the number of substitutions per site. Evolutionary analyses were conducted in MEGA7 and rooted with C. *elegans* HSP70. The Genbank accession numbers of the different proteins are listed in Materials and methods.

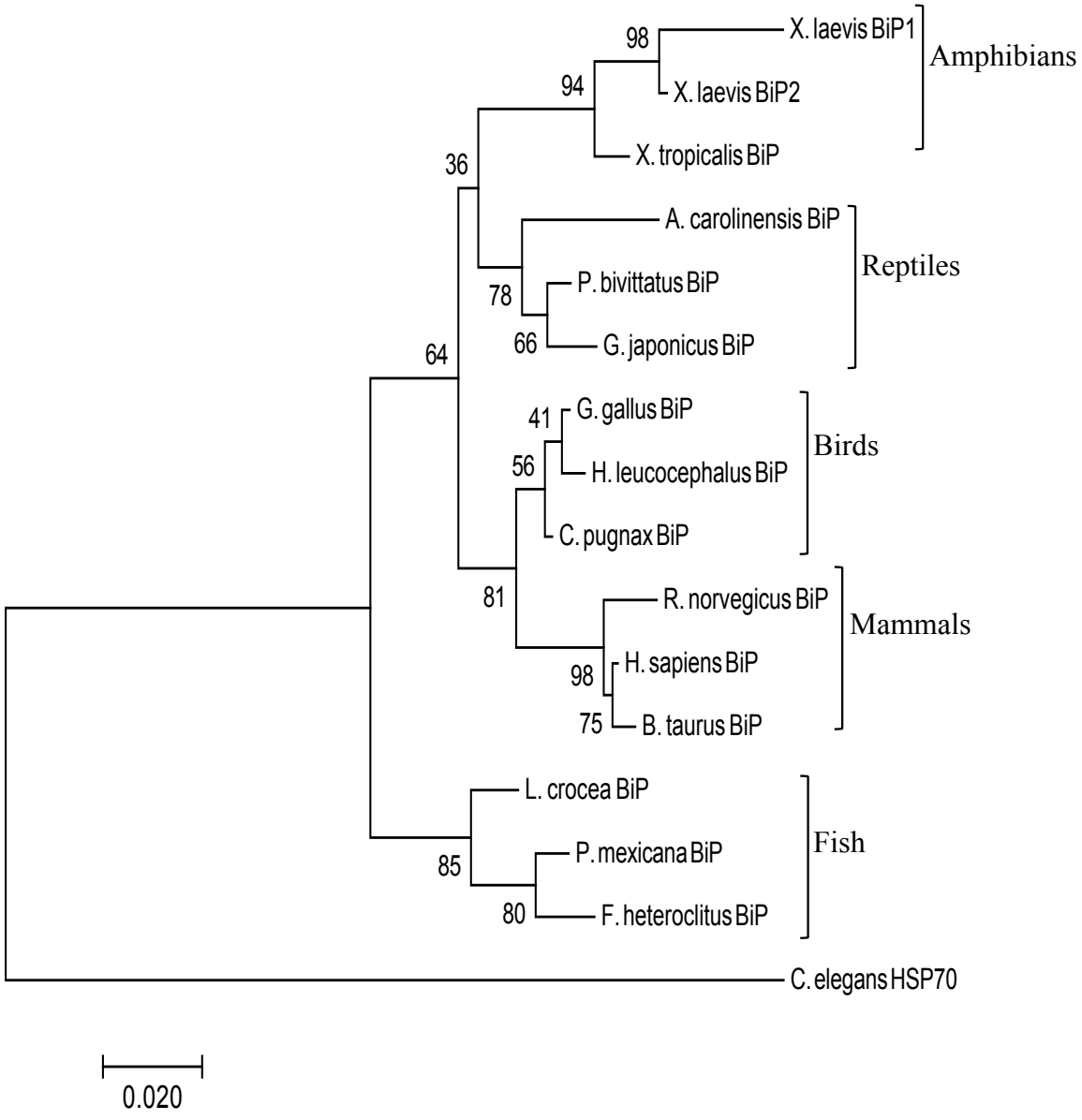
X. laevis BiP1
98
X. laevis BiP2
94
X. tropicalis BiP
Amphibians
36
A. carolinensis BiP
P. bivittatus BiP
78
G. japonicus BiP
66
Reptiles
64
G. gallus BiP
41
H. leucocephalus BiP
56
C. pugnax BiP
Birds
81
R. norvegicus BiP
H. sapiens BiP
98
B. taurus BiP
75
Mammals
L. crocea BiP
P. mexicana BiP
85
F. heteroclitus BiP
80
Fish
C. elegans HSP70
0.020

Figure 8. Putative *cis*-acting elements in the upstream regulatory region of the *X. laevis bip* gene. The upstream DNA sequence was obtained from V9.1 of the *Xenopus laevis* genome available from Xenbase (Karpinka et al., 2015). The transcribed nucleotide sequence is shown in capital letters while the transcriptional start site is indicated by +1. CAAT sites, TATA box and endoplasmic reticulum stress element (ERSE) consensus sequences are indicated by black lines. Consensus sequences for ERSE were obtained from mammalian studies (Yoshida et al., 1998; Kokame et al., 2001; Misiewicz et al., 2013).

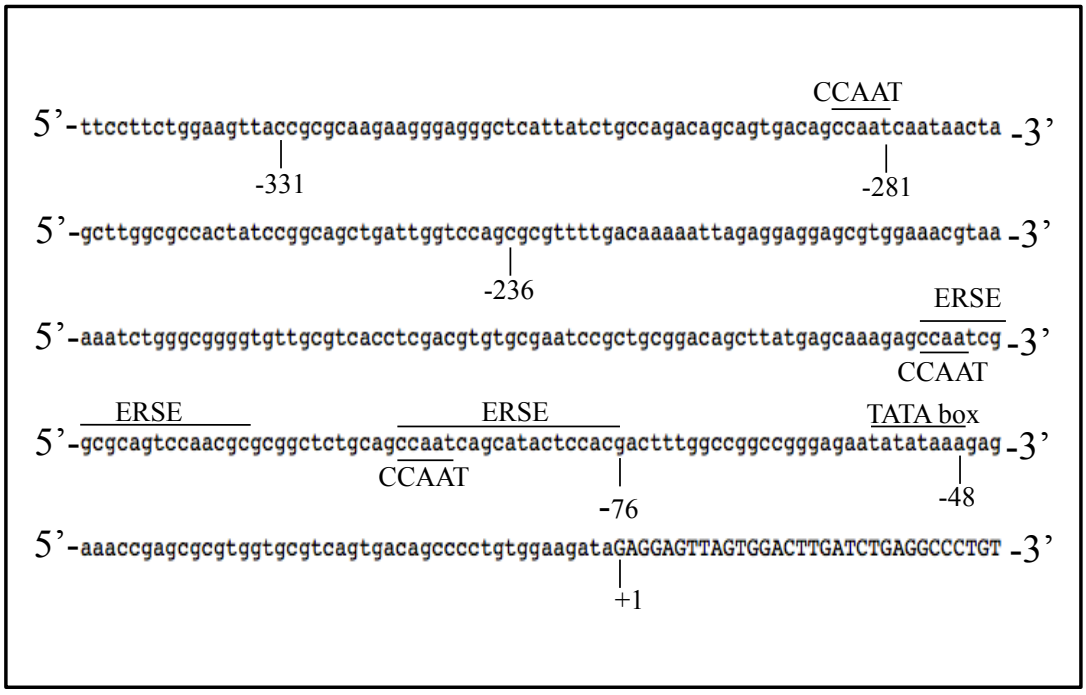
CCAAT
5'-ttccttctggaagttaccgcgcaagaagggagggctcattatctgccagacagcagtgacagccaatcaataacta-3'
-331
-281
5'-gcttggcgccactatccggcagctgattggtccagcgcgttttgacaaaaattagaggaggagcgtggaaacgtaa-3'
-236
ERSE
5'-aaatctgggcggggtgttgcgtcacctcgacgtgtgcgaatccgctgcggacagcttatgagcaaagagccaatcg-3'
CCAAT
ERSE
ERSE
TATA box
5'-gcgcagtccaacgcgcggctctgcagccaatcagcatactccacgactttggccggccgggagaatatataaagag-3'
CCAAT
-76
-48
5'-aaaccgagcgcgtggtgcgtcagtgacagcccctgtggaagataGAGGAGTTAGTGGACTTGATCTGAGGCCCTGT-3'
+1

Figure 9. Multiple sequence alignment of the promoter region of *bip* genes from *X. laevis*, *X. tropicalis* and *H. sapiens*. The upstream regions were aligned using the Clustal Omega program. Asterisks under the sequences indicate identical nucleotides while putative *cis*-acting elements are designated by black lines. Distances from the transcriptional start sites are indicated on the right side of the sequences. Consensus sequence for ERSE was obtained from mammalian studies (Yoshida et al., 1998; Kokame et al., 2001; Misiewicz et al., 2013). Sequences for *X. laevis* (Xenbase ID: XB-GENE-865337) and *X. tropicalis* (Xenbase ID: XB-GENE-480060) are available in the Xenbase genome browser. The nucleotide sequence for the *H. sapiens* regulatory region was obtained from NCBI (accession no. X59969).

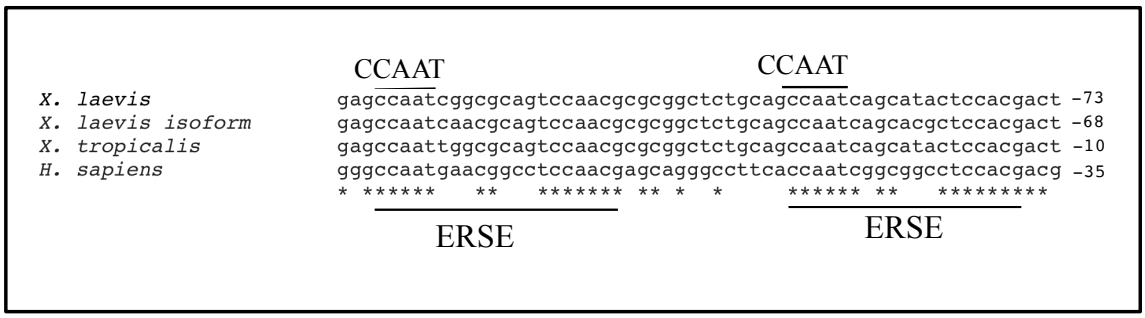
CCAAT
CCAAT
X. laevis gagccaatcggcgcagtccaacgcgcggctctgcagccaatcagcatactccacgact -73
X. laevis isoform gagccaatcaacgcagtccaacgcgcggctctgcagccaatcagcacgctccacgact -68
X. tropicalis gagccaattggcgcagtccaacgcgcggctctgcagccaatcagcatactccacgact -10
H. sapiens gggccaatgaacggcctccaacgagcagggccttcaccaatcggcggcctccacgacg -35
ERSE
ERSE

proteasomal inhibitor, MG132 (Winning et al., 1989; Miskovic et al., 1997; Khan et al., 2012). Consistent with the previous studies, immunoblot analyses revealed an increase in the relative levels of BiP accumulation in A6 cells treated with 2 μg/mL tunicamycin or 7 μM A23187 for 14 h compared to control cells maintained at 22 °C (Fig. 10A). Additionally, treatment of A6 cells with 200 μM cadmium chloride for 14 h also induced BiP accumulation. Densitometric analysis determined that BiP accumulation increased by 2.5-fold in cadmium chloride-treated cells compared to control cells (Fig 10B). In comparison, treatment of A6 cells with tunicamycin and A23187 caused a 1.4- and 1.6-fold increase, respectively, compared to control. Examples of the time course of BiP accumulation in response to A23187 or MG132 in A6 cells are shown in Figure 11. Both A23187 and MG132 induced the accumulation of BiP in a time-dependent fashion with peak levels after 24 h of treatment.

3.3 Cadmium chloride-induced BiP accumulation in A6 cells is concentration- and time-dependent

An initial characterization of the effect of cadmium chloride on BiP accumulation in A6 cells involved an examination of the effect of different concentrations and exposure times. For comparison, the effect of cadmium chloride on the accumulation of other previously characterized stress proteins, including HSP70, HO-1 and a representative constitutive protein, actin, was examined (Woolfson & Heikkila, 2009; Khamis & Heikkila, 2013; Music et al., 2014). The concentration-dependent effect of cadmium chloride (25 to 400 μM for 14 h) on BiP, HSP70 and HO-1 accumulation by means of immunoblot analysis is shown in Figure 12. Densitometric analysis determined that cadmium chloride-induced BiP accumulation was detectable at 100 μM and maximal at

Figure 10. Accumulation of BiP in A6 cells treated with cadmium chloride, tunicamycin or A23187. A) Cells were incubated at 22 °C for 14 h (C) or treated with either 200 μM cadmium chloride, 2 μg/mL tunicamycin or 7 μM A23187 for 14 h. Immunoblot analyses employing anti-BiP, anti-HSP70 or anti-actin antibodies were performed as described in the Materials and methods. B) Densitometric analysis of BiP and HSP70 accumulation was carried out as detailed in Materials and methods. The results were expressed as % mean relative density. The error bars indicate standard error of the mean. The significance ($p < 0.05$) relative to control was determined by the one-way ANOVA test and Tukey's post-hoc test and represented by an asterisk. The results were obtained from 3 separate experiments.

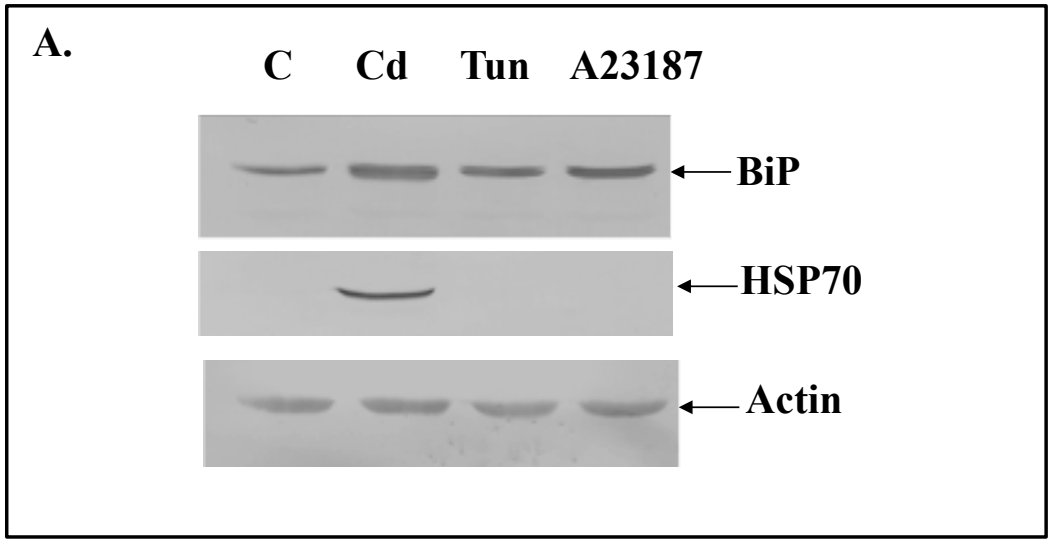
A.
C
Cd
Tun
A23187
BiP
HSP70
Actin

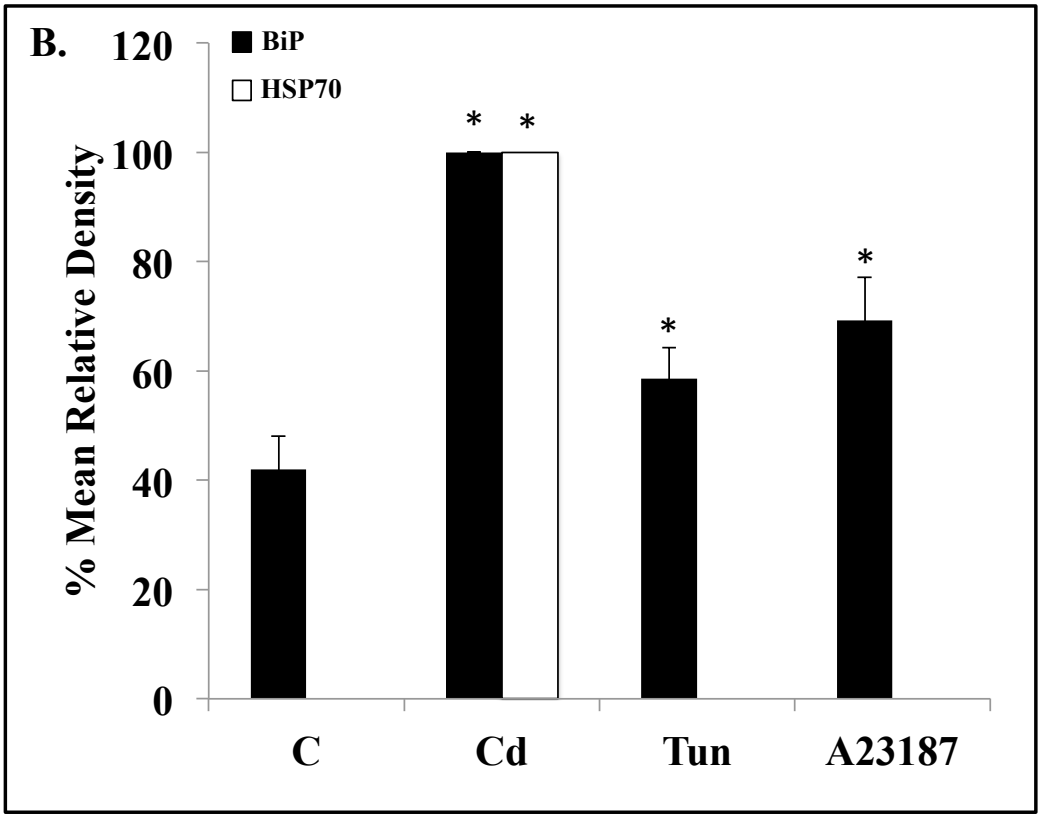
B.
BiP
HSP70
% Mean Relative Density
120
100
80
60
40
20
0
*
*
*
*
C
Cd
Tun
A23187

Figure 11. Time-course of BiP accumulation in A6 cells treated with MG132 or A23187. A) Cells were incubated at 22 °C for 24 h (C) or treated with 7 μM A23187 for 4, 8 12, 16 or 24 h. B) Cells were incubated at 22 °C for 24 h (C) or treated with 30 μM MG132 for 4, 8 12, 16 or 24 h. Immunoblot analyses with anti-BiP, anti-HSP70 or anti-actin antibodies were performed as described in the Materials and methods. These results are representative of 2 separate experiments.

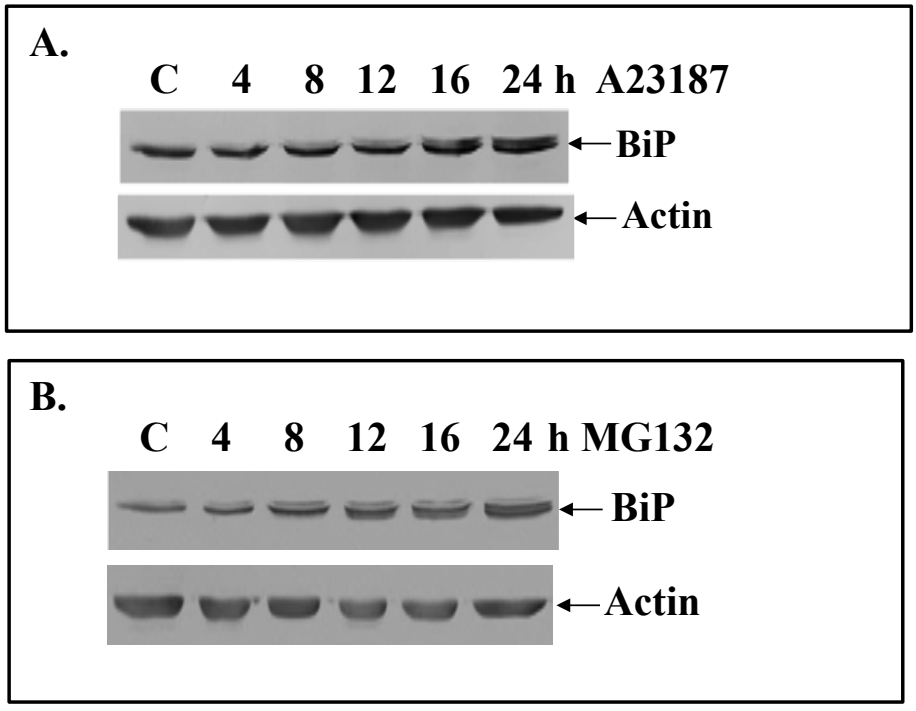
A.
C 4 8 12 16 24 h A23187
BiP
Actin
B.
C 4 8 12 16 24 h MG132
BiP
Actin

Figure 12. Effect of different cadmium chloride concentrations on BiP accumulation in A6 cells. Cells were incubated for 14 h at 22 °C or treated with 25, 50, 100, 200 or 400 μM cadmium chloride for 14 h at 22 °C. A) Immunoblot analysis was performed as stated in the Materials and methods employing anti-BiP, anti-HSP70, anti-HO-1 or anti-actin antibodies. B) Densitometric analysis of BiP (black), HSP70 (white), and HO-1 (grey) accumulation. The results were expressed as % mean relative density. The error bars indicate standard error of the mean. The significance ($p < 0.05$) relative to control was determined by the one-way ANOVA test and Tukey's post-hoc test and represented by an asterisk. These results were obtained from 3 separate experiments

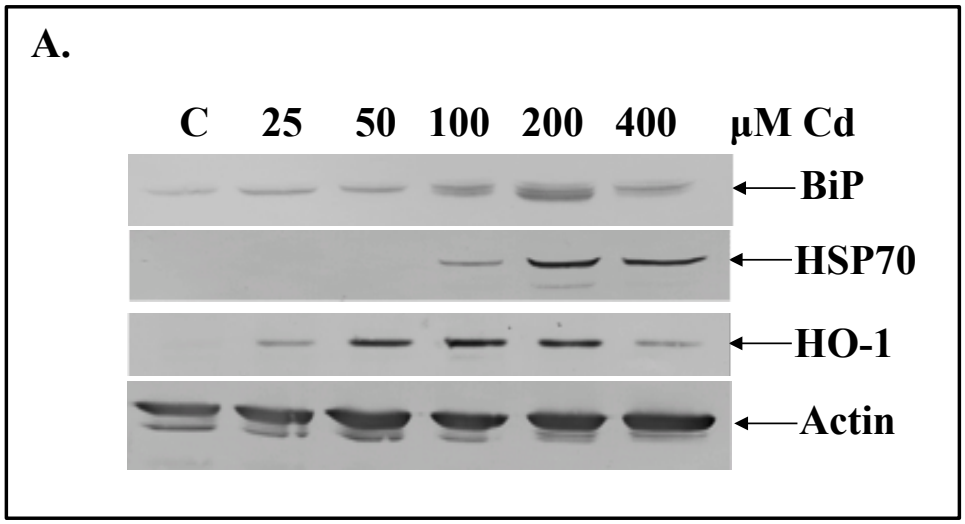
A.
C
25
50
100
200
400
µM Cd
BiP
HSP70
HO-1
Actin

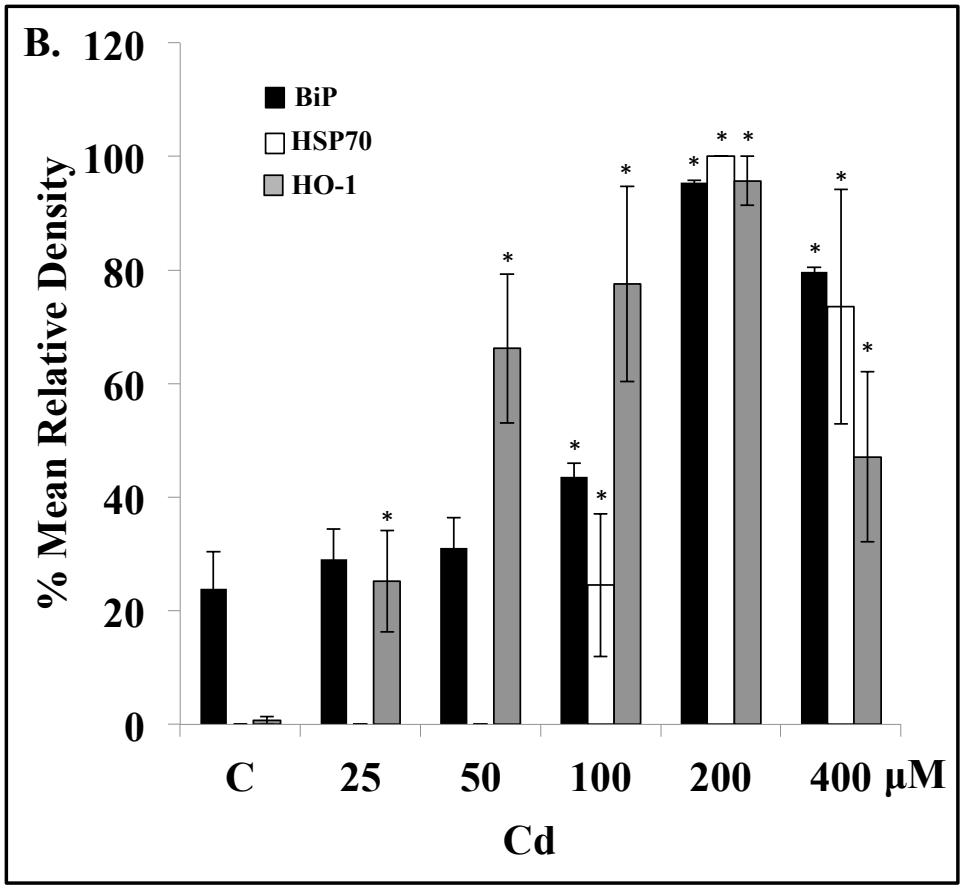
B.
120
100
80
60
40
20
0
% Mean Relative Density
BiP
HSP70
HO-1
C
25
50
100
200
400 µM
Cd

200 μM whereas increasing the concentration to 400 μM resulted in a reduction of 25% from the peak level (Figure 12B). HSP70 accumulation was first detectable at 100 μM cadmium chloride followed by a relatively large increase with 200 μM and then a slight decrease with 400 μM. Enhanced HO-1 accumulation relative to control was detected in cells treated with 25 μM cadmium chloride, reached peak levels at 100-200 μM and then decreased at 400 μM. In time course experiments, A6 cells were treated with 200 μM cadmium chloride for 4, 8, 12, 16 and 24 h at 22°C (Fig. 13). Immunoblot and densitometric analyses revealed a time-dependent increase in cadmium chloride-induced BiP, HSP70 and HO-1 accumulation. For example, the relative level of BiP increased by 1.5-fold and 2-fold at 12 and 24 h, respectively, compared to control. Relative levels of HSP70 increased by 24-fold after 8 h of cadmium chloride exposure with further increases from 12 (43-fold) to 24 h (53-fold). The levels of HO-1 increased by 82-fold at 8 h relative to control followed by 146-fold at 12 h and 200-fold at 24 h. In both cadmium chloride concentration and time course studies the relative level of actin remained relatively constant.

3.4 Effect of transcriptional and translational inhibitors on cadmium-induced BiP accumulation

Cadmium chloride-induced BiP accumulation in A6 cells appears to involve de novo transcription and translation. Pretreatment of cells with 2 μg/mL actinomycin D inhibited the 200 μM cadmium chloride-induced accumulation of BiP and HSP70 to control levels (Fig. 14). Furthermore, pretreatment of A6 cells with 100 μM

Figure 13. Time course of cadmium chloride-induced BiP accumulation in A6 cells. Cells were incubated in media alone at 22 °C for 24 h (C) or in media supplemented with 200 μM cadmium chloride for 4, 8, 12, 16, 24 h at 22 °C. **A**) Immunoblot analysis was performed as stated in Materials and methods employing anti-BiP, anti-HSP70, anti-HO-1 or anti-actin antibodies. **B**) Densitometric analysis BiP (black), HSP70 (white) and HO-1 (grey) accumulation. The results were expressed as % mean relative density. The error bars indicate standard error of the mean. The significance ($p < 0.05$) relative to control was determined by the one-way ANOVA test and Tukey's post-hoc test represented by an asterisk. These results were obtained from 3 separate experiments.

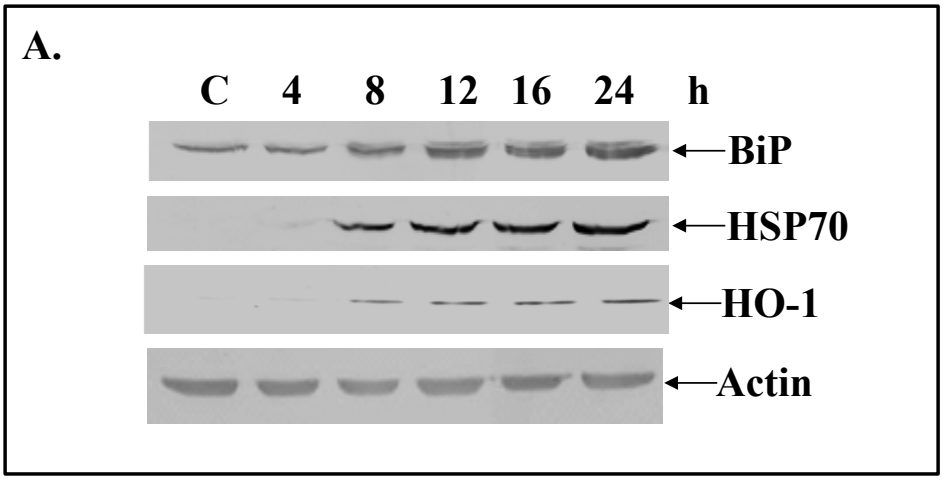
A.
C
4
8
12
16
24
h
BiP
HSP70
HO-1
Actin

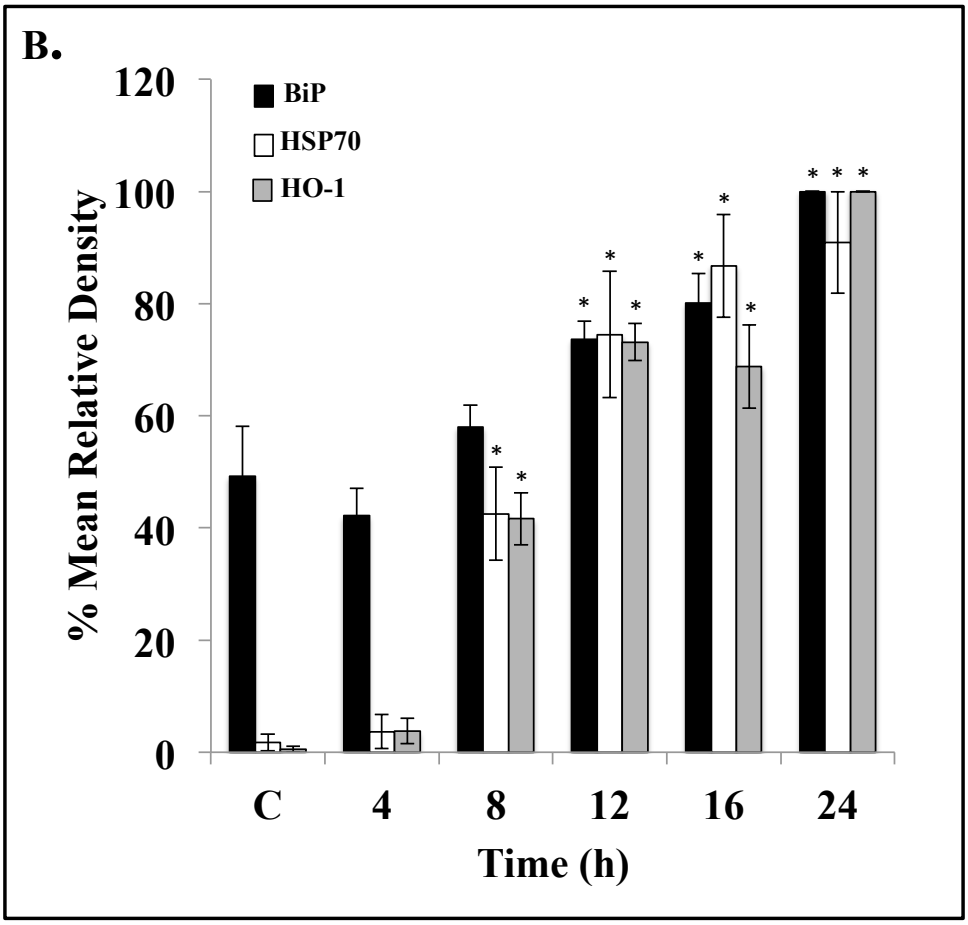
B.
BiP
HSP70
HO-1
% Mean Relative Density
120
100
80
60
40
20
0
C
4
8
12
16
24
Time (h)

Figure 14. Accumulation of cadmium chloride-induced BiP in cells pretreated with the transcriptional inhibitor actinomycin D. Cells were incubated at 22 °C with media (control) or pretreated with 2 μg/mL actinomycin D (Act. D) for 30 min. Cells were then treated with 200 μM cadmium chloride for 14 h at 22 °C. **A**) Immunoblot analysis was performed as stated in the Materials and methods section with anti-BiP, anti-HSP70 or anti-actin antibodies. **B)** Densitometric analysis of BiP (black) and HSP70 (white). The results were expressed as % mean relative density. The error bars indicate standard error of the mean. The significance ($p < 0.05$) relative to control was determined by the one-way ANOVA test and Tukey's post-hoc test represented by an asterisk. These results are representative of at least 3 separate experiments

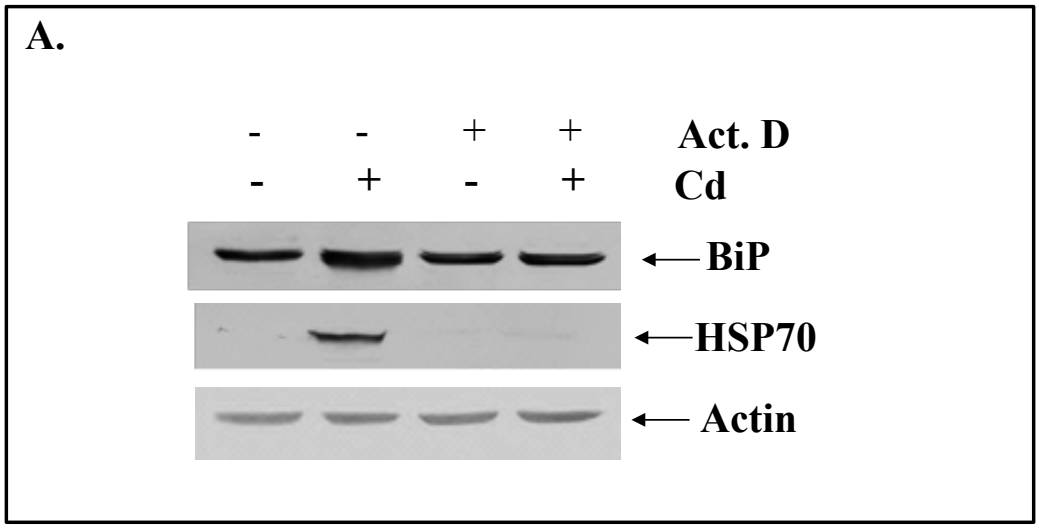
A.
- - + + Act. D
- + - + Cd
BiP
HSP70
Actin

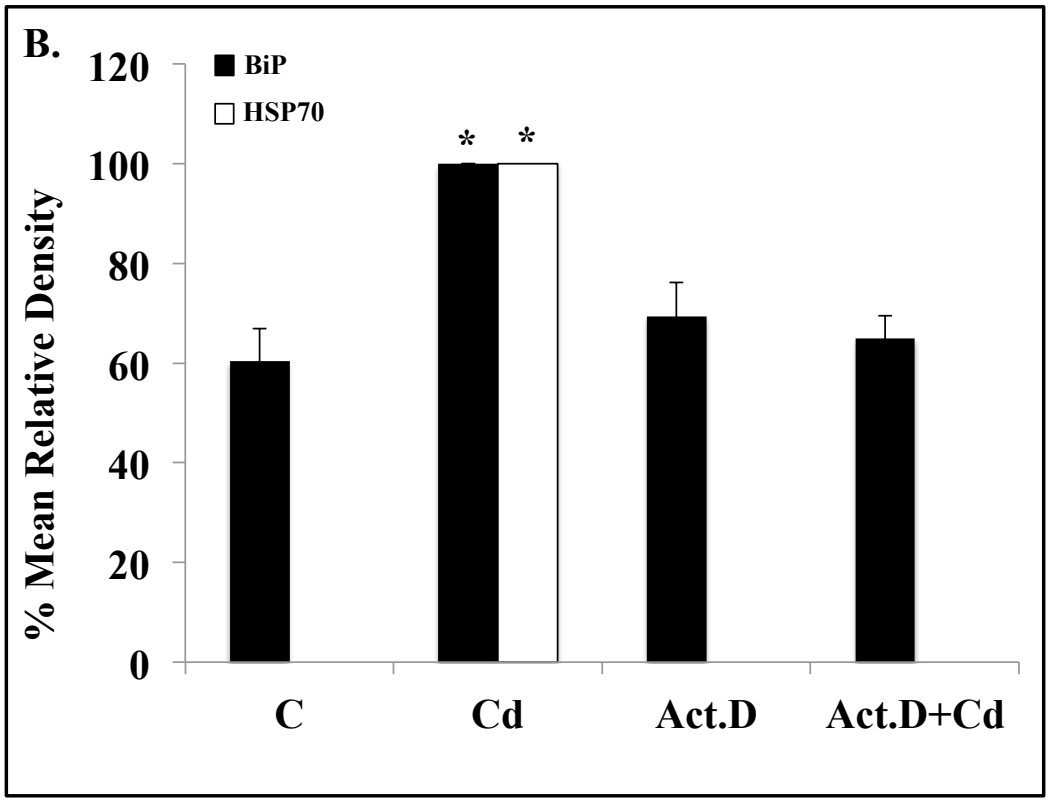
B.
BiP
HSP70
% Mean Relative Density
120
100
80
60
40
20
0
* *
C
Cd
Act.D
Act.D+Cd

cycloheximide, an inhibitor of protein synthesis, prevented 200 μM cadmium chloride-induced BiP and HSP70 accumulation (Fig. 15).

3.5 BiP accumulation in cells recovering from cadmium chloride

In previous studies, Woolfson and Heikkila (2009) reported that treatment of A6 cells with cadmium chloride for 8 h followed by recovery in fresh media resulted in a transient increase in HSP70 and HSP30 during the initial recovery period. In the present study, the effect of this cadmium chloride treatment protocol was employed to examine its effect on BiP accumulation. Thus, A6 cells were treated with 200 μM cadmium chloride for 8 h prior to recovery in fresh L-15 media. As shown in Figure 16, the levels of BiP increased 1.4-fold in A6 cells given 12 h of recovery compared to cells exposed to cadmium chloride with no recovery. After 24 h of recovery, the relative levels of BiP dropped slightly to 1.3-fold compared to no recovery followed by a further decrease to 1.1-fold after 48 and 72 h. The relative levels of HSP70 increased 1.5-fold after 12 h of recovery compared to no recovery with a drop to 1.3-fold after 24 h followed by further decreases at 48 h and 72 h. The relative levels of HO-1 increased 1.5-fold at 12 h and 2.3-fold at 24 h compared to cells with no recovery, followed by a 1.9-fold increase after 48 h and a 1.5-fold increase at 72 h. In this experiment, the levels of actin remained relatively constant.

3.6 Localization of BiP in A6 cells treated with cadmium chloride

Immunocytochemistry and laser scanning confocal microscopy (LSCM) were employed to examine the effect of cadmium chloride on BiP localization in A6 cells. Cells

Figure 15. Accumulation of cadmium chloride-induced BiP in cells treated with the translational inhibitor cycloheximide (CHX). Cells were incubated at 22 °C with media (control) or pre-treated with 100 μM CHX for 6 h. Cells were then treated with 200 μM cadmium chloride for 14 h at 22 °C. **A**) Immunoblot analysis was performed as stated in the Materials and methods section with anti-BiP, anti-HSP70 or anti-actin antibodies. **B)** Densitometric analysis of BiP (black) and HSP70 (white). The results were expressed as % mean relative density. The error bars indicate standard error of the mean. The significance ($p < 0.05$) relative to control was determined by the one-way ANOVA test and Tukey's post-hoc test represented by an asterisk. These results are representative of at least 3 separate experiments.

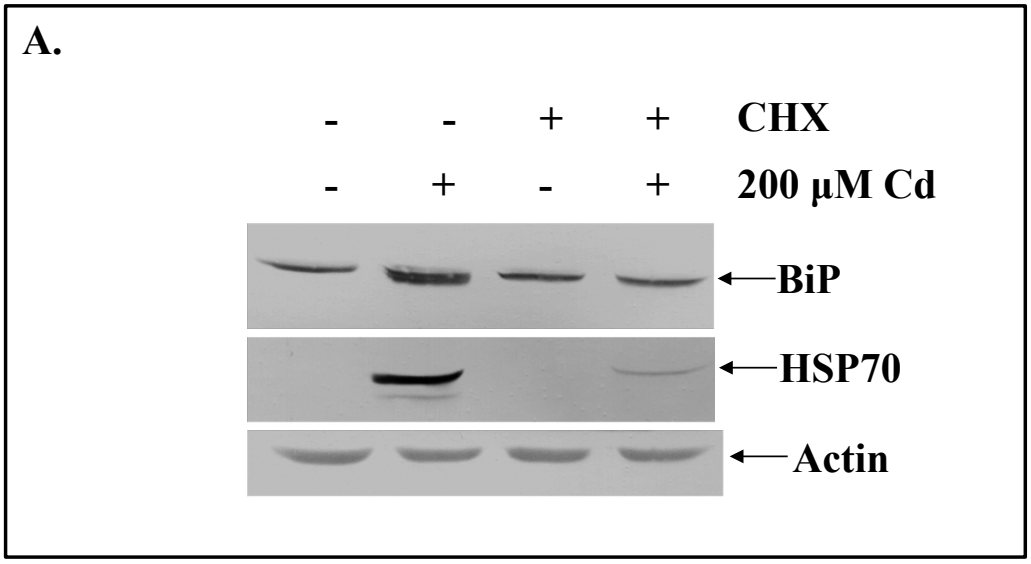
A.
- - + + CHX
- + - + 200 µM Cd
BiP
HSP70
Actin

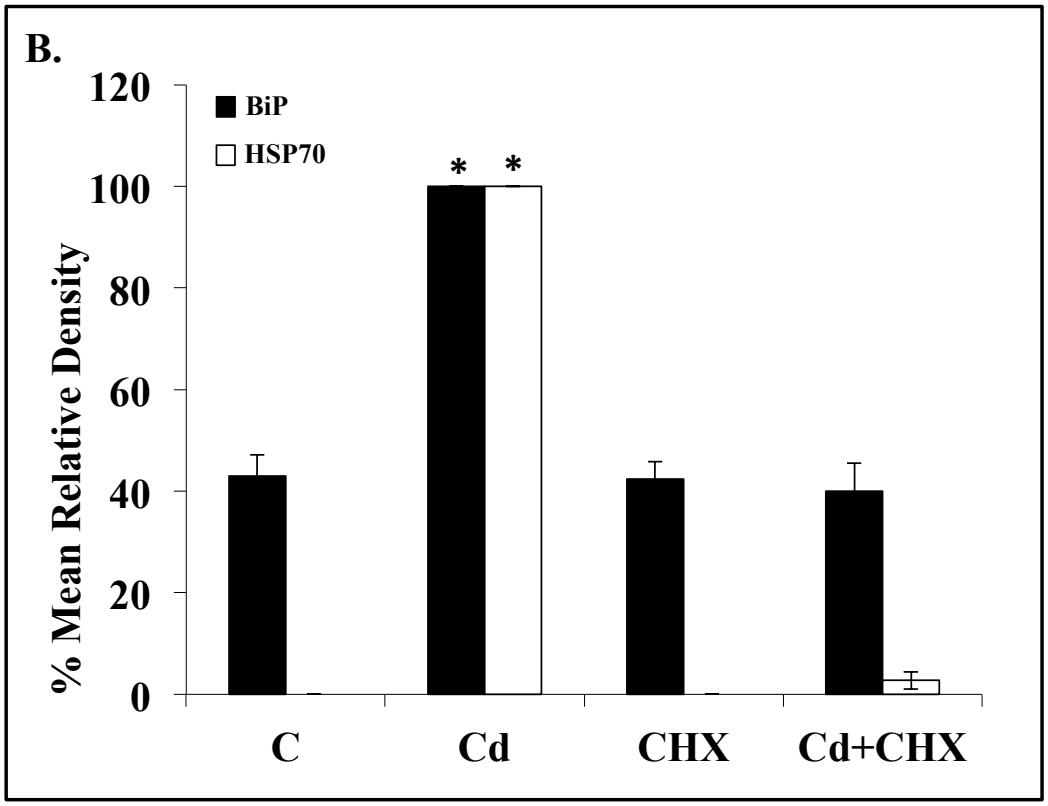
B.
BiP
HSP70
% Mean Relative Density
120
100
80
60
40
20
0
* *
C
Cd
CHX
Cd+CHX

Figure 16. BiP accumulation in A6 cells recovering from an 8 h 200 µM cadmium chloride treatment. Cells were incubated at 22 °C with media (C) or treated with media that included 200 µM cadmium chloride at 22 °C for 8 h. Cells were washed 3 times with HBSS and then allowed to recover in media for 0, 12, 24, 48 or 72 h. **A**) Immunoblot analysis was performed as stated in the Materials and methods section with anti-BiP, anti-HSP70, anti-HO-1 or anti-actin antibodies. **B**) Densitometric analysis of BiP (black), HSP70 (white) and HO-1 (grey) accumulation. The results were expressed as % mean relative density. The error bars indicate standard error of the mean. The significance ($p < 0.05$) relative to control was determined by the one-way ANOVA test and Tukey's post-hoc test represented by an asterisk. These results were obtained from 3 separate experiments.

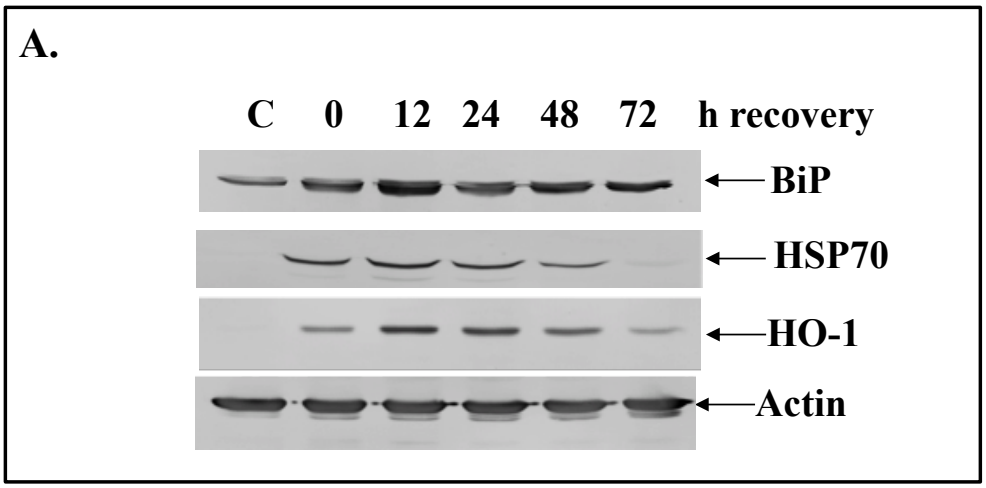
A.
C 0 12 24 48 72 h recovery
BiP
HSP70
HO-1
Actin

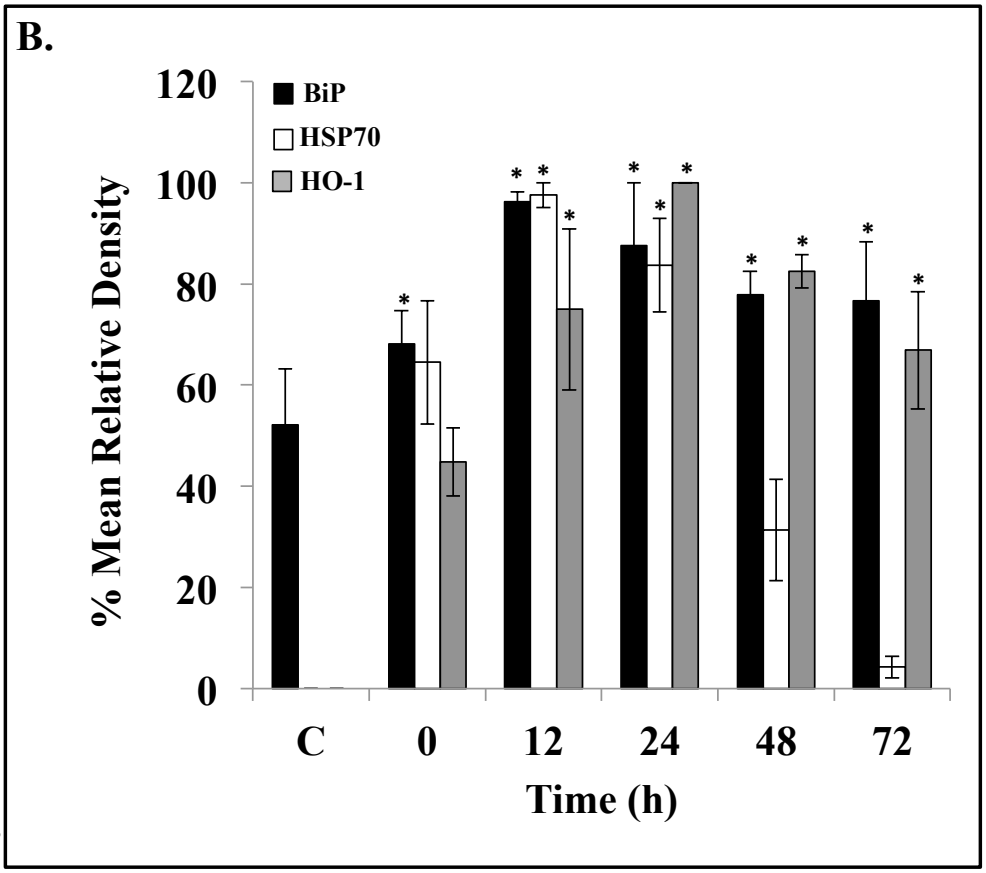
B.
BiP
HSP70
HO-1
% Mean Relative Density
120
100
80
60
40
20
0
C 0 12 24 48 72
Time (h)

were grown on coverslips and maintained at 22 °C or treated with 100 or 200 μM cadmium chloride for 12 h. In control cells, BiP accumulation was detected in a punctate pattern in the perinuclear region (Fig. 17). However, treatment of cells with 100 μM cadmium chloride enriched the accumulation of BiP near the nucleus. A further enhancement was observed when cells were exposed to 200 μM cadmium chloride. In addition, relatively large anti-BiP antibody staining structures, approximately 2 μM in diameter (Fig. 17, indicated by white arrows), were observed near the nucleus in approximately 10% of cells treated with 200 μM cadmium chloride. Examination of the actin cytoskeleton revealed slight disorganization and membrane ruffling in cells treated with 100 μM cadmium chloride, which was more intense at 200 μM (indicated by asterisks).

3.7 Co-localization of large perinuclear structures with anti-BiP antibody and Proteostat dye in A6 cells exposed to cadmium chloride or MG132

Since BiP is a molecular chaperone that binds to unfolded protein in the ER, it was possible that the relatively large anti-BiP antibody staining structures, observed in Figure 17, may result from an association with aggregated protein as described previously in both yeast and human embryonic kidney cells overexpressing mutant cystic fibrosis conductance regulator (CFTR) tagged protein and monkey kidney cells expressing mutant ubiquitin carboxy-terminal hydrolase-1 (UCH-L1; Kopito & Sitia, 2000; Huyer et al., 2004; Ardley et al., 2004; Bagola & Sommer, 2008). Previously, our laboratory employed a Proteostat dye to detect the presence of aggregated protein and/or aggresome-like structures in A6 cells subjected to recovery from heat shock or to cadmium chloride, sodium arsenite or proteasomal inhibitor stress (Khan & Heikkila, 2014; Khan et al.,

Figure 17. Localization of BiP in cells treated with 100 or 200 μM cadmium chloride. Cells were maintained at 22 °C or treated with either 100 or 200 μM cadmium chloride for 12 h at 22 °C. Actin and nuclei were stained with TRITC (red) and DAPI (blue), respectively. BiP was detected with anti-BiP antibody and the secondary antibody conjugate, Alexa Fluor 488 (green). The 20 μm white scale bars are indicated at the bottom right corner of each panel. Examples of disruptions found in the actin cytoskeleton are indicated by asterisks. White arrows point to examples of large anti-BiP antibody staining structure. These results are representative of at least 3 separate experiments.

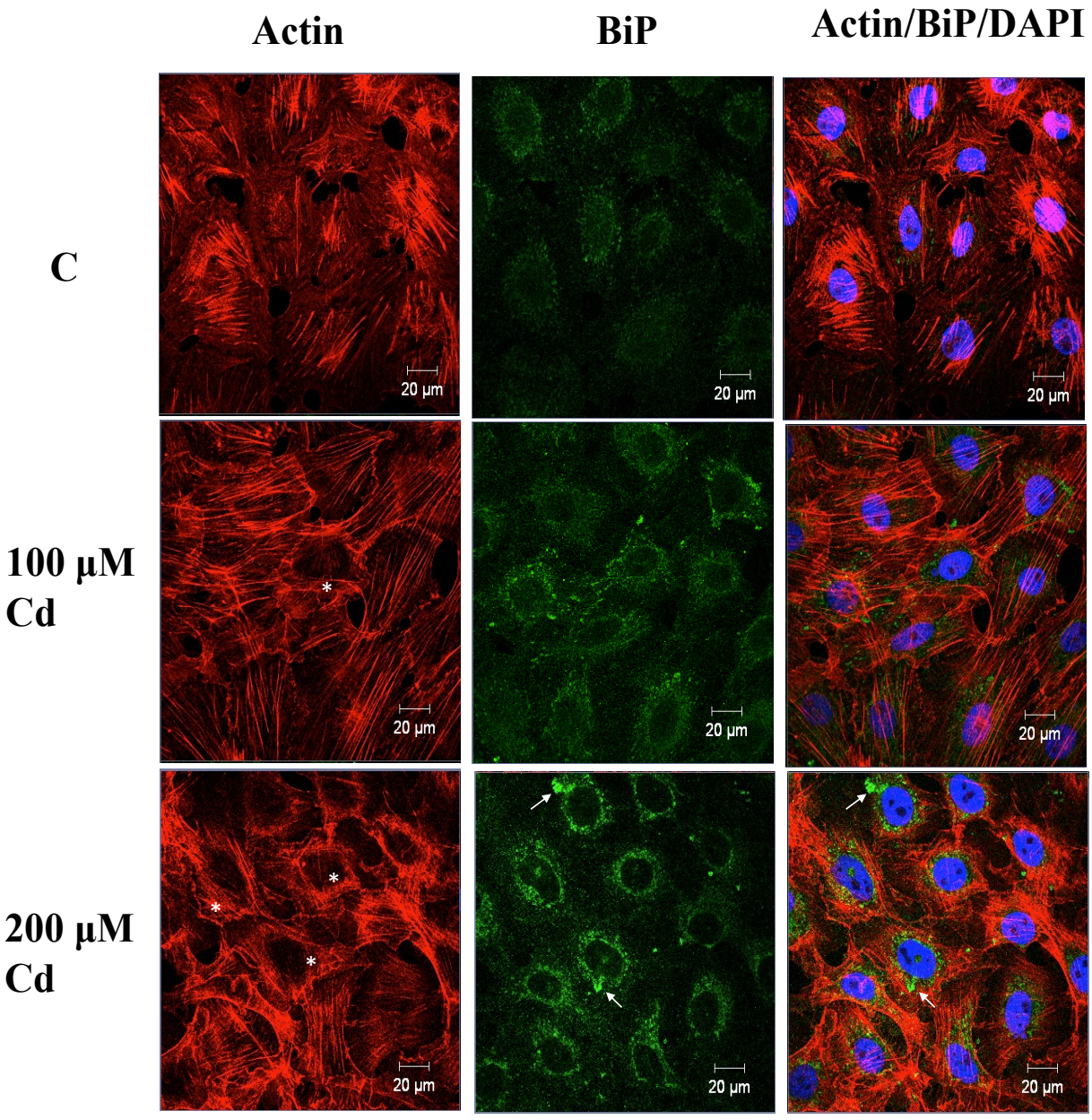
Actin
BiP
Actin/BiP/DAPI
C
100 µM Cd
200 µM Cd
20 µm

2015). In the present study, control and 100 μM cadmium chloride-treated cells displayed a weak level of staining with the Proteostat dye (Fig. 18). However, treatment of cells with 200 μM cadmium chloride induced the presence of relatively large Proteostat dye stained structures (approximately 1-2 μm in diameter) that co-localized with structures that were stained with the anti-BiP antibody in approximately 10% of cells. The association of the BiP structures with the Proteostat dye in the perinuclear region is shown more clearly in the bottom row of enlarged images, which reveal the presence of yellow/orange structures indicating the co-localization of BiP with the Proteostat dye (see white boxes in bottom row). Given that the proteasomal inhibitor, MG132, also induced BiP accumulation, a similar co-localization analysis was performed (Fig. 19). The treatment of cells with MG132 induced the accumulation of large and small granular Proteostat dye-stained structures in the perinuclear region in 90% of the cells. Some of the relatively large Proteostat dye-stained structures found in the perinuclear region were also detected with anti-BiP antibody and gave rise to yellow/orange structures in the merged image (see white arrows and boxes in the second and third rows, respectively). As shown in Figure 20, z-stacking analysis of the cadmium- and MG132-induced Proteostat dye and anti-BiP antibody stained structures revealed the presence of co-localized staining (yellow/orange) in the center of the structure with varying amounts of aggregated protein (red) at the periphery.

3.8 Comparison of the effect cadmium chloride has on BiP accumulation in cells maintained at 22 or 30 °C for 5 h.

Figure 18. Co-localization of Proteostat dye-stained structures with large BiP containing complexes in cadmium chloride-treated cells. Cells were grown on glass coverslips with L-15 media at 22 °C. Cells were maintained at 22 °C (C) or treated with 200 μM cadmium for 12 h at 22 °C. The Proteostat detection kit was used according to the manufacter's instructions. Nuclei were stained with DAPI (blue). BiP was detected with anti-BiP antibody and secondary antibody conjugate, Alexa Fluor 488 (green). The 10 or 20 μm white scale bars are indicated at the bottom right corner of each panel. In the third row, the white arrows indicate examples of aggregated protein complexes detected by Proteostat dye, large anti-BiP antibody staining structures, and their co-localization in the merged panel. In the bottom row, enlarged images of the large Proteostat- and anti-BiP antibody-stained structures (a and b) are found in the upper left and right corners, respectively. These results are representative of at least 3 separate experiments.

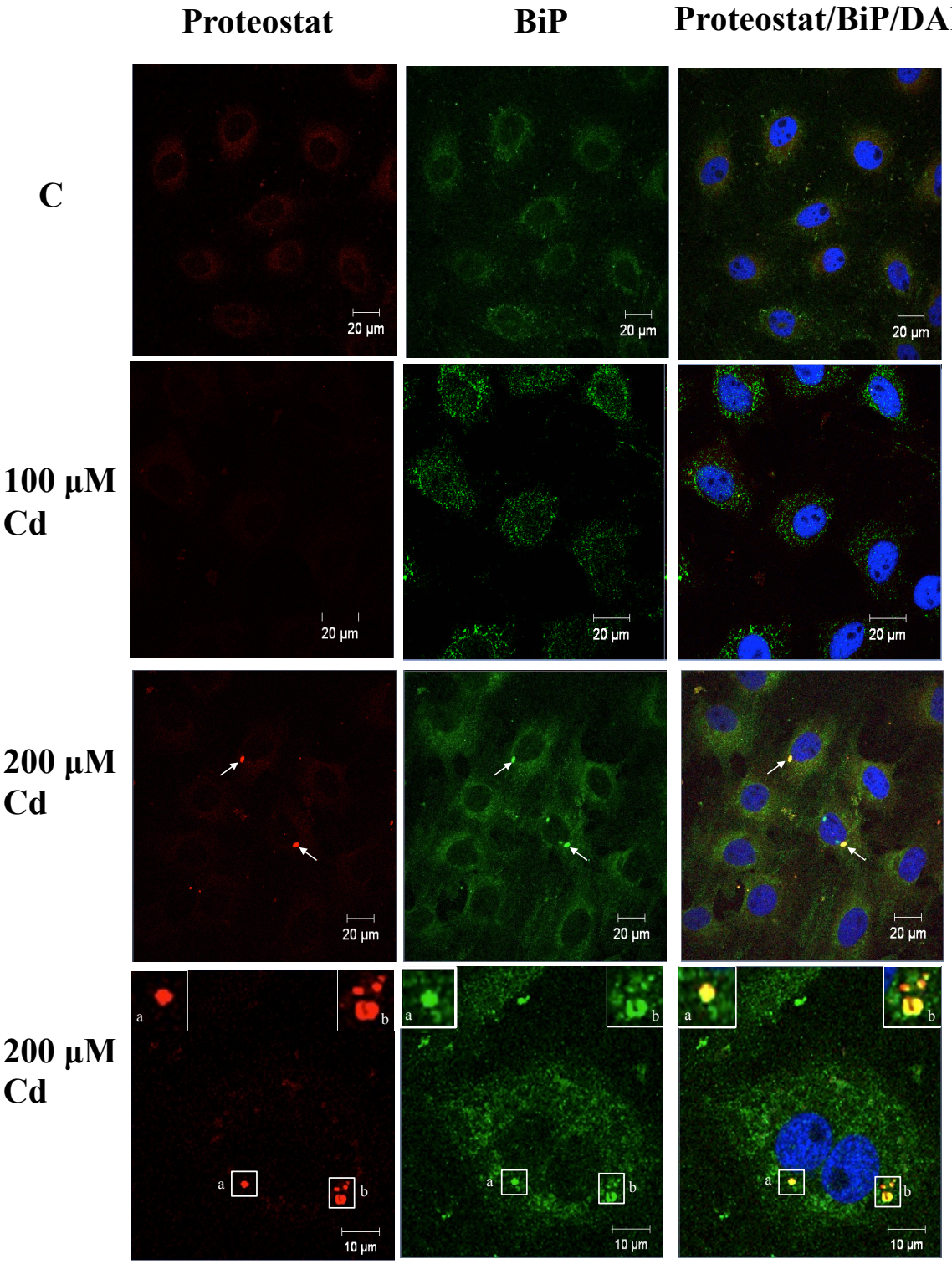
Proteostat
BiP
Proteostat/BiP/DAPI
C
100 µM Cd
200 µM Cd
200 µM Cd
20 µm
10 µm
a
b

Figure 19. Co-localization of Proteostat dye-stained structures with large BiP containing complexes in MG132-treated cells. Cells were grown on glass coverslips with L-15 media at 22 °C. Cells were maintained at 22 °C (C) or treated with 30 μM MG132 for 12 h at 22 °C. The Proteostat detection kit to detect aggregated protein was used according to the manufacter's instructions. Nuclei were stained with DAPI (blue). BiP was detected with anti-BiP antibody and the secondary antibody conjugate, Alexa Fluor 488 (green). The 10 or 20 μm white scale bars are indicated at the bottom right corner of each panel. White arrows and boxes indicate examples of protein aggregates detected by Proteostat dye and/or anti-BiP antibody staining. In the bottom row enlargments of the white boxes are shown in the top left corner of each panel. These results are representative of at least 3 separate experiments.

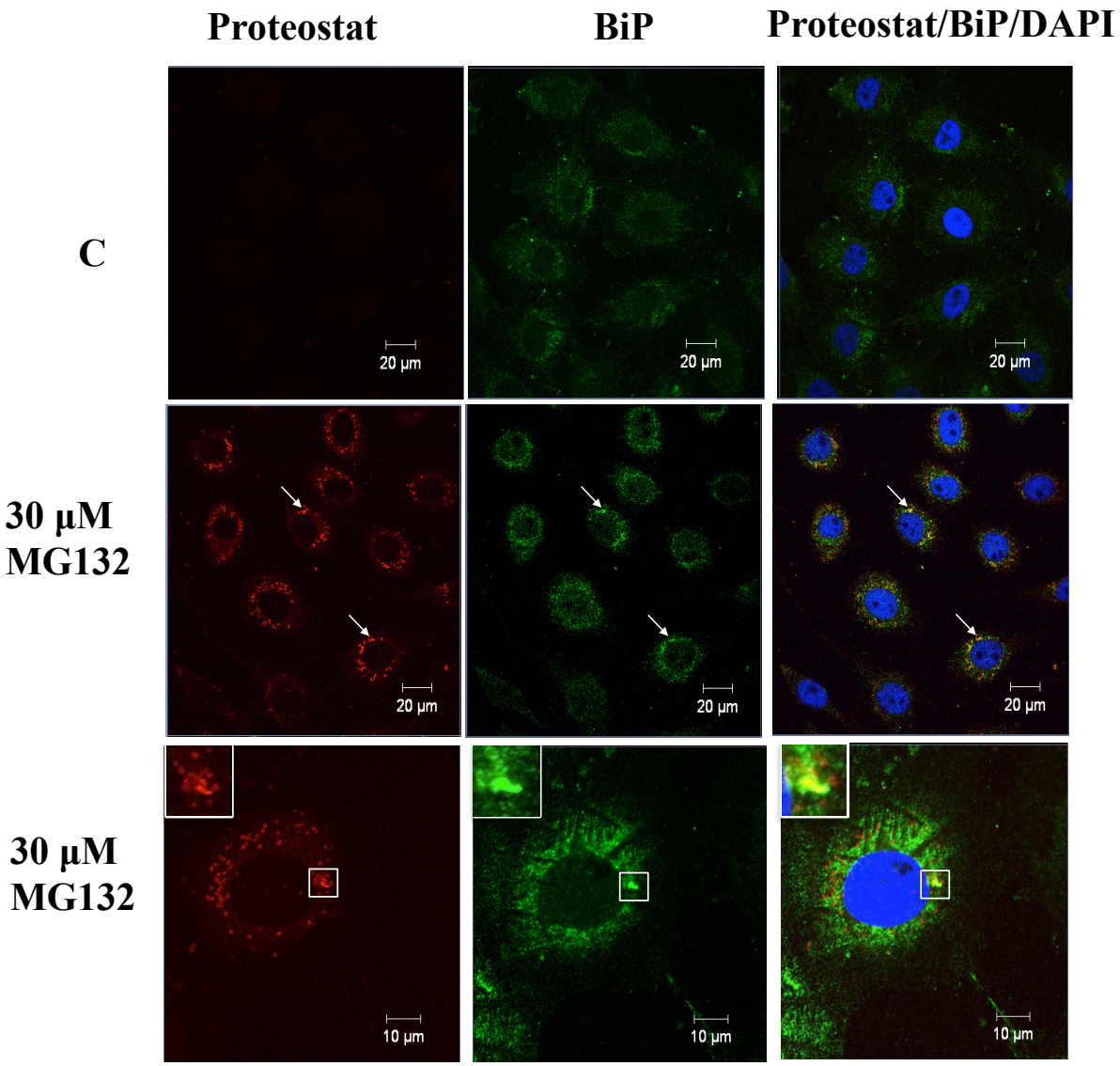
Proteostat
BiP
Proteostat/BiP/DAPI
C
30 µM MG132
30 µM MG132
20 µm
10 µm

Figure 20. Z-stacking analysis of BiP and Proteostat dye-stained complexes in cells treated with cadmium chloride or MG132. Cells were grown on glass coverslips with L-15 media at 22 °C. Cells were maintained at 22 °C (C) or treated with either 200 μM cadmium chloride or 30 μM MG132 for 12 h at 22 °C. The Proteostat detection kit was employed to detect aggregated protein. Nuclei were stained with DAPI (blue). BiP was detected with the anti-BiP antibody and the secondary antibody conjugate, Alexa Fluor 488 (green). The 10 μm white scale bars are indicated at the bottom right corner of each panel. Images A to D display merged images of Proteostat dye, anti-BiP antibody and DAPI with z-stack planes separated by 1 μm. White boxes indicate examples of large aggregated protein/BiP containing structures. Enlarged white boxes of these structures are shown in the top right corner of each panel.

200 µM Cd

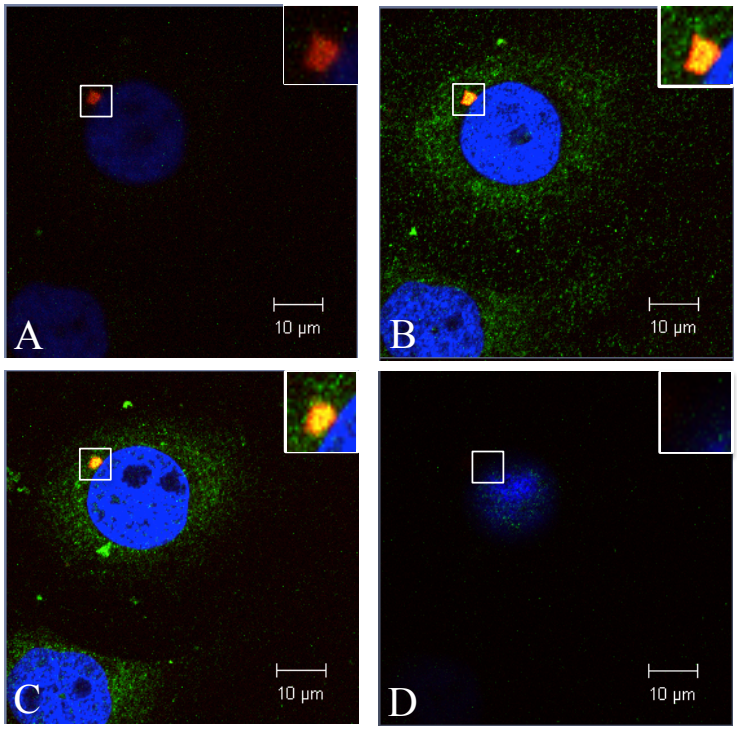

30 µM MG132

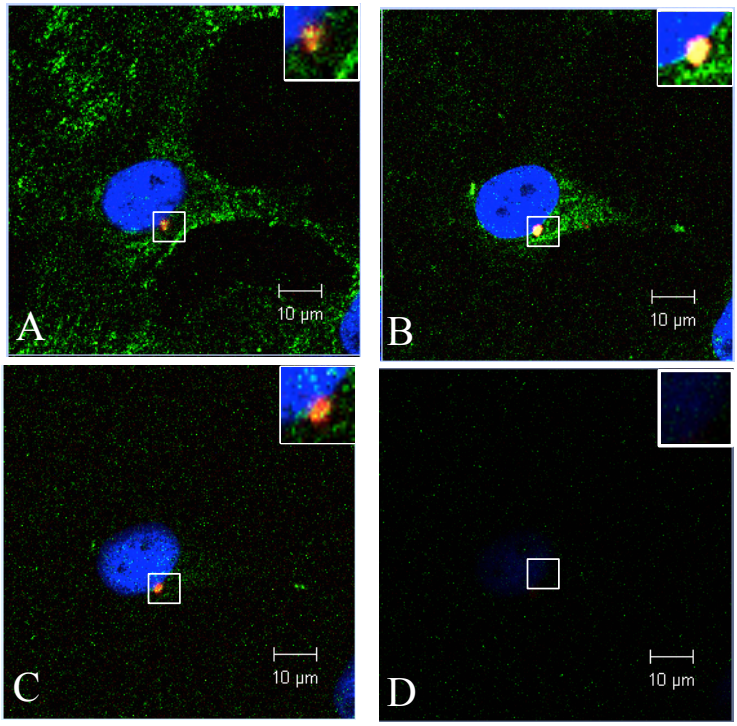

Previously, our laboratory determined that elevation of the incubation temperature enhanced the extent of cadmium chloride-induced *hsp70* gene expression in A6 cells (Woolfson & Heikkila, 2009). In the present study, the same protocol was used to examine the effect of 100 μM cadmium chloride at either 22 °C or 30 °C for 5 h on BiP accumulation in A6 cells. Immunoblot and densitometric analyses revealed that treatment of A6 cells with 100 μM cadmium chloride at 30 °C produced a 60% increase in BiP accumulation relative to cadmium chloride treatment at 22 °C or with 30°C alone (Figure 21). Immunocytochemical analysis revealed similar patterns of BiP accumulation in cells maintained at 22 °C or 30 °C in addition to cells treated with cadmium chloride at 22 °C (Figure 22). BiP accumulation in cells treated with cadmium chloride at 30°C was enriched next to the nucleus and included the presence of relatively large anti-BiP staining structures, approximately 1-2 μM in diameter, in 10% of the cells. Examination of cells treated with cadmium chloride at 30 °C revealed increased actin cytoskeleton disorganization in cells compared to control or with individual stressors of either 30 °C or 100 μM cadmium chloride. As shown in Figure 23, the relatively large anti-BiP staining structures induced by the combined stressors were also stained with the Proteostat dye and appeared yellow/orange in color in the merged image. Analysis of individual z-planes by confocal microscopy determined that these structures contained co-localized aggregated protein and BiP (red/orange) in its core as well as aggregated protein at the periphery (data not shown).

3.9 DL-Buthionine sulfoximine enhances cadmium-induced BiP accumulation in A6 cells

Figure 21. Comparison of BiP accumulation in cells subjected to cadmium chloride treatment at 22 or 30 °C. Cells were maintained in media at 22 °C or subjected to either a 100 μM cadmium chloride treatment at 22 °C or 30 °C for 5 h. **A**) Immunoblot analysis performed as stated in the Materials and Methods section with anti-BiP, anti-HSP70 or anti-actin antibodies. These results are representative of at least 3 separate experiments. **B**) Densitometric analysis of BiP and HSP70 accumulation. The results were expressed as % mean relative density. The error bars indicate standard error of the mean. The significance ($p < 0.05$) relative to control was determined by the one-way ANOVA test and Tukey's post-hoc test and represented by an asterisk. These results were obtained from 3 separate experiments.

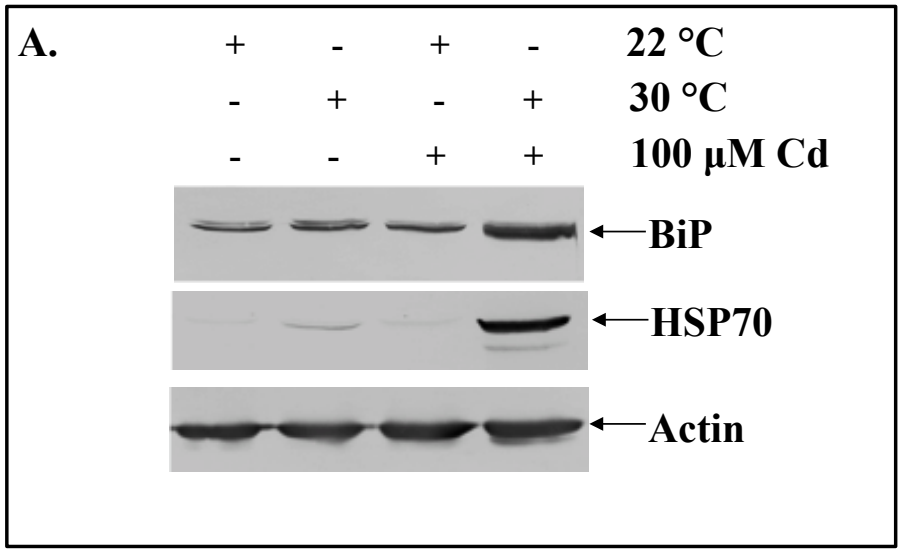
A.
+ - + - 22 °C
- + - + 30 °C
- - + + 100 µM Cd
BiP
HSP70
Actin

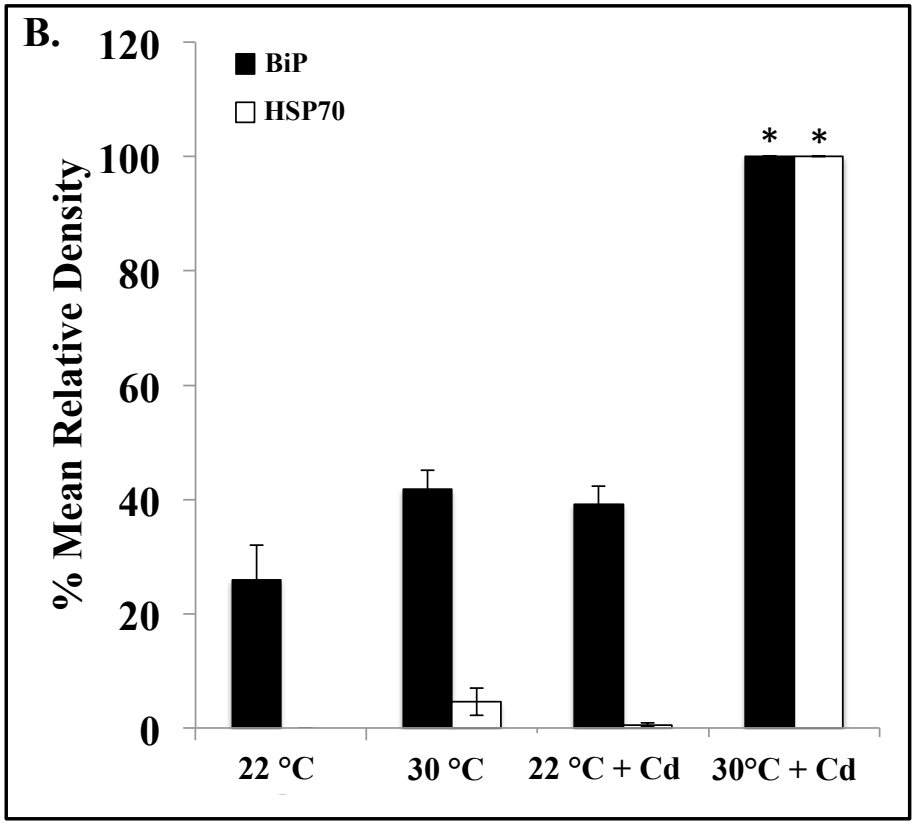
B.
BiP
HSP70
% Mean Relative Density
120
100
80
60
40
20
0
* *
22 °C
30 °C
22 °C + Cd
30°C + Cd

Figure 22. Intracellular localization of BiP in A6 cells treated with 100 cadmium chloride at 30 °C for 5 h. Cells were grown on glass coverslips with L-15 media at 22 °C. Cells were maintained at 22 °C or subjected to either a 100 μM cadmium chloride treatment at 22 °C or 30 °C for 5 h. Actin and nuclei were stained with TRITC (red) and DAPI (blue), respectively. BiP was detected with anti-BiP antibody and the secondary antibody conjugate, Alexa Fluor 488 (green). The 20 μm white scale bars are indicated at the bottom right corner of each panel. Examples of disruptions found in the actin cytoskeleton are indicated by asterisks. White arrows point to examples of large anti-BiP antibody staining structures. These results are representative of at least 2 separate experiments.

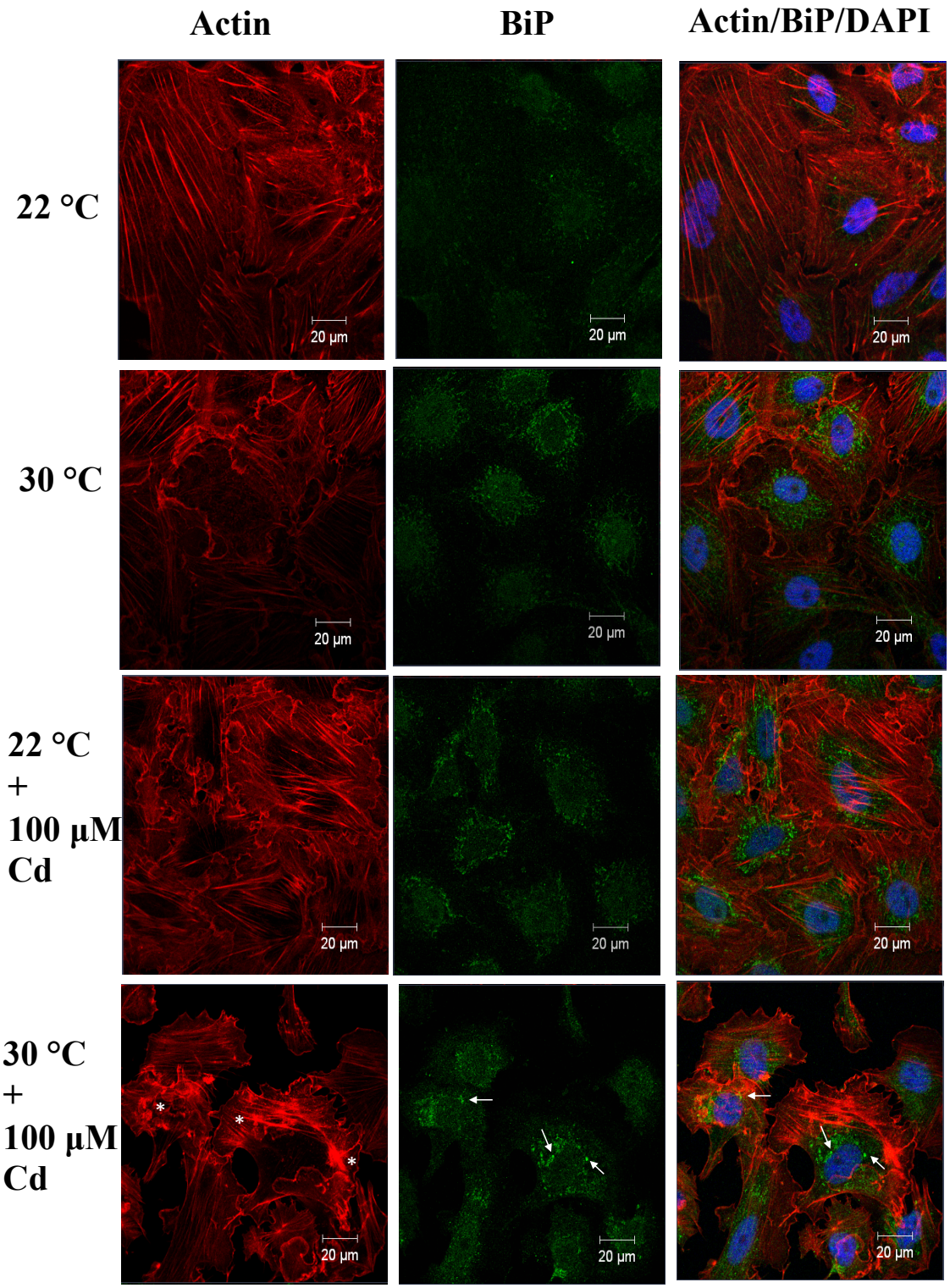
Actin
BiP
Actin/BiP/DAPI
22 °C
30 °C
22 °C + 100 µM Cd
30 °C + 100 µM Cd
20 µm

Figure 23. Co-localization of Proteostat dye with large BiP complexes in cells treated with 100 cadmium chloride at 30 °C for 5 h. Cells were grown on glass coverslips with L-15 media at 22 °C. Cells were maintained at 22 °C or subjected to either a 100 μM cadmium chloride treatment at 22 °C or 30 °C for 5 h. The Proteostat detection kit was employed to detect aggregated protein. Nuclei were stained with DAPI (blue). BiP was detected with anti-BiP antibody and the secondary antibody conjugate, Alexa Fluor 488 (green). The 20 μm white scale bars are indicated at the bottom right corner of each panel. White arrows and boxes indicate examples of complexes detected by Proteostat dye, anti-BiP antibody staining or both. In the bottom row, enlargements of the white boxes are located in the top left corner of the panels. These results are representative of at least 3 separate experiments.

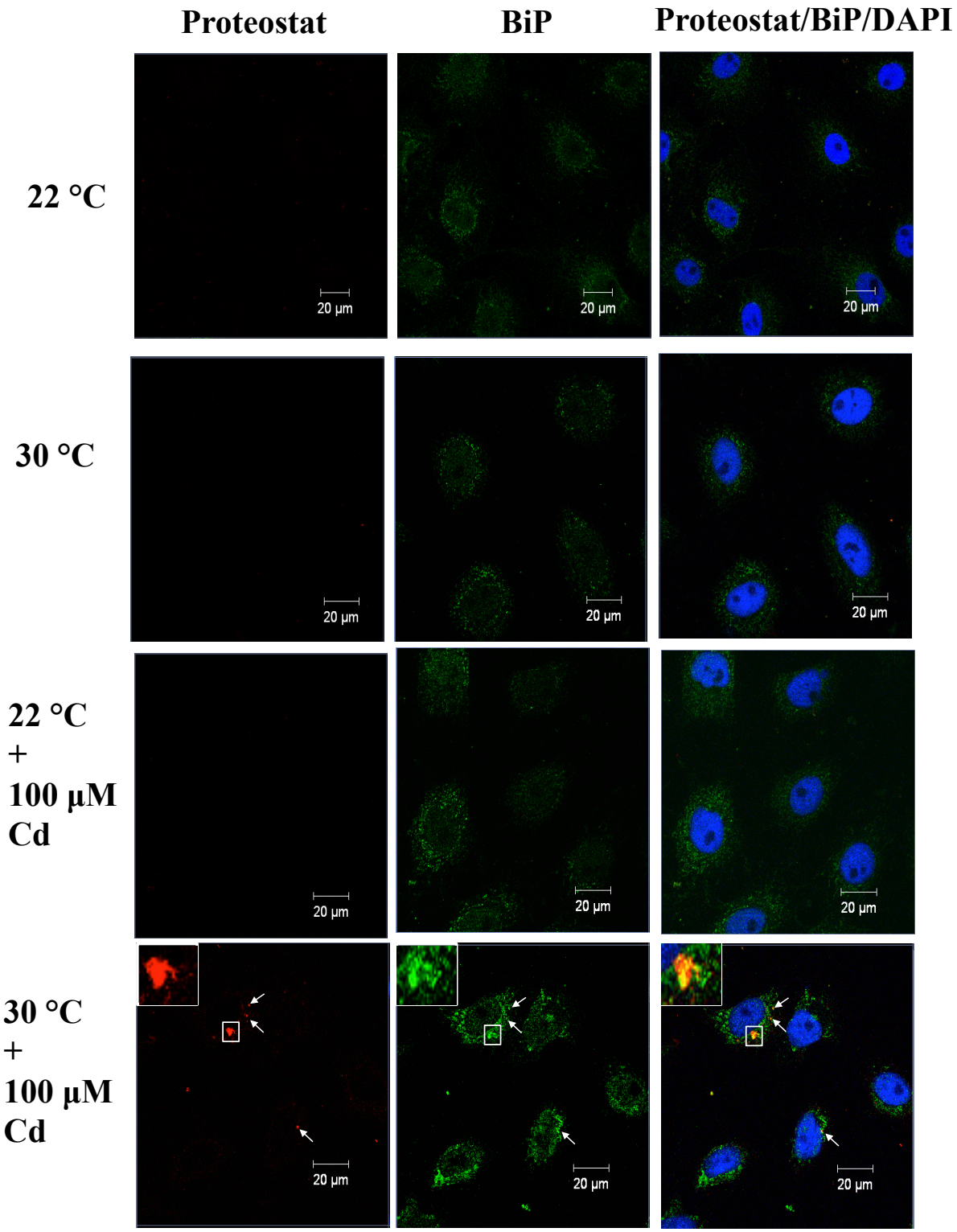
Proteostat
BiP
Proteostat/BiP/DAPI
22 °C
30 °C
22 °C + 100 µM Cd
30 °C + 100 µM Cd
20 µm

In the present study, the effect of DL-buthionine sulfoximine (BSO) on cadmium-induced BiP accumulation was examined in A6 cells. BSO, a glutathione synthesis inhibitor, has been reported to deplete intracellular glutathione and enhance ROS in mammalian, fish and plant cell cultures (Reese & Wagner, 1987; Abe et al., 1994; Babich et al., 1993; Beyersemann & Hechtenberg, 1997; Galan et al., 2001; Abdelhamid & El-kadi, 2015; Chen et al., 2015). Furthermore, previous studies demonstrated decreased levels of cytosolic glutathione in *X. laevis* oocytes and spermatogenic cells treated with BSO (Li et al., 1989; Kannan et al., 1996; Kannan et al., 1998; Tong et al., 2015). Since previous studies have indicated that cadmium chloride can also decrease levels of intracellular glutathione, it was hypothesized that ROS may enhance this effect leading to the unfolded protein response and increased BiP accumulation (Abe et al., 1994; Beyersemann & Hechtenberg, 1997; Galan et al., 2001; Liu et al., 2009; Chen et al., 2015). In the present study, A6 cells were pretreated with 10 mM BSO, a concentration of BSO previously used in studies examining glutathione uptake in *X. laevis* oocytes (Keenan et al., 1996; Kannan et al., 1998), for 4 h before a co-treatment with 100 μM cadmium chloride for 16 h. As shown in Figure 24, cells treated with BSO plus cadmium had a 40% increase in BiP and a 42% increase in HSP70 accumulation compared to values found with cells treated with cadmium chloride alone. Immunocytochemical analysis revealed that treatment of A6 cells with BSO had a similar granular BiP staining pattern compared to control (Fig. 25). Treatment of cells with 100 μM cadmium chloride had a more intense anti-BiP antibody staining pattern in the perinuclear region compared to control. However, exposure of cells to both BSO and cadmium chloride displayed the presence of relatively

Figure 24. Enhanced accumulation of cadmium chloride-induced BiP in A6 cells treated with DL-buthionine-L-sulfoximine (BSO). Cells were incubated at 22 °C with media (C) or pre-treated with 10 mM BSO for 4 h before adding 100 μM cadmium chloride for 16 h. **A**) Immunoblot analysis performed as stated in the Materials and methods section with anti-BiP, anti-HSP70 or anti-actin antibodies. **B**) Densitometric analysis of BiP and HSP70 accumulation. The results were expressed as % mean relative density. The error bars indicate standard error of the mean. The significance ($p < 0.05$) relative to control was determined by the one-way ANOVA test and Tukey's post-hoc test and represented by an asterisk. These results were obtained from 3 separate experiments.

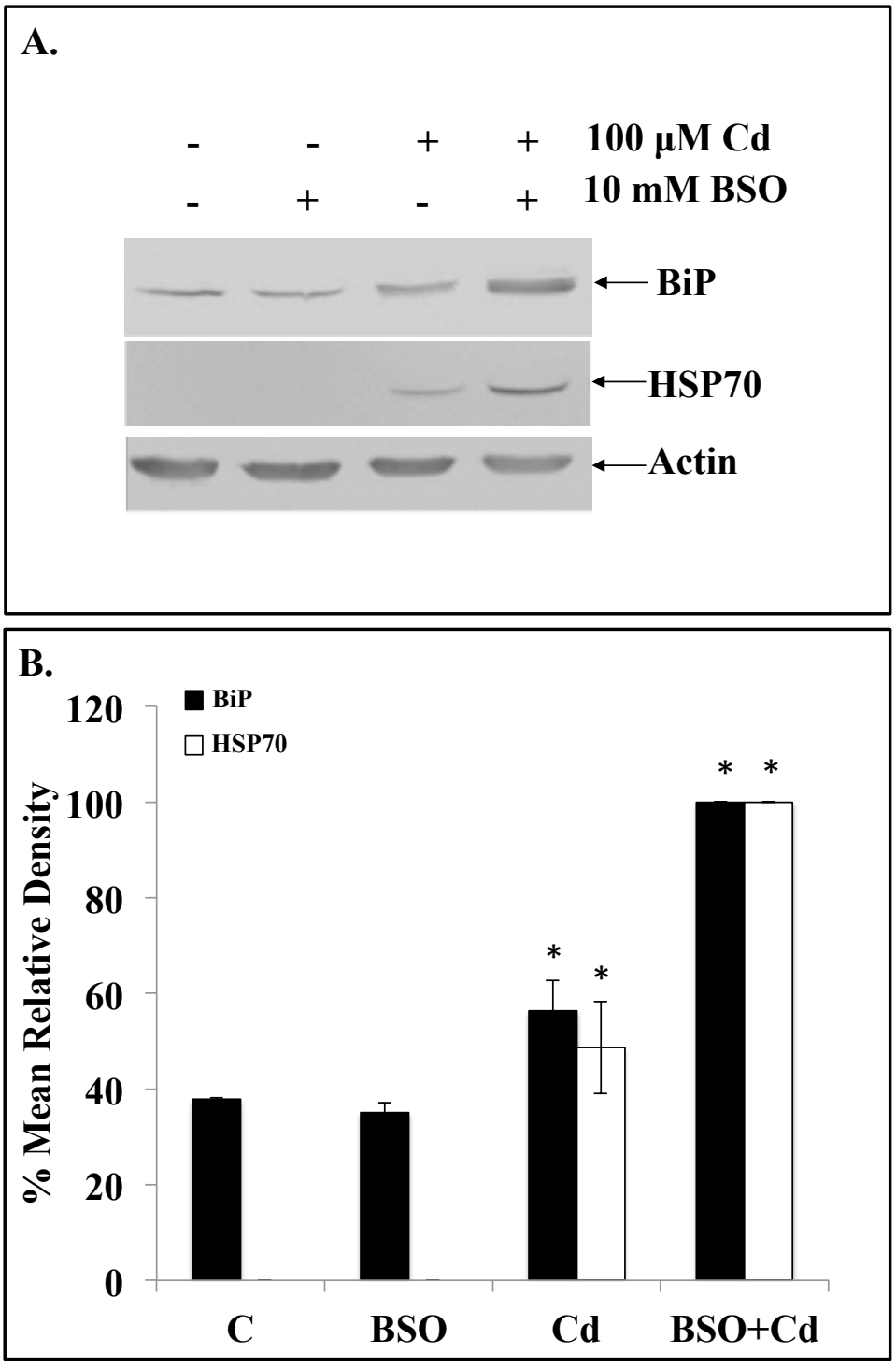
A.
- - + + 100 µM Cd
- + - + 10 mM BSO
BiP
HSP70
Actin
B.
BiP
HSP70
% Mean Relative Density
120
100
80
60
40
20
0
* *
* *
C
BSO
Cd
BSO+Cd

Figure 25. Localization of BiP in A6 cells subjected to simultaneous DL-buthionine-sulfoximine and cadmium chloride treatment. Cells were grown on glass coverslips with L-15 media at 22 °C. Cells were maintained at 22 °C (C) or pretreated for 4 h with 10 mM BSO before incubation with 100 μM cadmium chloride for 16 h at 22 °C. Actin and nuclei were stained with TRITC (red) and DAPI (blue), respectively. BiP was detected with anti-BiP antibody and the secondary antibody conjugate, Alexa Fluor 488 (green). The 20 μm white scale bars are indicated at the bottom right corner of each panel. Examples of disruptions found in the actin cytoskeleton are indicated by asterisks.

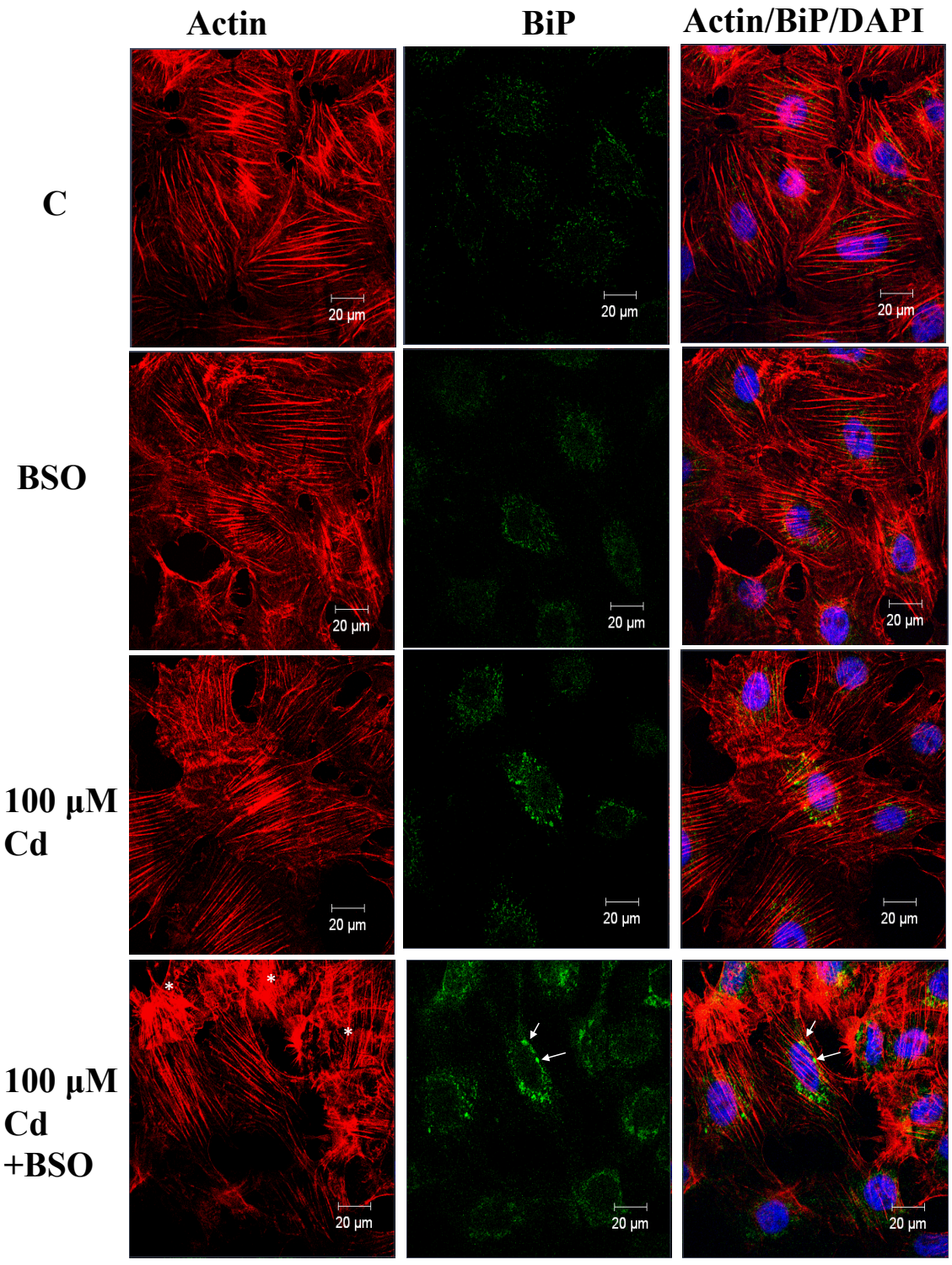
Actin
BiP
Actin/BiP/DAPI
C
BSO
100 µM Cd
100 µM Cd +BSO
20 µm

large BiP structures (approximately 1-2 μm in diameter) in approximately 8% of the cells. As shown in Figure 26, the large anti-BiP antibody staining structures co-localized with the Proteostat dye in cells treated with BSO and cadmium chloride, which revealed yellow/orange structures in the merged image (see white boxes in bottom row). A more detailed analysis of these structures revealed the presence of BiP in the core of these particles with aggregated protein components at the periphery similar to the BiP/aggregated protein structures observed in cells treated with 200 μM cadmium chloride, 30 μM MG132 and 100 μM cadmium chloride at 30 °C (data not shown). Cells treated with both BSO and cadmium chloride displayed areas of actin cytoskeleton disorganization. Additional immunocytochemical experiments determined that treatment of cells with 150 μM cadmium chloride resulted in the formation of large anti-BiP antibody stained structures (Fig. 27). However, these structures were not observed in cells given BSO pretreatment prior to incubation with 150 μM cadmium chloride. An increase in actin disorganization was displayed in cells treated with 150 μM cadmium chloride, which was further enhanced in cells treated with both cadmium chloride and BSO. As shown in Figure 28, the large anti-BiP antibody staining structures observed in cells treated with 150 μM cadmium chloride co-localized with the Proteostat dye stained aggregated protein (see white arrows). Finally, A6 cells incubated with 200 μM cadmium chloride plus BSO for 16 h were not examined since the cells were unable to adhere to the glass coverslips during the treatment (data not shown).

Figure 26. Co-localization Proteostat dye-stained structures with large BiP containing complexes in cells treated with 100 µM cadmium chloride plus BSO. Cells were grown on glass coverslips with L-15 media at 22 °C. Cells were maintained at 22 °C (C) or pre-treated with or without 10 mM BSO for 4 h before adding media with and without 100 µM cadmium for 16 h. The Proteostat detection kit to detect aggregated protein was used according to the manufacter's instructions. Nuclei were stained with DAPI (blue). BiP was detected with the anti-BiP antibody and the secondary antibody conjugate, Alexa Fluor 488 (green). The 20 µm white scale bars are indicated at the bottom right corner of each panel. White arrows and boxes indicate examples of large complexes detected by Proteostat dye, anti-BiP antibody staining or both. Enlargements of the white boxes are shown at top left corner of the panels in the bottom row. These results are representative of at least 3 separate experiments.

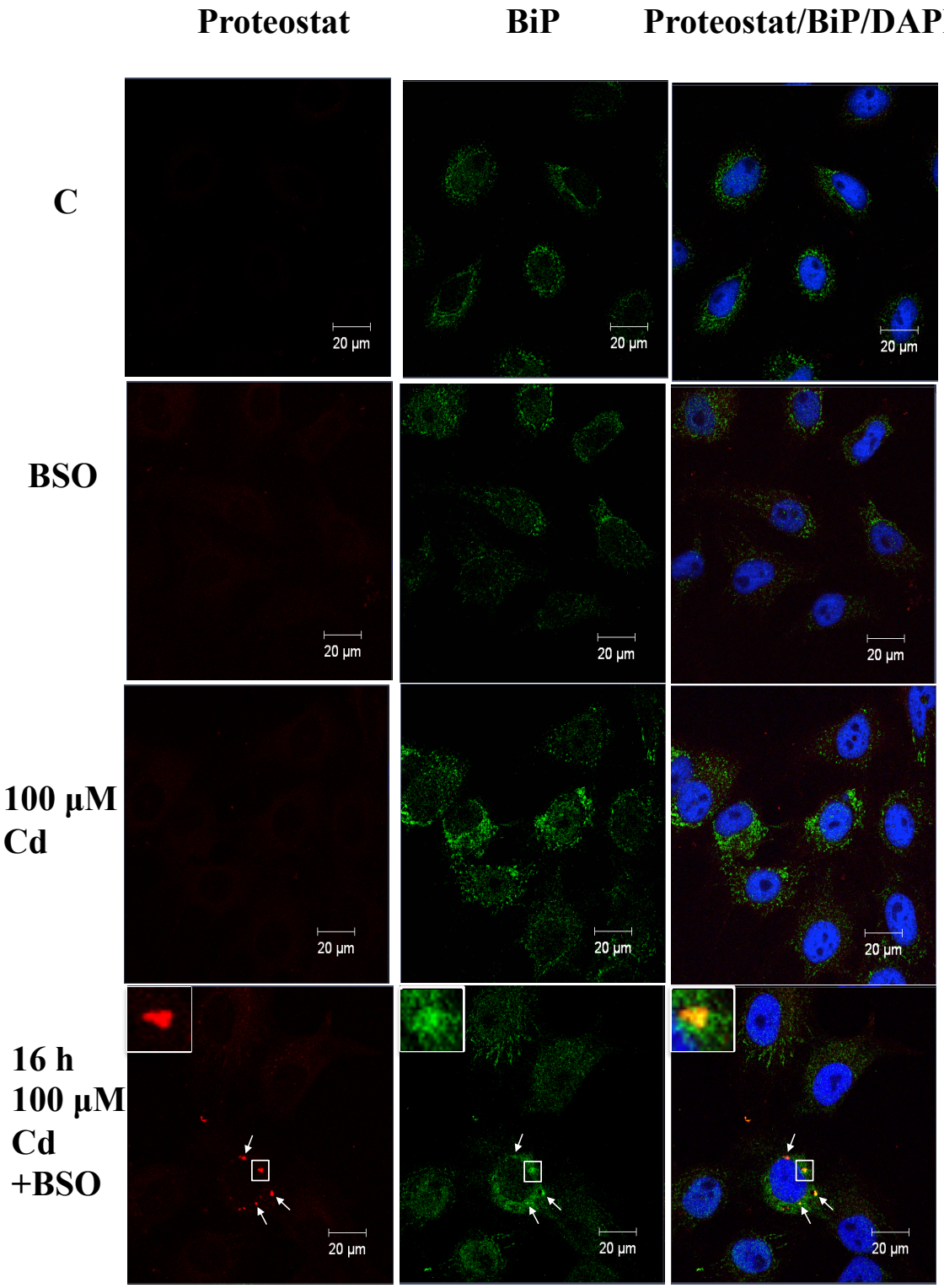
Proteostat
BiP
Proteostat/BiP/DAPI
C
BSO
100 µM Cd
16 h 100 µM Cd +BSO
20 µm

Figure 27. Intracellular localization of BiP in A6 cells treated with 150 µM cadmium chloride plus BSO. Cells were grown on glass coverslips with L-15 media at 22 °C. Cells were maintained at 22 °C (C) or pretreated for 4 h with 10 mM BSO before incubation with 150 µM cadmium chloride for 16 h at 22 °C. Actin and nuclei were stained with TRITC (red) and DAPI (blue), respectively. BiP was detected with anti-BiP antibody and the secondary antibody conjugate, Alexa Fluor 488 (green). The 20 µm white scale bars are indicated at the bottom right corner of each panel. Examples of disruptions found in the actin cytoskeleton are indicated by asterisks. White arrows point to examples of large BiP staining structures. These results are representative of a single experiment.

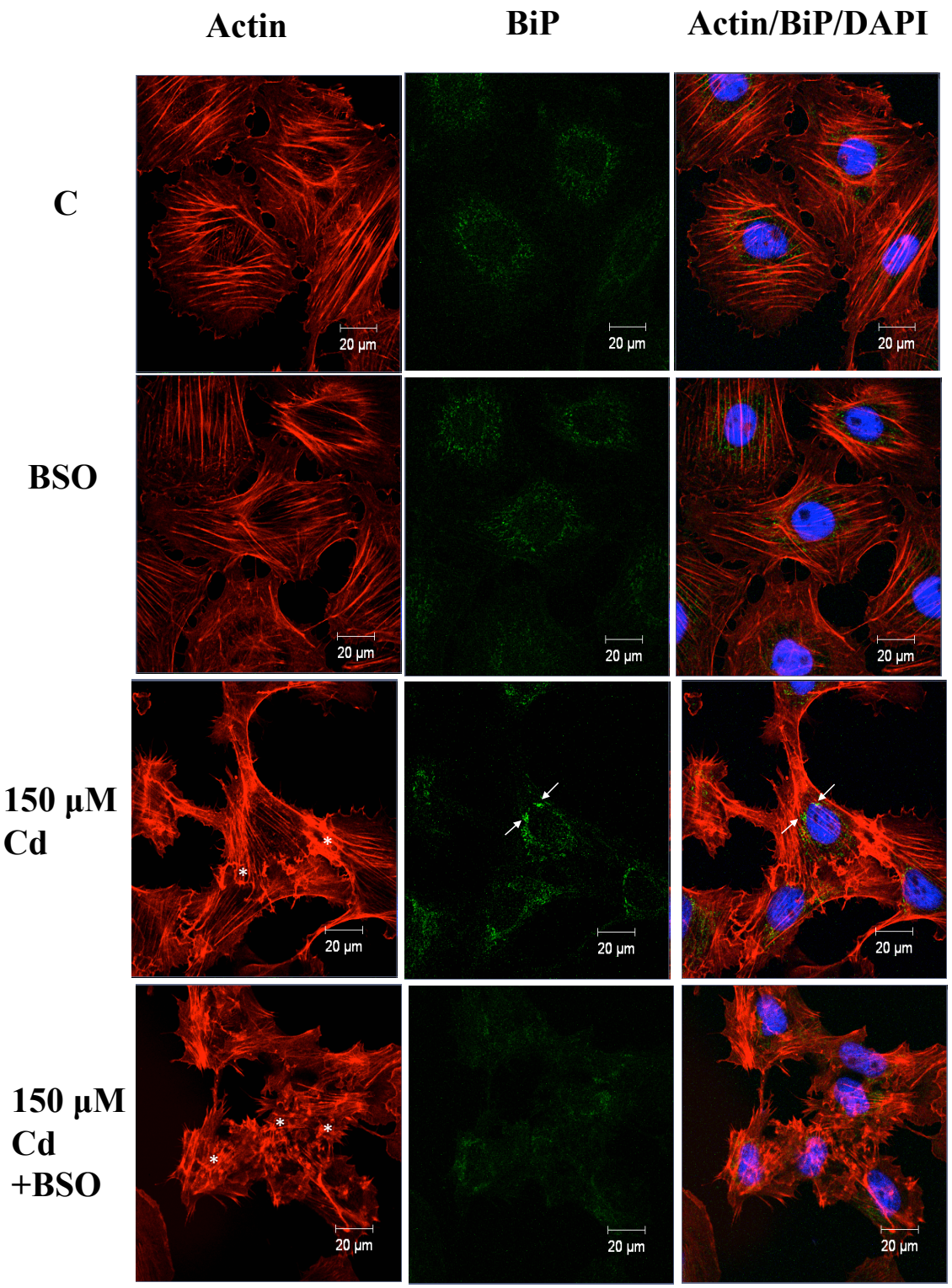
Actin
BiP
Actin/BiP/DAPI
C
BSO
150 µM Cd
150 µM Cd +BSO
20 µm

Figure 28. Effect of BSO on the formation of 150 µM cadmium chloride-induced BiP complexes and their detection with the Proteostat dye. Cells were grown on glass coverslips with L-15 media at 22 °C. Cells were maintained at 22 °C (C) or pre-treated with or without 10 mM BSO for 4 h before adding media with and without 150 µM cadmium for 16 h. The Proteostat detection kit to detect aggregated protein was used according to the manufacter's instructions. Nuclei were stained with DAPI (blue). BiP was detected with anti-BiP antibody and the secondary antibody conjugate, Alexa Fluor 488 (green). White arrows indicate examples of large complexes detected by Proteostat dye, anti-BiP antibody staining or both. The 20 µm white scale bars are indicated at the bottom right corner of each panel. These results are representative of at least 2 separate experiments.

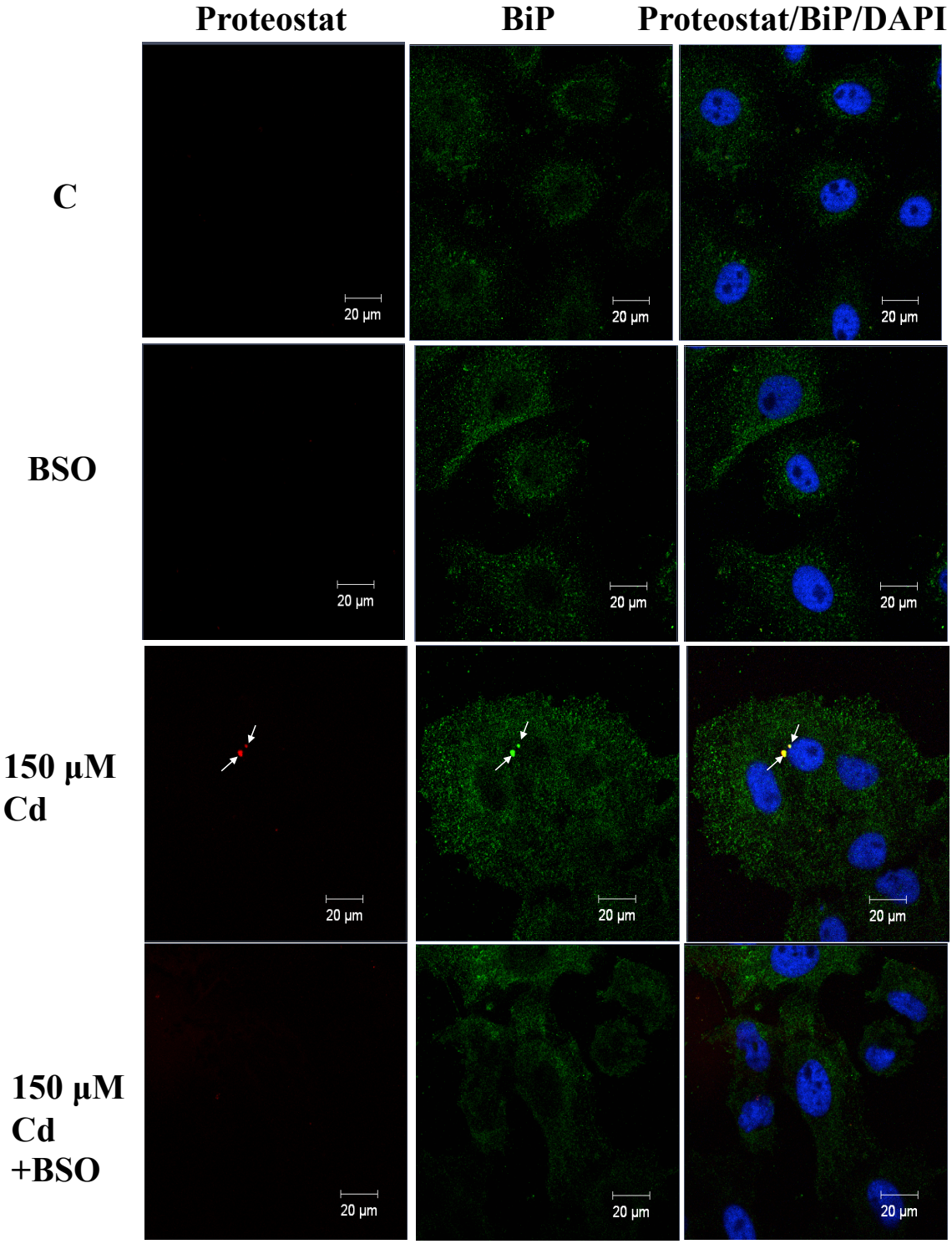
Proteostat
BiP
Proteostat/BiP/DAPI
C
BSO
150 µM Cd
150 µM Cd +BSO
20 µm

4.0 Discussion

The present study has characterized, for the first time in *X. laevis*, cadmium chloride-induced accumulation of BiP. Initial studies compared the amino acid sequence of *X. laevis* BiP with newly available BiP sequence information from other vertebrates that were not available when the *bip* gene was originally isolated (Beggah et al., 1996; Miskovic et al., 1997). Alignment of the *X. laevis* BiP amino acid sequence with BiP proteins from various organisms indicated it had 98% identity with *X. tropicalis* BiP in addition to having more than 90% identity with BiP from selected mammals, birds, reptiles and fish. Interestingly, *X. laevis* BiP only shared 63% and 62% identity with *X. laevis* HSP70 and HSC70, respectively. These findings support the results of previous studies that found higher conservation of BiP between species compared to BiP and HSP70 family members within the same organism (Haas, 1994; Miskovic et al., 1997; Quinones et al., 2008; Brocchieri et al., 2008). It was suggested that the *bip* gene diverged from other *hsp70* genes with the appearance of the first eukaryotes (Nicholson et al., 1990; Brocchieri et al., 2008).

A pairwise sequence alignment of the BiP amino acid sequence from both *X. laevis* and *H. sapiens* indicated high identity in key regions, such as the nucleotide-binding domain, substrate-binding interface and the KDEL retention sequence. The pairwise sequence alignment suggested conservation of these regions in *X. laevis* BiP and *H. sapiens* BiP. It was reported that three amino acids of the nucleotide-binding domain of *H. sapiens* BiP were involved in ATPase activity, namely Thr-37, Glu-201 and Thr-229 (Gaut & Hendershot, 1993). These three amino acids were present in the *X. laevis* BiP amino acid sequence which suggested functional ATPase activity. A recent study with human BiP determined that the nucleotide-binding domain bound to the lumenal domains of IRE1 and PERK in vitro (Carrara et al., 2015). Given this finding, it is

possible that *X. laevis* BiP could also interact with the lumenal domain of *X. laevis* IRE1 and PERK given the high amino acid identity shared between the nucleotide-binding domain of *X.laevis* and *H. sapiens* BiP in addition to a high identity between *X. laevis* IRE1 (77%) and PERK (79%) with their *H. sapiens* homologs. The presence of a KDEL retention sequence in the C-terminal end of both *X. laevis* and *H. sapiens* BiP is also present in other lumenal ER proteins, such as GRP94 and protein disulfide isomerase (Pagny et al., 1999). Proteins containing a KDEL sequence are retrieved from post-ER compartments, such as the Golgi apparatus, via receptors on the ER (Haas, 1994; Pagny et al., 1999; Young et al., 2013).

Phylogenetic analysis revealed that *X. laevis* BiP grouped more closely with BiP from reptiles, birds and mammals compared to fish. These results are consistent with findings of Brocchieri et al. (2008) in their phylogenetic analysis of BiP from a variety of different organisms. This latter study also determined that during evolution there was an early separation of fish from amphibians, mammals and birds. The separation of fish from tetrapod vertebrates is consistent with the hypothesis that tetrapod vertebrates and fish shared a common ancestor, the lobe-finned fish, at the start of the Devonian period approximately 390 million years ago (Daeschler et al., 2006; Amemiya et al., 2013).

Additional preliminary studies determined that tunicamycin and A23187 treatment of A6 cells induced the accumulation of BiP in contrast to HSP70, which was not detectable. Both tunicamycin and A23187 were previously demonstrated to upregulate A6 cell *bip* gene expression in our laboratory (Winning et al., 1989; Miskovic et al., 1999; Khan et al., 2012). Previous mammalian studies also observed an increase in BiP accumulation in cells treated with A23187 or tunicamycin (Li et al., 1997; Ron & Walter, 2007; Oslowski et al., 2012). Tunicamycin inhibits the initial step of glycoprotein biosynthesis in the ER, which likely causes

an accumulation of unfolded glycoproteins within the ER (Oslowski et al., 2012; Wang et al., 2015). A23187 is a calcium ionophore that depletes calcium stores within the ER lumen, which is thought to alter protein folding and stability leading to an increase in unfolded protein in the ER (Li et al., 1997; Sun et al., 2006). The rise in accumulation of unfolded protein in the ER and not in the cytosol may explain why cells treated with A23187 or tunicamycin had greater BiP accumulation and no detectable increase in HSP70 accumulation.

In addition to tunicamycin and A23187, the present study determined that cadmium chloride treatment of A6 cells enhanced the relative levels of BiP. Furthermore, pre-treatment of A6 cells with actinomycin D or cycloheximide prevented cadmium-induced BiP accumulation in A6 cells. These results support evidence from a mammalian study that examined the effect of actinomycin D and cycloheximide on cadmium-induced BiP in porcine LLC-PK1 cells (Liu et al., 2006). These studies suggest that cadmium-induced BiP accumulation involves de novo transcription and translation. Earlier studies determined that cadmium altered calcium homeostasis, inhibited the proteasome, increased levels of reactive oxygen species (ROS) and caused protein instability by interacting with thiol groups and replacing metal co-factors (Jungmann et al., 1993; Waisberg et al., 2003; Kitamura & Hiramatsu, 2010; Moulis & Thevenod, 2010; Brunt et al., 2012). These various cadmium-induced effects resulted in unfolded protein accumulation in the ER, which can trigger the UPR and upregulate *bip* gene expression (Moulis & Thevenod, 2010). Additionally, these cadmium-induced effects likely resulted in an increase in unfolded protein in the cytosol, which can elicit the HSR and upregulate *hsp70* gene expression. In the current study, analysis of the *X. laevis* BiP promoter region revealed the presence of putative *cis*-regulatory regions such as a TATA box, two endoplasmic reticulum stress elements (ERSE) and three CAAT sites. Multiple sequence

analysis of a segment of the promoter region for *bip* genes from *X. laevis*, *X. tropicalis*, and *H. sapiens* revealed the presence of conserved regulatory elements, namely two CAAT sites and two ERSEs. Previous mammalian studies reported the presence of multiple CAAT sites and ERSEs upstream of a TATA box in mammalian *bip* genes (Yoshida et al., 1998; Roy & Lee, 1999; Beaumeister et al., 2005). Studies with mammalian cells determined that duplicate copies of the ERSE could fully activate the tunicamycin-induced expression of a heterologous promoter fused to a chloramphenicol acetyltransferase (CAT) gene, in a sequence-specific but orientation-independent manner (Roy & Lee, 1999). Furthermore, deletion analysis of a rat BiP promoter region revealed that a CCAAT site and a TATA box were necessary for full constitutive and tunicamycin-inducible expression of a fusion gene microinjected into *X. laevis* embryos (Winning et al., 1992). This latter study suggested a conservation of *cis*-regulatory elements in rat and *X. laevis* BiP promoter regions. Given these findings, it is possible that the ERSE and CCAAT sites detected in the promoter region of *X. laevis* BiP are required for cadmium chloride-induced expression.

In *X. laevis* A6 cells, the magnitude of cadmium chloride-induced BiP protein accumulation was concentration-dependent. For example, treatment of A6 cells with 100 μM cadmium chloride enhanced BiP accumulation with maximal accumulation at 200 μM. Previous studies reported a cadmium chloride concentration-dependent increase in BiP accumulation in chicken hepatocytes and LLC-PK1 renal epithelial cells (Shao et al., 2014). In the present study, cadmium chloride also induced HSP70 and HO-1 protein accumulation in a concentration-dependent manner, which was consistent with our previous findings (Woolfson & Heikkila, 2009; Music et al., 2014). Increased HO-1 accumulation was first detected in A6 cells treated with 25 μM cadmium chloride, which suggests that the activation pathway for HO-1 expression

was more sensitive to a lower concentration of cadmium compared to the activation pathways for HSP70 or BiP expression. It is possible that treating A6 cells with 25 μM cadmium chloride for 14 h increased levels of ROS, which modified cysteine residues on KEAP-1 and increased levels of NRF2 in the nucleus to activate HO-1 expression. Furthermore, A6 cells treated with 400 μM cadmium chloride displayed a decrease in relative levels of BiP, HSP70 and HO-1 compared to 200 μM. The decrease in stress protein accumulation at relatively high levels of cadmium chloride may be due to an inhibition of protein synthesis, which has been reported in other systems (Gamulin & Narancsik, 1982; Ovelgonne et al., 1995; Smalinskiene et al., 2005).

In time course studies, continuous exposure of A6 cells to cadmium chloride resulted in an increased accumulation of BiP over a 24-hour period. These findings are of interest since previous studies demonstrated that cadmium accumulated in kidney cells in a time-dependent manner in a variety of organisms including frogs (Goering et al., 1993; Vogiatzis & Lombourdis, 1997; Barbier et al., 2004; Simoncelli et al., 2015). Time-dependent accumulation of cadmium chloride-induced BiP accumulation was reported in porcine LLC-PK1 renal epithelial cells and plant cells (Liu et al., 2006; Yokouchi et al., 2007; Xu et al., 2013). An increase in BiP accumulation over time is likely due to elevated levels of intracellular cadmium and its effects on ER proteostasis leading to a prolonged UPR (Liu et al., 2006; Yokouchi et al., 2007; Xu et al., 2013).

The present study also observed a transient increase in BiP levels during recovery of A6 cells from an 8 h exposure to cadmium chloride. It is possible that intracellular cadmium present within the cell after 8 h continues to exert its proteotoxic stress within the ER. The presence of elevated levels of BiP even after 48 and 72 h of recovery may be due, at least in part, to a reduction in the rate of its degradation. This possibility is viable given that previous studies in

our laboratory have shown that cadmium chloride treatment can inhibit the ubiquitin proteasome system that may be involved in BiP degradation (Brunt et al., 2012). Additionally, previous studies have reported the half-life of mouse and human BiP to be approximately 28 to 33 h (Gulow et al., 2002). It is possible that *X. laevis* BiP also has a long half-life, which could partly explain BiP remaining elevated during recovery. Transient increases in the relative levels of HSP70 and HO-1 were also detected, which is consistent with previous work in our laboratory (Woolfson & Heikkila, 2009; Music et al., 2014). It is possible HSP70 was being degraded by the proteasome during recovery since HSP70 has been previously reported to be degraded by the proteasome in A6 cells recovering from heat stress (Khan & Heikkila, 2014). HO-1

Immunocytochemical and LCSM studies of A6 cells determined that cadmium chloride- and MG132-induced BiP accumulation was enriched in the perinuclear region compared to control and that it occurred in a punctate pattern. Previous immunocytochemical studies performed in our laboratory also reported the perinuclear enrichment of BiP in a punctate pattern in A6 cells treated with A23187 and the proteasomal inhibitors, withaferin A and MG132 (Khan et al., 2012). Additionally, mammalian immunocytochemical studies have reported the enriched perinuclear accumulation of BiP in mouse pancreatic β-cells treated with tunicamycin (Kitiphongspattana et al., 2005). Furthermore, approximately 10% of cells treated with 200 μM cadmium chloride or with 30 μM MG132 contained relatively large anti-BiP antibody staining structures that co-localized with complexes that were also stained with the Proteostat dye. This latter result was confirmed by Z-stacking analysis, which verified that BiP was enriched within Proteostat-stained structures. It is possible that these cadmium chloride- or MG132-induced large aggregate-like structures may be aggresomes. Aggresomes are large microtubule-dependent perinuclear inclusion bodies wrapped in a vimentin cage that can develop in the cytoplasm as a

result of an overwhelmed or inhibition of the UPS with agents like MG132 (Johnston et al., 1998; Kopito, 2000; Bauer & Richter-Landsberg, 2006; Bolhuis & Richter-Landsberg, 2010; Shen et al., 2011; Ito et al., 2012; Taylor et al., 2012; Bang et al., 2014; Corchero et al., 2016). In previous studies, our laboratory reported the presence of MG132-induced aggresome-like complexes that co-localized with the small HSP, HSP30, in A6 cells (Khan et al., 2015). It has been suggested that cadmium-induced formation of aggresomes in human embryonic kidney 293 cells resulted from valosin-containing protein interacting with HDAC6, which directs ubiquitinated protein to aggresomes (Song et al., 2008). It is possible that a similar phenomenon occurs in *Xenopus* A6 cells since our laboratory has shown that cadmium chloride induced the inhibition of the UPS (Brunt et al., 2012; Khamis et al., 2013). Given these previous and current findings, it is possible that the inhibition and/or overwhelming of the UPS by cadmium chloride or MG132 in A6 cells could promote aggresome formation, possibly facilitated by retrograde transportation of BiP from the ER to the cytoplasm, in order to sequester toxic protein aggregates in the cytoplasm (Johnston et al., 1998; Garcia-Matas et al., 2002; Bagola et al., 2008). In support of this possibility BiP was detected in the core of aggresome-like structures in human embryonic cells overexpressing mutant Huntingtin protein (Waelter et al., 2001; Garcia-Matas et al., 2002).

Aggresomes have been previously reported to associate in close proximity with the microtubule-oragnizing center, also known as the centrosome (Garcia-Mata et al., 1999). It is possible BiP may be associating with the centrosome since the size and location of the BiP structures appear similar to HSP70 structures that have been previously been reported to co-localize with centrosomes in mammalian cells under heat stress (Hut et al., 2005). It is also

possible that BiP may be associating with both a centrosome and aggressome. However, further analysis is required to locate the centrosome in relation to the BiP structures.

It is also possible that these Proteostat dye and anti-BiP antibody staining complexes detected in A6 cells treated with cadmium chloride or MG132-treated cells are endoplasmic reticulum-associated compartments (ERACs; Huyer et al., 2004). ERACs are tubular-vesicles directly connected to the ER that have been observed in yeast cells overexpressing protein that misfolds and aggregates within the ER (Huyer et al., 2004). ERACs localize next to the nucleus and have been associated with BiP (Huyer et al., 2004, Bagola & Sommer, 2008). It is possible that protein unfolding and aggregation induced by cadmium and MG132 is sequestered in ERACs, which are facilitated by BiP, to protect the ER from toxic protein aggregates.

The treatment of A6 cells with 100 μM cadmium chloride at 30 °C for 5 h resulted in increased BiP accumulation in A6 cells compared to the stressors individually. Also, immunocytochemical analysis revealed the presence of large anti-BiP antibody stained structures that co-localized with the Proteostat dye. Previously our laboratory documented a synergistic increase in HSP30 and HSP70 accumulation in A6 cells subjected to 100 μM at 30 °C for 5 h (Woolfson & Heikkila, 2009; Khamis & Heikkila, 2013). The mechanism for increased accumulation of BiP in A6 cells treated with cadmium at elevated temperature is not known. Previous studies revealed that the cellular uptake of cadmium increased with increasing temperature in planktonic crustaceans and human hepatic cells (Souza et al., 1997; Heugens et al., 2003). It is possible that enhanced cadmium uptake in A6 cells treated at 30°C could result in an increased accumulation of unfolded protein in the ER, which activates the UPR and enhances BiP accumulation as well as inhibition of the ubiquitin- proteasome system which could result in the formation of aggresomes.

Finally, the present study examined the effect of BSO, an inhibitor of γ-glutamylcysteine synthetase, which is required for glutathione synthesis, on cadmium chloride-induced BiP accumulation (Griffith, 1982; Montero & Jassem, 2011). Previous studies found that mammalian and plant cells treated with BSO had lowered intracellular levels of glutathione, which increased sensitivity to cadmium stress (Abe et al., 1994; Galan et al., 2001; Waisberg et al., 2003; Mah & Jalilehvand, 2010; Chen et al., 2015). Additionally, depleted levels of glutathione were reported in *X. laevis* oocytes and spermatogenic cells treated with BSO (Kannan et al., 1996; Kannan et al., 1998; Tong et al., 2015). In the present study, A6 cells pretreated with BSO enhanced the effect of 100 μM cadmium chloride on BiP accumulation and the formation of aggresome-like structures. This is the first study to report the increased levels of BiP in cells treated with cadmium and BSO. Previous studies have reported an increase in HSP70 accumulation in human promonocytic cells and human amniotic WISH cells pretreated with BSO plus a treatment with a low concentration of cadmium (Abe et al., 1994; Galan et al., 2001). It is possible that a BSO pretreatment lowered the intracellular glutathione concentration in A6 cells, which sensitized them to cadmium chloride-induced oxidative stress, leading to an increase in the accumulation of unfolded protein and activation of the UPR. Furthermore, it is possible that the combination of BSO-induced glutathione depletion and cadmium chloride stimulated oxidative stress resulted in UPS inhibition and sequesteration of toxic protein aggregates in the form of aggresomes.

In the present study, it should be pointed out that a portion of the cadmium chloride- or MG132-induced anti-BiP antibody stained complexes did not co-localize with the Proteostat dye. It is possible that these BiP structures may have been large BiP oligomers, which do not display chaperone activity (Preissler et al., 2015). While the precise reason is not known, further analysis

may determine if the large anti-BiP antibody staining structures interact with unfolded rather than aggregated ER protein.

This study is of significance since it is the first study to examine cadmium-induced BiP in a poikilothermic vertebrate. Basic information on cadmium-induced BiP in *X. laevis* is important given that amphibians are considered sentinel species for environmental contaminants (Burggren & Warburton, 2007). Furthermore, the findings in this study suggest that BiP levels or the detection of aggregated protein may be used as biomarkers for cadmium exposure in amphibians. The techniques developed in this study may be applicable for use in cells and tissues derived from aquatic vertebrates found in North America (e.g. Rana catesbeiana). This study may also advance our understanding of the cytoxicity of cadmium telluride nanoparticles, which have been recently reported to activate the UPR in human umbilical cord epithelial cells (Yan et al., 2016). In addition, the detection of protein aggregates that associate with BiP in cadmium-treated A6 cells may provide insight into neurodegenerative diseases that have been associated with chronic cadmium exposure.

It is not known if other molecular chaperones are associated with the cadmium chloride-induced BiP-containing aggresomal structures. It is possible that HSP30 may be present since it was shown previously to associate with cadmium chloride-induced aggregates (Khan et al., 2015). Future studies examining the possible co-localization of HSP30 and BiP accumulation may shed light on this question. The effect of other stressors on BiP accumulation could also be examined, such as sodium arsenite and Withaferin A. Very little research has been devoted to an analysis of cadmium chloride-induced association of BiP with aggresome-like structures during early vertebrate development. The extensive information and techniques available for the study

of molecular chaperones and cellular structures in *Xenopus laevis* embryos may make this developmental system ideal for the analysis of these questions.

References

Abdelhamid, G., El-Kadi, A. O. 2015. Buthionine sulfoximine, an inhibitor of glutathione biosynthesis, induces expression of soluble epoxide hydrolase and markers of cellular hypertrophy in a rat cardiomyoblast cell line: roles of the NF-κB and MAPK signaling pathways. Free Radical Biology and Medicine, 82, 1-12.

Abe, T., Konishi, T., Katoh, T., Hirano, H., Matsukuma, K., Kashimura, M., Higashi, K. 1994. Induction of heat shock 70 mRNA by cadmium is mediated by glutathione suppressive and non-suppressive triggers. Biochimica et biophysica acta, 120, 29-36.

Åkerfelt, M., Morimoto, R. I., Sistonen, L. 2010. Heat shock factors: integrators of cell stress, development and lifespan. Nature Reviews: Molecular Cell Biology, 11, 545-555.

Alder, N. N., Shen, Y., Brodsky, J. L., Hendershot, L. M., Johnson, A. E. 2005. The molecular mechanisms underlying BiP-mediated gating of the Sec61 translocon of the endoplasmic reticulum. Journal of Cell Biology, 168, 389–399.

Alam, J., Wicks, C., Stewart, G., Pengfei, T., Cheri, O., Cherri, C., Augustine, B., Mathew, Tou J., S. 2000. Mechanism of heme oxygenase-1 gene activation by cadmium in MCF-7 mammary epithelial cells. Journal of Biological Chemistry. 275, 94–702.

Alam, J., Cook, J. L. 2007. How many transcription factors does it take to turn on the heme oxygenase-1 gene? American Journal of Respiratory Cell and Molecular Biology, 32, 166-174.

Allen, S., Polazzi, J., Gierse, J., Easton, A. 1992. Two novel heat shock genes encoding proteins produced in response to heterologous protein expression in *Escherichia coli*. Journal of Bacteriology, 174, 6938–6947.

Amemiya, C. T., Alföldi, J., Lee, A. P., Fan, S., Philippe, H., MacCallum, I., Organ, C. 2013. The African coelacanth genome provides insights into tetrapod evolution. Nature, 496, 311-316.

Ardley, H. C., Robinson, P. A. 2005. E3 ubiquitin ligases. Essays in Biochemistry, 41, 15–30.

Ardley, H. C., Scott, G. B., Rose, S. A., Tan, N. G., Robinson, P. A. 2004. UCH-L1 aggresome formation in response to proteasome impairment indicates a role in inclusion formation in Parkinson's disease. Journal of Neurochemistry, 90, 379-391.

Arnason, J. G., Fletcher, B. A. 2003. A 40+ year record of Cd, Hg, Pb, and U deposition in sediments of Patroon Reservoir, Albany County, NY, USA. Environmental Pollution, 123, 383-391.

Arrigo, P. 2007. The cellular "networking" of mammalian Hsp27 and its functions in the control of protein folding, redox state and apoptosis. Molecular Aspects of the Stress Response: Chaperones, Membranes and Networks. 14–26.

Audry, S., Schäfer, J., Blanc, G., Jouanneau, J. M. 2004. Fifty-year sedimentary record of heavy metal pollution (Cd, Zn, Cu, Pb) in the Lot River reservoirs (France). Environmental Pollution, 132, 413-426.

Babich, H., Palace, M. R., Stern, A. 1993. Oxidative stress in fish cells: in vitro studies. Archives of Environmental Contamination and Toxicology, 24, 173-178.

Bagola, K., Sommer, T. 2008. Protein quality control: on IPODs and other JUNQ. Current Biology, 18, R1019-R1021.

Balch, W. E., Morimoto, R. I., Dillin, A., Kelly, J. W. 2008. Adapting proteostasis for disease intervention. Science, 319, 916-919.

Bang, Y., Kang, B. Y., Choi, H. J. 2014. Preconditioning stimulus of proteasome inhibitor enhances aggresome formation and autophagy in differentiated SH-SY5Y cells. Neuroscience letters, 566, 263-268.

Bauer, N., Richter-Landsberg, C. 2006. The dynamic instability of microtubules is required for aggresome formation in olgodengroglial cells after proteolytic stress. Journal of Molecular Neuroscience, 29, 101–108.

Baumeister, P., Luo, S., Skarnes, W. C., Sui, G., Seto, E., Shi, Y., Lee, A. S. 2005. Endoplasmic reticulum stress induction of the Grp78/BiP promoter: activating mechanisms mediated by YY1 and its interactive chromatin modifiers. Molecular and Cellular Biology, 25, 4529-4540.

Barbier, O., Jacquillet, G., Tauc, M., Poujeol, P., Cougnon, M. 2004. Acute study of interaction among cadmium, calcium, and zinc transport along the rat nephron in vivo. American Journal of Physiology-Renal Physiology, 287, F1067-F1075.

Beckmann, R. P., Mizzen, L. E., Welch, W. J. 1990. Interaction of Hsp 70 with newly synthesized proteins: implications for protein folding and assembly. Science, 248, 850-854.

Beggah, A., Mathews, P., Beguin, P., Geering, K. 1996. Degradation and endoplasmic reticulum retention of unassembled α-and β-subunits of Na, K-ATPase correlate with interaction of BiP. Journal of Biological Chemistry, 271, 20895-20902.

Berendes, H. D. 1968. Factors involved in the expression of gene activity in polytene chromosomes. Chromosoma, 24, 418-437.

Bertin, G., Averbeck, D. 2006. Cadmium: cellular effects, modifications of biomolecules, modulation of DNA repair and genotoxic consequences. Biochimie. 88, 1549–1559.

Bertolotti, A., Zhang, Y., Hendershot, L. M., Harding, H. P., Ron, D. 2000. Dynamic interaction of BiP and ER stress transducers in the unfolded-protein response. Nature Cell Biology, 2, 326-332.

Beyersmann, D., Hechtenberg, S. 1997. Cadmium, gene regulation, and cellular signalling in mammalian cells. Toxicology and Applied Pharmacology, 144, 247-261.

Bienz, M. 1984. *Xenopus* hsp 70 genes are constitutively expressed in injected oocytes. The EMBO journal, 3, 2477.

Bjerregaard, H. 2007. Effects of cadmium on differentiation and cell cycle progression in cultured *Xenopus* kidney distal epithelial (A6) cells. Alternatives to Laboratory Animals, 35, 343-348.

Bolhuis, S., Richter-Landsberg, C. 2010. Effect of proteasome inhibition by MG-132 on HSP27 oligomerization, phosphorylation, and aggresome formation in the OLN-93 oligodendroglia cell line. Journal of Neurochemistry, 114, 960-971.

Boyault, C., Sadoul, K., Pabion, M., Khochbin, S. 2007. HDAC6, at the crossroads between cytoskeleton and cell signaling by acetylation and ubiquitination. Oncogene, 26, 5468-5476.

Bratt, A., Rosenwasser, S., Meyer, A., Fluhr, R. 2016. Organelle redox autonomy during environmental stress. Plant, Cell Environment, 97, 85-94.

Brocchieri, L., Conway de Macario, E., Macario, A. J. L. 2008. Hsp70 genes in the human genome: Conservation and differentiation patterns predict a wide array of overlapping and specialized functions. BMC: Evolutionary Biology, 8-19.

Brodsky, J. L., Werner, E. D., Maria, E., Goeckeler, J. L., Kristina, B., Mccracken, A. A., Kruse, K. B. 1999. The requirement for molecular chaperones during endoplasmic reticulum-associated protein degradation demonstrates that protein export and import are mechanistically distinct the requirement for molecular chaperones during. Journal of Biological Chemistry, 274, 3453–3460.

Brumbaugh, W. G., Schmitt, C. J., May, T. W. 2005. Concentrations of cadmium, lead, and zinc in fish from mining-influenced waters of Northeastern Oklahoma: sampling of blood, carcass, and liver for aquatic biomonitoring. Archives of Environmental Contamination and Toxicology, 49, 76-88.

Brunt, J. J., Khan, S., Heikkila, J. J. 2012. Sodium arsenite and cadmium chloride induction of proteasomal inhibition and HSP accumulation in *Xenopus laevis* A6 kidney epithelial cells. Comparative Biochemistry and Physiology Part C: Toxicology Pharmacology, 155, 307-317

Burggren, W. W., Warburton, S. 2007. Amphibians as animal models for laboratory research in physiology. Ilar Journal, 48, 260-269.

Cai, L. 2013. Preventive and therapeutic effects of MG132 by activating Nrf2-ARE signaling pathway on oxidative stress-induced cardiovascular and renal injury. Oxidative Medicine and Cellular Longevity, 239-241.

Capitani, M. Sallese, M. 2009. The KDEL receptor: New functions for an old protein. FEBS Letters. 583, 3863–3871.

Carrara, M., Prischi, F., Nowak, P. R., Kopp, M. C., Ali, M. M. 2015. Noncanonical binding of BiP ATPase domain to Ire1 and Perk is dissociated by unfolded protein CH1 to initiate ER stress signaling. Elife, 4, e03522.

Carroll, D., Howard, D., Zhu, H., Paumi, C. M., Vore, M., Bondada, S., Clair, D. K. S. 2016. Simultaneous quantitation of oxidized and reduced glutathione via LC-MS/MS: An insight into the redox state of hematopoietic stem cells. Free Radical Biology and Medicine, 97, 85-94.

Chen, J., Yang, L., Gu, J., Bai, X., Ren, Y., Fan, T., Cao, S. 2015. MAN3 gene regulates cadmium tolerance through the glutathione-dependent pathway in *Arabidopsis thaliana*. New Phytologist, 205, 570-582.

Chiti, F., Dobson, C. M. 2009. Amyloid formation by globular proteins under native conditions. Nature Chemical Biology, 5, 15–22.

Ciechanover, A. 1994. The ubiquitin-proteasome proteolytic pathway. Cell. 79, 13–21.

Corchero, J. L. 2016. Eukaryotic aggresomes: from a model of conformational diseases to an emerging type of immobilized biocatalyzers. Applied Microbiology and Biotechnology, 100, 559-569.

Cullen, J. T., Maldonado, M. T. 2013. Chapter 2: Biogeochemistry of cadmium and its release to the environment. In cadmium: From toxicity to essentiality. 31–62.

Daeschler, E. B., Shubin, N. H., Jenkins, F. A. 2006. A Devonian tetrapod-like fish and the evolution of the tetrapod body plan. Nature, 440, 757-763.

Daniel, R. M., Dines, M., Petach, H. H. 1996. The denaturation and degradation of stable enzymes at high temperatures. The Biochemical Journal, 317, 1–11.

Daugaard, M., Rohde, M., Jäättelä, M. 2007. The heat shock protein 70 family: Highly homologous proteins with overlapping and distinct functions. FEBS letters, 581, 3702-3710.

De Jong, W. W., Caspers, G. J., Leunissen, J. A. 1998. Genealogy of the α-crystallin—small heat-shock protein superfamily. International Journal of Biological Macromolecules, 22, 151-162.

DeMartino, G. N., Gillette, T. G. 2007. Proteasomes: machines for all reasons. Cell, 129, 659-662.

Ellis, R. J., Minton, A. P. 2006. Protein aggregation in crowded environments. Biological chemistry, 387, 485-497.

Ewing, J. F., Maines, M. D. 1993. Glutathione depletion induces heme oxygenase-1 (HSP32) mRNA and protein in rat brain. Journal of Neurochemistry, 60, 1512–9.

Fan, C., Lee, S., Cyr, D. M. 2003. Mechanisms for regulation of Hsp70 function by Hsp40. Cell Stress Chaperones, 8, 309–316.

Fauchon, M., Lagniel, G., Aude, J. C., Lombardia, L., Soularue, P., Petat, C., Labarre, J. 2002. Sulfur sparing in the yeast proteome in response to sulfur demand. Molecular Cell, 9, 713-723.

Faurskov, B., Bjerregaard, H. F. 2002. Evidence for cadmium mobilization of intracellular calcium through a divalent cation receptor in renal distal epithelial A6 cells. Pflügers Archiv, 445, 40-50.

Feder, M. E., Hofmann, G. E. 1999. Heat-shock proteins, molecular chaperones, and the stress response: Evolutionary and ecological physiology. Annual Reviews of Physiology, 61, 243–282.

Flynn, G. C., Pohl, J., Flocco, M. T., Rothman, J. E. 1991. Peptide-binding specificity of the molecular chaperone BiP. Nature, 353, 726–730.

Fort, D. J., Stover, E. L., Bantle, J. A., Dumont, J. N., Finch, R. A. 2001. Evaluation of a reproductive toxicity assay using *Xenopus laevis*: boric acid, cadmium and ethylene glycol monomethyl ether. Journal of Applied Toxicology, 21, 41-52.

Fox, M. A., Nieuwesteeg, M. A., Willson, J. A., Cepeda, M., Damjanovski, S. 2014. Knockdown of Pex11β reveals its pivotal role in regulating peroxisomal genes, numbers, and ROS levels in *Xenopus laevis* A6 cells. In Vitro Cellular Developmental Biology-Animal, 50, 340-349

Friedman, P. A., Gesek, F. A. 1994. Cadmium uptake by kidney distal convoluted tubule cells. Toxicology and Applied Pharmacology, 128, 257-263.

Frydman, J. 2001. Folding of newly translated proteins in vivo: the role of molecular chaperones. Annual Review of Biochemistry, 70, 603–647.

Fujimoto, M., Hayashida, N., Katoh, T., Oshima, K., Shinkawa, T., Prakasam, R., Nakai, A. 2010. A novel mouse HSF3 has the potential to activate nonclassical heat-shock genes during heat shock. Molecular Biology of the Cell, 21, 106-116.

Fujishiro, H., Yano, Y., Takada, Y., Tanihara, M., and Himeno, S. 2012. Roles of ZIP8, ZIP14, and DMT1 in transport of cadmium and manganese in mouse kidney proximal tubule cells. Metallomics : Integrated Biometal Science. 4, 700–8.

Galan, A., Troyano, A., Vilaboa, N.E., Fernandez, C., de Blas, E., Aller, P. 2001. Modulation of the stress response during apoptosis and necrosis induction in cadmium-treated U-937 human promonocytic cells. Biochimica et biophysica acta 1538, 38-46.

Gamerdinger, M., Kaya, M., Wolfrum, U., Clement, A. M., Behl, C. 2011. BAG3 mediates chaperone-based aggresome-targeting and selective autophagy of misfolded proteins. EMBO Reports, 12, 149–156.

Gamulin, S., Narancsik, P. 1982. Effects of cadmium on mouse liver polyribosome function. Pathobiology, 50, 72-78.

García-Mata, R., Bebök, Z., Sorscher, E. J., Sztul, E. S. 1999. Characterization and dynamics of aggresome formation by a cytosolic GFP-chimera. The Journal of cell biology, 146, 1239-1254.

Garcia-Mata, R., Gao, Y. S., Sztul, E. 2002. Hassles with taking out the garbage: aggravating aggresomes. Traffic, 3, 388-396.

Gauley, J., Young, J. T. F., Heikkila, J. J. 2008. Intracellular localization of the heat shock protein, HSP110, in *Xenopus laevis* A6 kidney epithelial cells. Comparative Biochemistry and Physiology Part A: Molecular Integrative Physiology, 151, 133-138.

Gaut, J. R., Hendershot, L. M. 1993. The immunoglobulin-binding protein in vitro autophosphorylation site maps to a threonine within the ATP binding cleft but is not a detectable site of in vivo phosphorylation. Journal of Biological Chemistry, 268, 12691-12698.

Goering, P. L., Fisher, B. R., Kish, C. L. 1993. Stress protein synthesis induced in rat liver by cadmium precedes hepatotoxicity. Toxicology and Applied Pharmacology, 122, 139-148.

Goldbaum, O., Riedel, M., Stahnke, T., Richter-Landsberg, C., 2009. The small heat shock protein HSP25 protects astrocytes against stress induced by proteasomal inhibition. Glia, 57, 1566–1577.

Goodson, M. L., Park-Sarge, O. K., Sarge, K. D. 1995. Tissue-dependent expression of heat shock factor 2 isoforms with distinct transcriptional activities. Molecular and Cellular Biology, 15, 5288–5293.

Grayfer, L., De Jesús Andino, F., Robert, J. 2014. The amphibian (*Xenopus laevis*) type I interferon response to frog virus 3: new insight into ranavirus pathogenicity. Journal of Virology, 88, 5766–77.

Griffith, OW. 1982. Mechanism of action, metabolism, and toxicity of buthionine sulfoximine and its higher homologs, potent inhibitors of glutathione synthesis. Journal of Biological Chemistry. 257, 13704-13712.

Groten, J. P., Sinkeldam, E. J., Luten, J. B., van Bladeren, P. J. 1991. Cadmium accumulation and metallothionein concentrations after 4-week dietary exposure to cadmium chloride or cadmium-metallothionein in rats. Toxicology and Applied Pharmacology. 111, 504–513

Gülow, K., Bienert, D., Haas, I. G. 2002. BiP is feed-back regulated by control of protein translation efficiency. Journal of cellular science, 115, 2443-2452.

Haas, I. G. 1994. BiP (GRP78), an essential hsp70 resident protein in the endoplasmic reticulum. Experientia, 50, 1012–1020.

Haas, I, Wabl, J. 1983. Immunoglobulin heavy chain binding protein. Nature, 306, 387–389.

Hentze, N., Le Breton, L., Wiesner, J., Kempf, G., Mayer, M. P. 2016. Molecular mechanism of thermosensory function of human heat shock transcription factor Hsf1. eLife, 5, e11576.

Heugens, E. H., Jager, T., Creyghton, R., Kraak, M. H., Hendriks, A. J., Van Straalen, N. M., Admiraal, W. 2003. Temperature-dependent effects of cadmium on Daphnia magna: accumulation versus sensitivity. Environmental Science Technology, 37, 2145-2151.

Heikkila, J. J. 2010. Heat shock protein gene expression and function in amphibian model systems. Comparative Biochemistry and Physiology Part A: Molecular Integrative Physiology, 156, 19-33.

Heir, R., Ablasou, C., Dumontier, E., Elliott, M., Fagotto-Kaufmann, C., Bedford, F. K. 2006. The UBL domain of PLIC-1 regulates aggresome formation. EMBO reports, 7, 1252-1258.

Hilgarth, R. S., Murphy, L. a, O'Connor, C. M., Clark, J. a, Park-Sarge, O.-K., Sarge, K. D. 2004. Identification of *Xenopus* heat shock transcription factor-2: conserved role of sumoylation in regulating deoxyribonucleic acid-binding activity of heat shock transcription factor-2 proteins. Cell Stress Chaperones, 9, 214–20.

Horrell, A., Shuttleworth, J., Colman, A. 1987. Transcript levels and translational control of hsp70 synthesis in *Xenopus* oocytes. Genes Development, 1, 433-444.

Hunt, C., Morimoto, R. I. 1985. Conserved features of eukaryotic hsp70 genes revealed by comparison with the nucleotide sequence of human hsp70. Proceedings of the National Academy of Sciences of the United States of America, 82, 6455–9.

Hut, H. M., Kampinga, H. H., Sibon, O. C. 2005. Hsp70 protects mitotic cells against heat-induced centrosome damage and division abnormalities. Molecular biology of the cell, 16, 3776-3785.

Huyer, G., Longsworth, G. L., Mason, D. L., Mallampalli, M. P., McCaffery, J. M., Wright, R. L., Michaelis, S. 2004. A striking quality control subcompartment in *Saccharomyces cerevisiae*: the endoplasmic reticulum-associated compartment. Molecular biology of the cell, 15, 908-921.

Ito, H., Okamoto, K., Kato, K. 1998. Enhancement of expression of stress proteins by agents that lower the levels of glutathione in cells. Biochimica et Biophysica Acta (BBA)-Gene Structure and Expression, 1397, 223-230.

Ito, D., Yagi, T., Ikawa, M., Suzuki, N. 2012. Characterization of inclusion bodies with cytoprotective properties formed by seipinopathy-linked mutant seipin. Human Molecular Genetics, 21, 635-646.

Jacobson, T., Navarrete, C., Sharma, S. K., Sideri, T. C., Ibstedt, S., Priya, S., Tamás, M. J. 2012. Arsenite interferes with protein folding and triggers formation of protein aggregates in yeast. Journal of Cell Science, 125, 5073-5083.

Jones, D. T., Taylor, W. R., Thornton, J. M. 1992. The rapid generation of mutation data matrices from protein sequences. Computer Applications in the Biosciences: CABIOS, 8, 275-282.

Johnson, N., Powis, K., High, S. 2013. Post-translational translocation into the endoplasmic reticulum. Biochimica et Biophysica Acta - Molecular Cell Research, 1833, 2403–2409.

Johnston, J. A., Ward, C. L., Kopito, R. R. 1998. Aggresomes: a cellular response to misfolded proteins. The Journal of Cell Biology, 143, 1883-1898.

Jungmann, J., Reins, H. A., Schobert, C., Jentsch, S. 1993. Resistance to cadmium mediated by ubiquitin-dependent proteolysis. Nature, 361, 369-371.

Kaldis, A., Atkinson, B. G., Heikkila, J. J. 2004. Molecular chaperone function of the *Rana catesbeiana* small heat shock protein, hsp30. Comparative Biohemistry and Physiology, 139, 175–182.

Kang, P. J., Ostermann, J., Shilling, J., Neupert, W., Craig, E., Pfanner, N. 1990. Requirement for hsp70 in the mitochondrial matrix for translocation and folding of precursor proteins. Nature, 348, 137–143.

Kapitinulk, J., Maines, M. D. 2009. Pleiotropic functions of biliverdin reductase: cellular signaling and generation of cytoprotective and cytotoxic bilirubin. Trends in Pharmacological Sciences, 30, 129–37.

Karpinka, J. B., Fortriede, J. D., Burns, K. A., James-Zorn, C., Ponferrada, V. G., Lee, J. Vize, P. D. 2015. Xenbase, the *Xenopus* model organism database; new virtualized system, data types and genomes. Nucleic acids Research, 43, D756-D763.

Katschinski, D.M. 2004. On heat and cells and proteins. Physiology, 19, 11-15.

Kawaguchi, Y., Kovacs, J. J., McLaurin, A., Vance, J. M., Ito, A., Yao, T. P. 2003. The deacetylase HDAC6 regulates aggresome formation and cell viability in response to misfolded protein stress. Cell, 115, 727-738.

Kannan, R., Bao, Y., Mittur, A., Andley, U. P., Kaplowitz, N. 1998. Glutathione transport in immortalized HLE cells and expression of transport in HLE cell poly (A)+ RNA-injected *Xenopus laevis* oocytes. Investigative Ophthalmology Visual Science, 39, 1379-1386.

Kannan, R., Yi, J. R., Tang, D., Zlokovic, B. V., Kaplowitz, N. 1996. Identification of a novel, sodium-dependent, reduced glutathione transporter in the rat lens epithelium. Investigative Ophthalmology Visual Science, 37, 2269-2275.

Khamis, I., Heikkila, J. J. 2013. Enhanced HSP30 and HSP70 accumulation in *Xenopus* cells subjected to concurrent sodium arsenite and cadmium chloride stress. Comparative Biochemistry and Physiology, Part C, 158, 165–172.

Khan, S., Heikkila, J. J. 2011. Curcumin-induced inhibition of proteasomal activity, enhanced HSP accumulation and the acquisition of thermotolerance in *Xenopus laevis* A6 cells. Comparative Biochemistry and Physiology Part A: Molecular Integrative Physiology, 158, 566-576.

Khan, S., Rammeloo, A. W., Heikkila, J. J. 2012. Withaferin A induces proteasome inhibition, endoplasmic reticulum stress, the heat shock response and acquisition of thermotolerance. PloS one, 7, e50547.

Khan, S., Heikkila, J. J. 2014. Distinct patterns of HSP30 and HSP70 degradation in *Xenopus laevis* A6 cells recovering from thermal stress. Comparative Biochemistry and Physiology - A Molecular and Integrative Physiology, 168, 1–10.

Khan, S., Khamis, I., Heikkila, J. J. 2015. The small heat shock protein , HSP30 , is associated with aggresome-like inclusion bodies in proteasomal inhibitor- , arsenite- , and cadmium-treated *Xenopus* kidney cells. Comparative Biochemistry and Physiology, Part A, 189, 130–140.

Kitamura, M., Hiramatsu, N. 2010. The oxidative stress: endoplasmic reticulum stress axis in cadmium toxicity. Biometals, 23, 941-950.

Kitiphongspattana, K., Mathews, C. E., Leiter, E. H., Gaskins, H. R. 2005. Proteasome inhibition alters glucose-stimulated (pro) insulin secretion and turnover in pancreatic β-cells. Journal of Biological Chemistry, 280, 15727-15734.

Kregel, K. C. 2002. Invited review: heat shock proteins: modifying factors in physiological stress responses and acquired thermotolerance. Journal of Applied Physiology, 92, 2177-2186.

Kokame, K., Kato, H., Miyata, T. 2001. Identification of ERSE-II, a new cis-acting element responsible for the ATF6-dependent mammalian unfolded protein response. Journal of Biological Chemistry, 276, 9199-9205.

Kobayashi, A., Kang, M., Okawa, H., Ohtsuji, M., Zenke, Y., Chiba, T., Igarashi, K., Yamamoto, M. 2004. Oxidative stress sensor Keap1 functions as an adaptor for Cul3-based E3 ligase to regulate proteasomal degradation of Nrf2. Molecular and Cellular Biology, 24, 7130–7139.

Kopito, R. R. 2000. Aggresomes, inclusion bodies and protein aggregation. Trends in Cell Biology, 10, 524–530.

Kopito, R. R., Sitia, R. 2000. Aggresomes and Russell bodies. EMBO reports, 1, 225-231.

Kumar, P., Singh, A. 2010. Cadmium toxicity in fish: An overview. GERF Bulletin of Biosciences, 1, 41–47.

Kumar, S., Stecher, G., Tamura, K. 2016. MEGA7: Molecular Evolutionary Genetics Analysis version 7.0 for bigger datasets. Molecular Biology and Evolution, 1870-1874.

Landis-Piwowar, K. R., Milacic, V., Chen, D., Yang, H., Zhao, Y., Chan, T. H., Dou, Q. P. 2006. The proteasome as a potential target for novel anticancer drugs and chemosensitizers. Drug Resistance Updates, 9, 263–273.

Lee, A. S. 1987. Coordinated regulation of a set of genes by glucose and calcium ionophores in mammalian cells. Trends in Biochemical Sciences, 12, 20-23.

Lee, A. S. 1992. Mammalian stress response: induction of the glucose-regulated protein family. Current Opinion in Cell Biology, 4, 267–273.

Lee, A. S. 2001. The glucose-regulated proteins: Stress induction and clinical applications. Trends in Biochemical Sciences, 26, 504–510.

Lee, A. S. 2005. The ER chaperone and signaling regulator GRP78/BiP as a monitor of endoplasmic reticulum stress. Methods, 35, 373-381.

Lee, D. H., Goldberg, A. L. 1998. Proteasome inhibitors: valuable new tools for cell biologists. Trends in Cell Biology, 8, 397-403.

Lentze, N., Narberhaus, F. 2004. Detection of oligomerisation and substrate recognition sites of small heat shock proteins by peptide arrays. Biochemical and Biophysical Research Communications, 325, 401–407.

Li, L. Y., Seddon, A. P., Meister, A. Risley, M. S. 1989. Spermatogenic cell-somatic cell interactions are required for maintenance of spermatogenic cell glutathione. Biology of Reproduction, 40, 317-331.

Li, W. W., Hsiung, Y., Zhou, Y., Roy, B., Lee, A. S. 1997. Induction of the mammalian GRP78/BiP gene by Ca2+ depletion and formation of aberrant proteins: activation of the conserved stress-inducible grp core promoter element by the human nuclear factor YY1. Molecular and Cellular Biology, 17, 54-60.

Li, H., Wu, S., Chen, J., Wang, B., Shi, N. 2013. Effect of glutathione depletion on Nrf2/ARE activation by deltamethrin in PC12 Cells. Arhiv Za Higijenu Rada I Toksikologiju, 64, 87–97.

Li, L., Yang, H., Chen, D., Cui, C., Dou, Q. P. 2008. Disulfiram promotes the conversion of carcinogenic cadmium to a proteasome inhibitor with pro-apoptotic activity in human cancer cells. Toxicology and Applied Pharmacology. 229, 206–214.

Lièvremont, J. P., Rizzuto, R., Hendershot, L., Meldolesi, J. 1997. BiP, a major chaperone protein of the endoplasmic reticulum lumen, plays a direct and important role in the storage of the rapidly exchanging pool of Ca2+. Journal of Biological Chemistry, 272, 30873-30879.

Linder, B., Jin, Z., Jonathan, H., Rubin, C. S., Freedman, J. H. 1996. Molecular characterization of a novel, developmentally regulated small embryonic chaperone from *Caenorhabditis elegans*. The Journal of Biological Chemistry, 271, 30158–30166.

Lindquist, S., Craig, E. A. 1988. The heat shock proteins. Annual Review of Genetics, 22, 631-677.

Liu, J., Qu, W., Kadiiska, M. B. 2009. Role of oxidative stress in cadmium toxicity and carcinogenesis. Toxicology and Applied Pharmacology, 238, 209-214.

Liu, F., Inageda, K., Nishitai, G., Matsuoka, M. 2006. Cadmium induces the expression of Grp78, an endoplasmic reticulum molecular chaperone, in LLC-PK1 renal epithelial cells. Environmental Health Perspectives, 859-864.

Lodish H, Berk A, Zipursky SL, 2000. Molecular Cell Biology. 4th edition. New York: W. H. Freeman. Section 17.3, Overview of the Secretory Pathway.

Loumbourdis, N. S., Vogiatzis, a K. 2002. Impact of cadmium on liver pigmentary system of the frog *Rana ridibunda*. Ecotoxicology and Environmental Safety, 53, 52–58.

Ma, Y., Hendershot, L. M. 2004. The role of the unfolded protein response in tumour development: friend or foe? Nature Reviews Cancer, 4, 966-977.

Macleod, A. K., Mcmahon, M., Plummer, S. M., Higgins, L. G., Penning, T. M., Igarashi, K., Hayes, J. D. 2009. Characterization of the cancer chemopreventive NRF2-dependent gene battery in human keratinocytes: Demonstration that the KEAP1-NRF2 pathway, and not the BACH1-NRF2 pathway, controls cytoprotection against electrophiles as well as redox-cycling compounds. Carcinogenesis, 30, 1571–1580.

MacIas, A. T., Williamson, D. S., Allen, N., Borgognoni, J., Clay, A., Daniels, Z., Massey, A. J. 2011. Adenosine-derived inhibitors of 78 kDa glucose regulated protein (Grp78) ATPase: Insights into isoform selectivity. Journal of Medicinal Chemistry. 54, 4034–4041.

Mah, V., Jalilehvand, F. 2010. Cadmium (II) complex formation with glutathione. Journal of Biological Inorganic Chemistry, 15, 441-458.

Malaker, K., Hurwitz, S. J., Bump, E. A., Griffith, O. W., Lai, L. L., Riese, N., Coleman, C. N. 1994. Pharmacodynamics of prolonged treatment with L, S-buthionine sulfoximine. International Journal of Radiation Oncology Biology Physics, 29, 407-412.

Malek, M. A. A., Jagannathan, S., Malek, E., Sayed, D. M., Elgammal, S. A., El-Azeem, H. G. A., Driscoll, J. J. 2015. Molecular chaperone GRP78 enhances aggresome delivery to autophagosomes to promote drug resistance in multiple myeloma. Oncotarget, 6, 3098.

Mason, R. P., Laporte, J. M., Andres, S. 2000. Factors controlling the bioaccumulation of mercury, methylmercury, arsenic, selenium, and cadmium by freshwater invertebrates and fish. Archives of Environmental Contamination and Toxicology, 38, 283-297.

Mason, P. B., Lis, J. T. 1997. Cooperative and competitive protein interactions at the Hsp70 promoter. Journal of Biological Chemistry, 272, 33227–33233.

Masuya, Y., Hioki, K., Tokunuga, R., Taketani, S. 1998. Involvement of the tyrosine phosphorylation pathway in induction of human heme oxygenase-1 by hemin, sodium arsenite and cadmium chloride. Journal of Biological Chemistry. 633, 628–633.

Mayer, M. P., Bukau, B. 2005. Hsp70 chaperones: cellular functions and molecular mechanism. Cellular and Molecular Life Sciences, 62, 670-684.

McWilliam, H., Li, W., Uludag, M., Squizzato, S., Park, Y. M., Buso, N., Lopez, R. 2013. Analysis tool web services from the EMBL-EBI. Nucleic Acids Research, 41, W597-W600.

Miskovic, D., Heikkila, J. J. 1999. Constitutive and stress-inducible expression of the endoplasmic reticulum heat shock protein 70 gene family member, immunoglobulin-binding protein (BiP), during *Xenopus laevis* early development. Developmental Genetics, 25, 31–39.

Miskovic, D., Salter-Cid, L., Ohan, N., Flajnik, M., Heikkila, J. J. 1997. Isolation and characterization of a cDNA encoding a *Xenopus* immunoglobulin binding protein, BiP (GRP78). Comparative Biochemistry and Physiology Part B: Biochemistry and Molecular Biology, 116, 227-234

Misiewicz, M., Déry, M. A., Foveau, B., Jodoin, J., Ruths, D., LeBlanc, A. C. 2013. Identification of a novel endoplasmic reticulum stress response element regulated by XBP1. Journal of Biological Chemistry, 288, 20378-20391.

Misra, U. K., Gonzalez-Gronow, M., Gawdi, G., Wang, F., Pizzo, S. V. 2004. A novel receptor function for the heat shock protein Grp78: Silencing of Grp78 gene expression attenuates induced signalling. Cellular Signalling, 16, 929–938.

Miyamoto, Y., Ohshida, K., Sasago, K. 2009. Protein assay for heme oxygenase-1 (HO-1) induced by chemicals in HepG2 cells. The Journal of Toxicological Sciences. 34, 709–14.

Montero, A. J., Jassem, J. 2011. Cellular redox pathways as a therapeutic target in the treatment of cancer. Drugs, 71, 1385-1396.

Morgan, W. D. 1989. Transcription factor Sp1 binds to and activates a human hsp70 gene promoter. Molecular and Cellular Biology, 9, 4099–4104.

Morgan, W. D., Williams, G. T., Morimoto, R. I., Greene, J., Kingston, R. E., Tjian, R. 1987. Two transcriptional activators, CCAAT-box-binding transcription factor and heat shock transcription factor, interact with a human hsp70 gene promoter. Molecular and Cellular Biology, 7, 1129–38.

Morimoto, R. I. 2008. Proteotoxic stress and inducible chaperone networks in neurodegenerative disease and aging. Genes Development, 22, 1427-1438.

Morrow, G., Heikkila, J. J., Tanguay, R. M. 2006. Differences in the chaperone-like activities of the four main small heat shock proteins of *Drosophila melanogaster*. Cell Stress and Chaperones, 11, 51-60.

Mosser, D. D., Caron, a W., Bourget, L., Meriin, a B., Sherman, M. Y., Morimoto, R. I., Massie, B. 2000. The chaperone function of hsp70 is required for protection against stress-induced apoptosis. Molecular and Cellular Biology, 20, 7146–7159.

Moulis, J. M., Thévenod, F. 2010. New perspectives in cadmium toxicity: An introduction. Biometals, 23, 763-768.

Mounier, N., Arrigo, A. P. 2002. Actin cytoskeleton and small heat shock proteins: how do they interact? Cell Stress and Chaperones, 7, 167-176.

Murphy, M. E. 2013. The HSP70 family and cancer. Carcinogenesis, 34, 1181–1188.

Muller, M., Gauley, J., Heikkila, J. J. 2004. Hydrogen peroxide induces heat shock protein and proto-oncogene mRNA accumulation in *Xenopus laevis* A6 kidney epithelial cells. Canadian Journal of Physiology and Pharmacology, 82, 523–529.

Munro, S., Pelham, H. R. 1986. An Hsp70-like protein in the ER: identity with the 78 kd glucose-regulated protein and immunoglobulin heavy chain binding protein. Cell, 46, 291-300.

Music, E., Khan, S., Khamis, I., Heikkila, J. J. 2014. Accumulation of heme oxygenase-1 (HSP32) in *Xenopus laevis* A6 kidney epithelial cells treated with sodium arsenite, cadmium chloride or proteasomal inhibitors. Comparative Biochemistry and Physiology, 166, 75–87.

Nakai, a, Morimoto, R. I. 1993. Characterization of a novel chicken heat shock transcription factor, heat shock factor 3, suggests a new regulatory pathway. Molecular and Cellular Biology, 13, 1983–97.

Ng, D. T., Watowich, S. S., Lamb, R. a. 1992. Analysis in vivo of GRP78-BiP/substrate interactions and their role in induction of the GRP78-BiP gene. Molecular Biology of the Cell, 3, 143–55.

Ni, Min., Zhang, Yi., Lee, A. 2011. Beyond the endoplasmic reticulum: atpycial GRP78 in cell viability, signaling and therapeutic targeting. Journal of Biochemistry, 72, 181–204.

Nicholson, R. C., Williams, D. B., Moran, L. A. 1990. An essential member of the HSP70 gene family of *Saccharomyces cerevisiae* is homologous to immunoglobulin heavy chain binding protein. Proceedings of the National Academy of Sciences, 87, 1159-1163.

Nioi, P., McMahon, M., Itoh, K., Yamamoto, M., Hayes, J. D. 2003. Identification of a novel Nrf2-regulated antioxidant response element (ARE) in the mouse NAD(P)H:quinone oxidoreductase 1 gene: reassessment of the ARE consensus sequence. The Biochemical Journal. 374, 337–48.

Nordberg, G. F. 2009. Historical perspectives on cadmium toxicology. Toxicology and Applied Pharmacology, 238, 192–200.

Nyathi, Y., Wilkinson, B. M., Pool, M. R. 2013. Co-translational targeting and translocation of proteins to the endoplasmic reticulum. Biochimica et Biophysica Acta - Molecular Cell Research, 1833, 2392–2402.

Ohan, N. W., Tam, Y., Fernando, P., Heikkila, J. J. 1998. Characterization of a novel group of basic small heat shock proteins in *Xenopus laevis* A6 kidney epithelial cells. Biochemistry and Cell Biology, 76, 665–71.

Okuda-Shimizu, Y., Hendershot, L. M. 2007. Characterization of an ERAD Pathway for Nonglycosylated BiP Substrates, which Require Herp. Molecular Cell, 28, 544–554.

Olden, K., Pratt, R. M., Jaworski, C., Yamada, K. M. 1979. Evidence for role of glycoprotein carbohydrates in membrane transport: specific inhibition by tunicamycin. Proceedings of the National Academy of Sciences, 76, 791–795.

Oslowski, C. M., Hara, T., O'Sullivan-Murphy, B., Kanekura, K., Lu, S., Hara, M., Greiner, D. 2012. Thioredoxin-interacting protein mediates ER stress-induced β cell death through initiation of the inflammasome. Cell Metabolism, 16, 265-273.

Otero, J. H., Lizák, B., Hendershot, L. M. 2010. Life and death of a BiP substrate. Cell Developmental Biology. 21, 472-478.

Othman, M. S., Khonsue, W., Kitana, J., Thirakhupt, K., Robson, M. G., Kitana, N. 2009. Cadmium accumulation in two populations of rice frogs (*Fejervarya limnocharis*) naturally exposed to different environmental cadmium levels. Bulletin of Environmental Contamination and Toxicology, 83, 703-707.

Ouyang, H., Ali, Y. O., Ravichandran, M., Dong, A., Qiu, W., MacKenzie, F. Zhai, R. G. 2012. Protein aggregates are recruited to aggresome by histone deacetylase 6 via unanchored ubiquitin C termini. Journal of Biological Chemistry, 287, 2317-2327.

Ovelgönne, J. H., Souren, J. E. M., Wiegant, F. A. C., Van Wijk, R. 1995. Relationship between cadmium-induced expression of heatshock genes, inhibition of protein synthesis and cell death. Toxicology, 99, 19-30.

Ovsenek, N., Heikkila, J. J. 1990. DNA sequence-specific binding activity of the heat-shock transcription factor is heat-inducible before the midblastula transition of early *Xenopus* development. Development, 110, 427–433.

Pagny, S., Lerouge, P., Faye, L., Gomord, V. 1999. Signals and mechanisms for protein retention in the endoplasmic reticulum. Journal of Experimental Botany, 50, 157-164.

Paine, A., Eiz-Vesper, B., Blasczyk, R., Immenschuh, S. 2010. Signaling to heme oxygenase-1 and its anti-inflammatory therapeutic potential. Biochemical Pharmacology, 80, 1895-1903.

Pardue, M. L., Ballinger, D. G., Hogan, N. C. 1992. The heat shock response. Cells coping with transient stress. Annals of the New York Academy of Sciences, 663, 125–38.

Parker, C. S., Topol, J. 1984. A drosophila RNA polymerase II transcription factor binds to the regulatory site of an hsp 70 gene. Cell, 37, 273–283.

Pernet, L., Faure, V., Gilquin, B., Dufour-Guérin, S., Khochbin, S., Vourc'h, C. 2014. HDAC6–ubiquitin interaction controls the duration of HSF1 activation after heat shock. Molecular Biology of the Cell, 25, 4187-4194

Phang, D., Joyce, E. M., Heikkila, J. J. 1999. Heat shock-induced acquisition of thermotolerance at the levels of cell survival and translation in *Xenopus* A6 kidney epithelial cells. Biochemistry and Cell Biology, 77, 141-151.

Pocernich, C. B., Butterfield, D. A. 2012. Elevation of glutathione as a therapeutic strategy in Alzheimer disease. Biochimica et Biophysica Acta (BBA)-Molecular Basis of Disease, 1822, 625-630.

Pompella, A., Visvikis, A., Paolicchi, A., De Tata, V., Casini, A. F. 2003. The changing faces of glutathione, a cellular protagonist. Biochemical pharmacology, 66, 1499-1503.

Pouyssegur, J., Shiu, R. P. C., Pastan, I. 1977. Induction of two transformation-sensitive membrane polypeptides in normal fibroblasts by a block in glycoprotein synthesis or glucose deprivation. Cell, 11, 941–947.

Powers, E. T., Morimoto, R. I., Dillin, A., Kelly, J. W., Balch, W. E. 2009. Biological and chemical approaches to diseases of proteostasis deficiency. Annual review of biochemistry, 78, 959-991.

Pirkkala, L., Nykänen, P., Sistonen, L. 2001. Roles of the heat shock transcription factors in regulation of the heat shock response and beyond. Official Publication of the Federation of American Societies for Experimental Biology, 15, 1118–1131.

Plemper, R. K., Böhmler, S., Bordallo, J., Sommer, T., Wolf, D. H. 1997. Mutant analysis links the translocon and BiP to retrograde protein transport for ER degradation. Nature, 388, 891–895.

Preissler, S., Chambers, J. E., Crespillo-Casado, A., Avezov, E., Miranda, E., Perez, J., Ron, D. 2015. Physiological modulation of BiP activity by trans-protomer engagement of the interdomain linker. eLife, 4, e08961.

Quinones, Q. J., de Ridder, G. G., Pizzo, S. V. 2008. GRP78: A chaperone with diverse roles beyond the endoplasmic reticulum. Histology and Histopathology, 23, 1409–1416.

Rafferty, K.A. 1968. Mass culture of amphibian cells: methods and observations concerning stability of cell type. Biology of Amphibian Tumors. New York, NY, USA: Springer Verlag. pp. 52-81.

Rafferty, K. A. 1975. Epithelial cells: Growth in culture of normal and neoplastic forms. Advances in Cancer Research, 21, 249-272.

Ravid, T., Hochstrasser, M. 2008. Degradation signal diversity in the ubiquitin-proteasome system. Nature Reviews. Molecular Cell Biology, 9, 679–690.

Ramirez-Gordillo, D., Trujillo-Provencio, C., Knight, V. B., Serrano, E. E. 2011. Optimization of gene delivery methods in *Xenopus laevis* kidney (A6) and Chinese hamster ovary (CHO) cell lines for heterologous expression of *Xenopus* inner ear genes. In Vitro Cellular Developmental Biology-Animal, 47, 640-652

Reese, R. N., Wagner, G. J. 1987. Effects of buthionine sulfoximine on Cd-binding peptide levels in suspension-cultured tobacco cells treated with Cd, Zn, or Cu. Plant Physiology, 84, 574-577.

Richter, K., Haslbeck, M., Buchner, J. 2010. The heat shock response: life on the verge of death. Molecular Cell, 40, 253-266.

Ritossa, F. M. 1964. Experimental activation of specific loci in polytene chromosomes of *Drosophila*. Experimental Cell Research, 35, 601-607.

Resendez, E., Attenello, J. W., Grafsky, A., Chang, C. S., Lee, S. 1985. Calcium ionophore A23187 induces expression of glucose-regulated genes and their heterologous fusion genes. Molecular and Cellular Biology, 5, 1212–9.

Ron, D., Walter, P. 2007. Signal integration in the endoplasmic reticulum unfolded protein response. Nature reviews Molecular Cell Biology, 8, 519-529.

Roy, B., Lee, A.S. 1999. The mammalian endoplasmic reticulum stress response element consists of an evolutionarily conserved tripartite structure and interacts with a novel stress-inducible complex. Nucleic acids research,27, pp.1437-1443.

Rubtsova, M. P., Sizova, D. V., Dmitriev, S. E., Ivanov, D. S., Prassolov, V. S., Shatsky, I. N. 2003. Distinctive properties of the 5'-untranslated region of human Hsp70 mRNA. Journal of Biological Chemistry, 278, 22350–22356.

Ryter, S. W., Alam, J., Choi, A. M. 2006. Heme oxygenase-1/carbon monoxide: from basic science to therapeutic applications. Physiological Reviews, 86, 583-650.

Sabatelli, P., Castagnaro, S., Tagliavini, F., Chrisam, M., Sardone, F., Demay, L., Sandri, M. 2014. Aggresome–autophagy involvement in a sarcopenic patient with rigid spine syndrome and a p. C150R mutation in FHL1 gene. Frontiers in Aging Neuorscience. 1-9.

Saitou, N., Nei, M. 1987. The neighbor-joining method: a new method for reconstructing phylogenetic trees. Molecular Biology and Evolution, 4, 406-425.

Salemi, L. M., Almawi, A. W., Lefebvre, K. J., Schild-Poulter, C. 2014. Aggresome formation is regulated by RanBPM through an interaction with HDAC6. Biology Open, 1-13.

Sanders, S. L., Schekman, R. 1992. Polypeptide translocation across the endodasmic reticulum membrane. The Journal of Biological Chemistry, 267, 13791–13794.

Saunders, E. L., Maines, M. D., Meredith, M. J., Freeman, M. L. 1991. Enhancement of heme oxygenase-1 synthesis by glutathione depletion in Chinese hamster ovary cells. Archives of Biochemistry and Biophysics, 288, 368–373.

Schafer, F. Q., Buettner, G. R. 2001. Redox environment of the cell as viewed through the redox state of the glutathione disulfide/glutathione couple. Free Radical Biology and Medicine, 30, 1191-1212.

Schokraie, E., Hotz-Wagenblatt, A., Warnken, U., Frohme, M., Dandekar, T., Schill, R. O., Schnölzer, M. 2011. Investigating heat shock proteins of tardigrades in active versus anhydrobiotic state using shotgun proteomics. Journal of Zoological Systematics and Evolutionary Research, 49, 111–11

Schröder, M., Kaufman, R. J. 2005. The mammalian unfolded protein response. Annual Review of Biochemistry, 74, 739-789.

Seiler, H., Sigel, A., Sigel, H. 1994. Handbook on metals in clinical and analytical chemistry. CRC Press. Pp. 295- 300.

Shalgi, R., Hurt, J. A., Krykbaeva, I., Taipale, M., Lindquist, S., Burge, C. B. 2013. Widespread regulation of translation by elongation pausing in heat shock. Molecular Cell, 49, 439–452.

Shao, C. C., Li, N., Zhang, Z. W., Su, J., Li, S., Li, J. L., Xu, S. W. 2014. Cadmium supplement triggers endoplasmic reticulum stress response and cytotoxicity in primary chicken hepatocytes. Ecotoxicology and environmental safety, 106, 109-114.

Sham, M., Wichase, O. Æ., Gregory, M., Noppadon, R. 2009. Cadmium accumulation in two populations of rice frogs (*Fejervarya limnocharis*) naturally exposed to different environmental cadmium levels. Bulletin of Environmental Contamination and Toxicology, 83, 703–707.

Shen, J., Chen, X., Hendershot, L., Prywes, R. 2002. ER stress regulation of ATF6 localization by dissociation of BiP/GRP78 binding and unmasking of Golgi localization signals. Developmental Cell, 3, 99-111.

Shen, D., Coleman, J., Chan, E., Nicholson, T. P., Dai, L., Sheppard, P. W., Patton, W. F. 2011. Novel cell-and tissue-based assays for detecting misfolded and aggregated protein accumulation within aggresomes and inclusion bodies. Cell biochemistry and biophysics, 60, 173-185.

Shi, J., Mei, W., Yang, J. 2008. Heme metabolism enzymes are dynamically expressed during *Xenopus* embryonic development. Biocell, 32, 259-263.

Shiu, R. P., Pouyssegur, J., Pastan, I. 1977. Glucose depletion accounts for the induction of two transformation-sensitive membrane proteinsin Rous sarcoma virus-transformed chick embryo fibroblasts. Proceedings of the National Academy of Sciences of the United States of America, 74, 3840–3844.

Skowronek, M. H., Hendershot, L. M., Haas, I. G. 1998. The variable domain of nonassembled Ig light chains determines both their half-life and binding to the chaperone BiP. Proceedings of the National Academy of Sciences of the United States of America, 95, 1574–8.

Sievers, F., Wilm, A., Dineen, D., Gibson, T. J., Karplus, K., Li, W., Thompson, J. D. 2011. Fast, scalable generation of high-quality protein multiple sequence alignments using Clustal Omega. Molecular Systems Biology, 7, 539.

Silver, J. T., Noble, E. G. 2012. Regulation of survival gene hsp70. Cell Stress and Chaperones, 17, 1–9.

Simoncelli, F., Belia, S., Di Rosa, I., Paracucchi, R., Rossi, R., La Porta, G., Fagotti, A. 2015. Short-term cadmium exposure induces stress responses in frog (*Pelophylax bergeri*) skin organ culture. Ecotoxicology and Environmental Safety, 122, 221-229.

Smalinskienė, A., Gailevičiūtė, R., Lesauskaitė, V., Sadauskienė, I., Abdrakhmanov, O., Ivanov, L. 2005. Effects of cadmium and zinc ions on mitotic activity and protein synthesis in mouse liver. Medicina, 41. 506-511.

Smith, M. H., Ploegh, H. L., Weissman, J. S. 2011. Road to ruin: targeting proteins for degradation in the endoplasmic reticulum. Science, 334, 1086-1090.

Song, C., Xiao, Z., Nagashima, K., Li, C. C. H., Lockett, S. J., Dai, R. M., Wang, Q. 2008. The heavy metal cadmium induces valosin-containing protein (VCP)-mediated aggresome formation. Toxicology and Applied Pharmacology, 228, 351-363.

Souza, V., Bucio, L., Gutierrez-Ruiz, M. C. 1997. Cadmium uptake by a human hepatic cell line (WRL-68 cells). Toxicology, 120, 215-220.

Stromer, T., Ehrnsperger, M., Gaestel, M., Buchner, J. 2003. Analysis of the interaction of small heat shock proteins with unfolding proteins. The Journal of Biological Chemistry, 278, 18015–18021.

Stone, M. 1974. Cross-validatory choice and assessment of statistical predictions. Journal of the Royal Statistical Society: Series B, 111-147

Stump, D. G., Landsberger, N., Wolffe, A. P. 1995. The cDNA encoding *Xenopus laevis* heat-shock factor 1 (XHSF1): nucleotide and deduced amino-acid sequences, and properties of the encoded protein. Gene, 160, 207-211.

Sudnitsyna, M. V, Mymrikov, E. V, Seit-nebi, A. S., Gusev, N. B. 2012. The Role of intrinsically disordered regions in the structure and functioning of small heat shock proteins. Current Protein and Peptide Science, 13, 76–85.

Sun, W., Van Montagu, M., Verbruggen, N. 2002. Small heat shock proteins and stress tolerance in plants. Biochimica et Biophysica Acta (BBA) - Gene Structure and Expression, 1577, 1–9.

Sun, Y., MacRae, T. H. 2005. Small heat shock proteins: molecular structure and chaperone function. Cellular and Molecular Life Sciences CMLS, 62, 2460-2476.

Sun, F. C., Wei, S., Li, C. W., Chang, Y. S., Chao, C. C., Lai, Y. K. 2006. Localization of GRP78 to mitochondria under the unfolded protein response. Biochemical Journal, 396, 31-39.

Tanabe, M., Sasai, N., Nagata, K., Liu, X. D., Liu, P. C. C., Thiele, D. J., Nakai, A. 1999. The mammalian HSF4 gene generates both an activator and a repressor of heat shock genes by alternative splicing. Journal of Biological Chemistry, 274, 27845–27856.

Tavaria, M., Gabriele, T., Kola, I., Anderson, R. L. 1996. A hitchhiker's guide to the human Hsp70 family. Cell Stress and Chaperones, 1, 23-28.

Taylor, J. M., Brody, K. M., Lockhart, P. J. 2012. Parkin co-regulated gene is involved in aggresome formation and autophagy in response to proteasomal impairment. Experimental Cell Research, 318, 2059-2070.

Thit, A., Selck, H., Bjerregaard, H. F. 2015. Toxic mechanisms of copper oxide nanoparticles in epithelial kidney cells. Toxicology in Vitro, 29, 1053–1059.

Thrower, J. S., Hoffman, L., Rechsteiner, M., Pickart, C. M. 2000. Recognition of the polyubiquitin proteolytic signal. The EMBO Journal, 19, 94–102.

Todd, D. J., Lee, A. H., & Glimcher, L. H. 2008. The endoplasmic reticulum stress response in immunity and autoimmunity. Nature reviews immunology, 8, 663-674.

Tong, X., Lopez, W., Ramachandran, J., Ayad, W. A., Liu, Y., Lopez-Rodriguez, A., Contreras, J. E. 2015. Glutathione release through connexin hemichannels: Implications for chemical modification of pores permeable to large molecules. The Journal of General Physiology, 146, 245-254.

Tyedmers, J., Mogk, A., Bukau, B. 2010. Cellular strategies for controlling protein aggregation. Nature Reviews. Molecular Cell Biology, 11, 777–788.

Vabulas, R. M., Raychaudhuri, S., Hayer-hartl, M., Hartl, F. U. 2010. Heat Shock Response. Perspective in Biology, 2, 1–18.

Vasil'eva, V. F., Gusev, G. P., Krestinskaia, T. V., Burovina, I. V., Ukhanov, K. 1986. Cadmium distribution in tissues and Na, K-ATPase activity of the skin of the frog *Rana temporaria* in different routes of cadmium uptake by the body. Zhurnal evoliutsionnoi biokhimii i fiziologii, 23, 300-304.

Vilaboa, N. E., García-Bermejo, L., Pérez, C., de Blas, E., Calle, C., Aller, P. 1997. Heat-shock and cadmium chloride increase the vimentin mRNA and protein levels in U-937 human promonocytic cells. Journal of Cell Science, 110, 201-207.

Voellmy, R. 2004. On mechanisms that control heat shock transcription factor activity in metazoan cells. Cell Stress and Chaperones, 9, 122-133

Voellmy, R., Boellmann, F. 2007. Chaperone regulation of the heat shock protein response. Molecular Aspects of the Stress Response: Chaperones, Membranes and Networks pp. 89-99.

Vogiatzis, A. K., Loumbourdis, N. S. 1997. Uptake, tissue distribution, and depuration of cadmium (Cd) in the frog *Rana ridibunda*. Bulletin of Environmental Contamination and Toxicology, 59, 770–776.

Waelter, S., Boeddrich, A., Lurz, R., Scherzinger, E., Lueder, G., Lehrach, H., Wanker, E. E. 2001. Accumulation of mutant huntingtin fragments in aggresome-like inclusion bodies as a result of insufficient protein degradation. Molecular Biology of the Cell, 12, 1393-1407.

Waisberg, M., Joseph, P., Hale, B., Beyersmann, D. 2003. Molecular and cellular mechanisms of cadmium carcinogenesis. Toxicology. 192, 95–117.

Walcott, S. E., Heikkila, J. J. 2010. Celastrol can inhibit proteasome activity and upregulate the expression of heat shock protein genes, hsp30 and hsp70, in *Xenopus laevis* A6 cells. Comparative Biochemistry and Physiology, Part A, 156, 285–293.

Walter, P., Ron, D. 2011. The unfolded protein response: from stress pathway to homeostatic regulation. Science, 334, 1081-1086.

Wang, N., Li, Q., Feng, N.-H., Cheng, G., Guan, Z.-L., Wang, Y., Sistonen, L. 2013. Heat shock factors: integrators of cell stress, development and lifespan. Nature Reviews. Molecular Cell Biology, 11, 735–41.

Wang, Q., Song, B., Jiang, S., Liang, C., Chen, X., Shi, J., Zhang, Z. 2014. Hydrogen sulfide prevents advanced glycation end-products induced activation of the epithelial sodium channel. Oxidative Medicine and Celullar Longevity, 2015, 1–10.

Wang, H., Wang, X., Ke, Z. J., Comer, A. L., Xu, M., Frank, J. A., Luo, J. 2015. Tunicamycin-induced unfolded protein response in the developing mouse brain. Toxicology and Applied Pharmacology, 283, 157-167.

Wen-Tung, W. U., Kwan-Hwa, C. H. I., Feng-Ming, H. O., Wei-Chia, T., Wan-Wan, L.. 2004. Proteasome inhibitors up-regulate haem oxygenase-1 gene expression: requirement of p38 MAPK (mitogen-activated protein kinase) activation but not of NF-kappaB (nuclear factor kappaB) inhibition. Biochemical Journal, 379, 587-593.

Wheeler, G. N., Brändli, A. W. 2009. Simple vertebrate models for chemical genetics and drug discovery screens: Lessons from zebrafish and *Xenopus*. Developmental Dynamics, 238, 1287–1308.

Wilke, N., Sganga, M. W., Gayer, G. G., Hsieh, K. P., Miles, M. F. 2000. Characterization of promoter elements mediating ethanol regulation of hsc70 gene transcription. Journal of Pharmacology Experimental Therapeutics, 292, 173–180.

Wisniewska, M., Karlberg, T., Lehti, L., Johansson, I., Kotenyova, T., Moche, M., Scheller, H. 2010. Crystal structures of the ATPase domains of four human Hsp70 isoforms: HSPA1L/Hsp70-hom, HSPA2/Hsp70-2, HSPA6/Hsp70B', and HSPA5/BiP/GRP78. PLoS ONE, 5, e8625.

World Health Organization (WHO). 2008. Guidelines for drinking-water quality, 3rd edition incorporating 1st and 2nd agenda. Geneva, World Health Organization. 1, 317– 319.

Wotton, D., Freeman, K., Shore, D. 1996. Multimerization of Hsp42p, a novel heat shock protein of *Saccharomyces cerevisiae*, is a dependent on a conserved caarboxyl-terminal sequence. Journal of Biological Chemistry, 271, 2717–2723.

Woolfson, J. P., Heikkila, J. J. 2009. Examination of cadmium-induced expression of the small heat shock protein gene, hsp30, in *Xenopus laevis* A6 kidney epithelial cells. Comparative Biochemistry and Physiology Part A: Molecular Integrative Physiology, 152, 91-99.

Winning, R. S., J. J. Heikkila, N. C. Bols. 1989. Induction of glucose-regulated proteins in *Xenopus laevis* A6 Cells. Journal of Cellular Physiology 140. 239-245.

Winning, R. S., Bols, N. C., Wooden, S. K., Lee, A. S., Heikkila, J. J. 1992. Analysis of the expression of a glucose-regulated protein (GRP78) promoter/CAT fusion gene during early *Xenopus laevis* development. Differentiation, 49, 1-6.

Winning, R. S., Shea, L. J., Marcus, S. J., Sargent, T. D. 1991. Developmental regulation of transcription factor AP-2 during *Xenopus laevis* embryogenesis. Nucleic Acids Research, 19, 3709-3714.

Wu, B. J., Kingston, R. E., Morimoto, R. I. 1986. Human HSP70 promoter contains at least two distinct regulatory domains. Proceedings of the National Academy of Sciences of the United States of America, 83, 629–33.

Xu, H., Xu, W., Xi, H., Ma, W., He, Z., Ma, M. 2013. The ER luminal binding protein (BiP) alleviates Cd 2+-induced programmed cell death through endoplasmic reticulum stress–cell death signaling pathway in tobacco cells. Journal of Plant Physiology, 170, 1434-1441.

Yamamoto, N., Izumi, Y., Matsuo, T., Wakita, S., Kume, T., Takada-Takatori, Y., Akaike, A. 2010. Elevation of heme oxygenase-1 by proteasome inhibition affords dopaminergic neuroprotection. Journal of Neuroscience Research, 88, 1934-1942.

Yang, J., Nune, M., Zong, Y., Zhou, L., Liu, Q. 2015. Close and allosteric opening of the polypeptide-binding site in a Human Hsp70 chaperone BiP. Structure, 23, 2191–2203.

Yan, M., Zhang, Y., Qin, H., Liu, K., Guo, M., Ge, Y.Zheng, X. 2016. Cytotoxicity of CdTe quantum dots in human umbilical vein endothelial cells: the involvement of cellular uptake and induction of pro-apoptotic endoplasmic reticulum stress. International journal of nanomedicine, 11, 529.

Yokouchi, M., Hiramatsu, N., Hayakawa, K., Kasai, A., Takano, Y., Yao, J., Kitamura, M. 2007. Atypical, bidirectional regulation of cadmium-induced apoptosis via distinct signaling of unfolded protein response. Cell Death Differentiation, 14, 1467-1474.

Yoshida, H., Haze, K., Yanagi, H., Yura, T., Mori, K., 1998. Identification of the cis-acting endoplasmic reticulum stress response element responsible for transcriptional induction of mammalian glucose-regulated proteins Involvement of basic leucine zipper transcription factors. Journal of Biological Chemistry, 273, pp.33741-33749.

Yoshida, M., Hiderou, T. 2001. XBP1 mRNA is induced by ATF6 and spliced by IRE1 in response to ER stress to produce a highly active transcription factor. Cell, 107, 881-891.

Young, J. T. F., Heikkila, J. J. 2010. Proteasome inhibition induces hsp30 and hsp70 gene expression as well as the acquisition of thermotolerance in *Xenopus laevis* A6 cells. Cell Stress and Chaperones, 15, 323–334.

Young, C. L., Raden, D. L., Robinson, A. S. 2013. Analysis of ER resident proteins in *Saccharomyces cerevisiae*: implementation of H/KDEL retrieval sequences. Traffic, 14, 365-381.

Yu, X., Sidhu, J. S., Hong, S., Robinson, J. F., Ponce, R. A., and Faustman, E. M. 2011. Cadmium induced p53-Dependent activation of stress signaling, accumulation of ubiquitinated proteins, and apoptosis in mouse embryonic fibroblast cells. Toxicological Sciences. 120, 403–412.

Zaarur, N., Meriin, A. B., Gabai, V. L., Sherman, M. Y. 2008. Triggering Aggresome Formation, dissecting aggresome-targeting and aggregation signals in synphilin 1. Journal of Biological Chemistry, 283, 27575-27584.

Zala, C., Salas-prato, M., Yan, W-T., Banjo, B., Perdue, J. 1980. In cultured chick embryo fibroblasts the hexose transport components are not the 75 000 and 95 000 dalton polypeptides synthesized following glucose deprivation. Canadian Journal of Biochemistry, 58, 1179–1118.

Zhang, D. D., Hannink, M. 2003. Distinct cysteine residues in Keap1 are required for Keap1-dependent ubiquitination of Nrf2 and for stabilization of Nrf2 by chemopreventive agents and oxidative stress. Molecular and Cellular Biology, 23, 8137–51.

Zhang, X., Qian, S. B. 2011. Chaperone-mediated hierarchical control in targeting misfolded proteins to aggresomes. Molecular Biology of the Cell, 22, 3277-3288.

Zhu, G., Lee, A. S. 2015. Role of the unfolded protein response, GRP78 and GRP94 in organ homeostasis. Journal of Cellular Physiology, 230, 1413-1420.

Zimmerman, S. B., Trach, S. O. 1991. Estimation of macromolecule concentrations and excluded volume effects for the cytoplasm of *Escherichia coli*. Journal of Molecular Biology, 222, 599–620.